The Dissertation Committee for Khalid Hossain Miah Certifies that this is the approved version of the following dissertation:

Three-Dimensional Broadband Intensity Probe for Measuring Acoustical Parameters

Committee:

Michael F. Becker, Supervisor

Elmer L. Hixson, Co-Supervisor

Francis X. Bostick

Mark F. Hamilton

John H. Davis

Ronald O. Stearman

Three-Dimensional Broadband Intensity Probe for Measuring Acoustical Parameters

by

Khalid Hossain Miah, B.S.; M.S.E

Dissertation

Presented to the Faculty of the Graduate School of

The University of Texas at Austin

in Partial Fulfillment

of the Requirements

for the Degree of

Doctor of Philosophy

The University of Texas at Austin

August 2009

Dedication

Dedicated to my parents: Khadiza Begum and Moazzem Hossain.

Acknowledgements

First, I would like to thank Dr. Hixson for motivating and inspiring me from the very beginning to the end in the long journey of the graduate school. I am very grateful and thankful to Dr. John S. Swinnea, Dr. Venkat Ganesan, Dr. James Chelikowsky from the Chemical Engineering dept; Dr. Baxter Womack from the ECE dept., and Dr. Mrinal Sen from UT Institute for Geophysics for funding (TA/GRA) me in some semesters during this long graduate school career. I would also like to thank my other committee members, Dr. Michael Becker, Dr. Mark Hamilton, Dr. Francis Bostick, Dr. John Davis, and Dr. Stearman for being in the committee. Special thanks to Dr. Hamilton for agreeing to attend the PhD Final Oral Examination with a very short notice.

I would like to express great respect and love to my mother, brother and sisters for their patience, and prayer for my very well being. My father was hardly around during my graduate school career but has always been a great inspiration for me when comes to the higher education and the health. He has taught me the importance of getting the highest formal education, maintaining a healthy life style, and traveling.

I am also quite lucky and grateful to have some great friends, especially to Chrystel Cassan, who helped me in going through some difficult emotional periods over the years. Now, I would like to wish very happiness and joy to a very special person. I know that she would still be very happy knowing that I have at last completed the PhD.

Thank you God!!

Three-Dimensional Broadband Intensity Probe for Measuring Acoustical Parameters

Publication No._____

Khalid Hossain Miah, PhD

The University of Texas at Austin, 2009

Supervisor: Michael F. Becker

Co-Supervisor: Elmer L. Hixson

Measuring different acoustical properties have been the key in reducing noise and improving the sound quality from various sources. In this report, a broadband (200 Hz – 6.5 kHz) three-dimensional seven-microphone intensity probe system is developed to measure the sound intensity, and total energy density in different acoustical environments. Limitations of most commercial intensity probes in measuring the three-dimensional intensity for a broadband sound field was the main motivation in developing this probe. The finite-difference error and the phase mismatch error which are the two main errors associated with the intensity measurements are addressed in this report.

As for the physical design, seven microphones were arranged in a two-concentric arrays with one microphone located at the center of the probe. The outer array is for low-frequencies (200 Hz – 1.0 kHz), and the inner one is for high-frequencies (1.0 kHz – 6.5 kHz). The screw adjustable center microphone is used for the microphone calibration, and as the reference microphone of the probe. The simultaneous calibrations of all the

microphones in the probe were done in the anechoic room. Theories for the intensity and the energy densities calculations for the probe were derived from the existing four-microphone probe configuration. Reflection and diffraction effects on the intensity measurements due to the presence of the microphones, and the supporting structures were also investigated in this report. Directivity patterns of the calculated intensity showed the omnidirectional nature of the probe.

The intensity, and total energy density were calculated and compared with the ideal values in the anechoic room environment. Characterization of sound fields in a reverberant enclosed space, and sound source identification are some applications that were investigated using this probe. Results of different measurements showed effectiveness of the probe as a tool to measure key acoustical properties in many practical environments.

Table of Contents

List of Tables

List of Figures

List of Illustrations

Chapter 1: Introduction

1.0 MOTIVATION

Precise measurement of acoustical quantities in different environments has been the key in improving sound quality and in reducing acoustical noise from various sources. Acoustic intensity is a key acoustic quantity, generally used in characterizing a sound field. The main objective of this dissertation research is to develop a three-dimensional probe to calculate the acoustic intensity from the pressure and the particle velocity measurements.

Sound intensity is defined as the rate of energy flow at a point in space through a unit area. By definition, the instantaneous sound intensity is the product of the instantaneous acoustic pressure and the instantaneous particle velocity [1].So, a sound intensity measuring device needs to incorporate transducers to measure both the pressure and the particle velocity. The particle velocity is calculated from the pressure difference between the two microphones, and is used for the intensity, energy densities, and impedance measurements.

Most one-dimensional sound intensity probes use two identical microphones in a face-to-face configuration. However, these systems have these inherent problems associated with their designs [2, 3, 4]:

- microphone phase mismatch error (when spacing between the microphones is very small, the physical phase difference can be masked by the instrumentation phase error. This increases the overall probe error. This error is defined and explained in Section 3.3),

- pressure measurement errors due to a misalignment between the two microphones, and
- limitations in a multi-dimensional vector measurement from the directional characteristic of a two-microphone system.

A two-microphone system can be used for three-dimensional measurements by rotating it around the sound source. The scanning process needs an extra device in addition to the probe. This need of an extra device prompted researchers to develop a three-dimensional intensity probe. Several three-dimensional intensity probes have been proposed and implemented to address concerns associated with the two-microphone system. These probes vary in their geometrical configurations, use different types of microphones, and have different applications. One of the configurations is the four-microphone tetrahedral configuration is first used by Moryl [5] to measure the energy density, and then was used by Poterek [6] to measure the intensity vectors. A commercial system (model: Tetra-phone MI-6420) made by a Japanese Company, Ono Sokki is also based on this configuration. Two commercial six-microphone intensity probes of different configuration were developed by the two different Companies, Brüel & Kjaer and GRAS, can be used to calculate the intensity vectors in a 3-D space [7]. The seven-microphone two-concentric array intensity probe developed in this report is the modified version of the four-microphone tetrahedral configuration used by Poterek [6]. The center microphone of the four-microphone tetrahedral configuration is used as the reference microphone of the probe. The difference between these configurations lies in methods for estimating the sound pressure at the center of the probe. The six-microphone configuration estimates the center pressure by averaging sound pressures from the

surrounding microphones while the four-microphone configuration directly measures the center pressure from the reference microphone [8, 9].

The effective spacing between the two microphones of an intensity probe has significant impact on the intensity measurements in broadband sound fields. The sound field around the microphones in a probe due to effects of diffractions and reflections from the microphones and the supporting structure can distort measurements, especially for closely spaced microphones with a large overall dimension. Microphone spacing in the probe has major effect on the finite-difference approximation error, especially at high frequencies where the signal wavelength must be large compared to the spacing between the two microphones. The four-microphone configuration used by Schumacher [10] for the acoustic energy density measurements has microphones arranged in a concentric array with one microphone at the center of the probe. The spacing between the microphones of the probe is fixed for measurements regardless of the frequency band of the sound field. This system works well for the frequency range of 300 Hz to 3.0 kHz, but needs spacing adjustment between the microphones to work with sound fields of a wide frequency band (200 Hz – 6.5 kHz). Both the four-microphone and the six-microphone configurations mentioned above need spacing adjustment for measurements involving sound source with a wide frequency band (200 Hz – 6.5 kHz). The six-microphone configuration has face-to-face microphone orientation, and is not suitable for many source localization applications without a peripheral rotating device.

In this dissertation research, the design and implementation of a seven-microphone three-dimensional intensity probe arranged in a two-concentric array are discussed. An inner array and an outer array together form the two-concentric array of the proposed probe. The inner array is for the high-frequency (1.0 kHz − 6.5 kHz), and the outer array is for the low-frequency (200 Hz – 1.0 kHz) measurements. This design does

not require any spacing adjustment during measurements. Microphones with a small dimension (0.25 inch in diameter) were used in a side-by-side configuration to reduce potential adverse effects due to the diffraction and reflection off the sensors. A screw adjustable center microphone was used for the calibration, and for the measurement of the center (origin) pressure.

1.1 APPLICATIONS

Acoustic intensity, and total energy density were all measured and calculated using the intensity probe developed in this study. One of the applications of the intensity probe discussed in this report is the acoustic source direction identification. Measurements were made in an anechoic chamber, and in a reverberation room for the calibration and evaluation of the probe.

In an acoustic environment, information about the direction and the pressure amplitude of a sound radiating source play an important role in many applications such as identifying speakers; steering microphones and video cameras in a conference room; noise cancellation in automobiles and in airplanes; tracking movements of sound radiating sources; and so on. Rating different household utilities (vacuum cleaner, refrigerator, microwave oven, heating and cooling units, etc) based on their respective noise level can also use the source direction information. Directional characteristics of this proposed intensity probe can be used in various source localization applications, both in anechoic and in reverberation environments. Source localization using the intensity probe is the subject of the future work. Improvements in signal-to-noise ratio, channel estimation, reduction of adverse effects due to the presence of other sources in a sound

field are some areas where the proposed three-dimensional intensity probe can also be used.

1.2 GOALS AND OBJECTIVES

The main objective of this dissertation research is to design, build and evaluate a three-dimensional acoustic intensity probe. Particular goals and objectives are,

- to develop a seven-microphone probe to measure intensity vectors in a three-dimensional space,
- to keep the microphone configuration and the supporting structure simple and small, in order to reduce adverse effects due to reflections and diffractions off the structure,
- to develop a simultaneous calibration method for the microphones of the system,
- to keep the sensitivity mismatch among the microphones less than 1.0 dB for the broad frequency band of 200 Hz to 6.5 kHz,
- to measure the intensity, total energy density, impedance, and probe frequency response for a broad frequency band (200 Hz – 6.5 kHz) , and
- to measure directivity patterns of the probe.

1.3 OUTLINE OF THIS REPORT

This report encompasses the physical design, calibration methods, error analysis, measurements of different acoustical quantities, and performance evaluations of the probe. Equations, charts, illustrations, and figures are used to present and to clarify key

concepts and results. Careful considerations are given in preserving continuation among subsequent chapters, and sections.

Chapter 2 provides sufficient background of the intensity measurements, and describes some previous studies of the development of different three-dimensional acoustic probes. Limitations of the existing probes and motivations of this research are also discussed in this chapter.

Different aspects of the physical probe design are described in Chapter 3. Sensor size, orientation, and configuration are also explained with the aid of schematics and plots.

Chapter 4 discusses inherent systematic errors due to design imperfections; the center (origin) microphone calibration; the plane wave justification in the anechoic chamber; diffraction and reflection effects of the probe structures on the center microphone calibrations; and effects of probe orientations on the center microphone pressure measurements.

Theories and principles used in the intensity, and the energy densities calculations are described in Chapter 5.

Chapter 6 focuses on the analysis of the intensity, energy densities, and probe frequency response measurements. Characteristics of sound fields in a reverberation room, directivity pattern, and source direction identification in an anechoic chamber using the newly developed intensity probe are also discussed in this chapter.

Chapter 7 wraps up this report with conclusions, limitations of the probe, and recommendations for the future work.

References

[1] M. Möser, "*Engineering Acoustics-An Introduction to Noise Control*," second edition, Springer, Berlin, 2004.

[2] F. J. Fahy, "*Sound Intensity*," second edition, E & FN SPON (Chapman & Hall), London, 1995.

[3] S. Nagata, K. Furihata, T. Wada, D. K. Asano, and T. Yanagisawa, "A three-dimensional sound intensity measurement system for source identification and sound power determination by ln models," *J. Acoust. Soc. Am.*, vol. 118, pp. 3691-3705, 2005.

[4] F. J. Fahy, "Measurement of acoustic intensity using the cross-spectral density of two microphone signals," *J. Acoust. Soc. Am.*, vol. 62, pp. 1057-1059, 1977.

[5] J. A. Moryl and E. L. Hixson, "A total acoustic energy density sensor with applications to energy density measurement in a reverberation room," *Proceedings of Inter-Noise*, vol. 87, pp. 1195-1198, 1987.

[6] T. J. Poterek, "*Energy density analysis of acoustic intensity*," Master's thesis, The University of Texas at Austin, 2001.

[7] B. S. Cazzolato and J. Ghan, "Frequency domain expressions for the estimation of time-averaged acoustic energy density," *J. Acoust. Soc. Am.*, vol. 117, pp. 3750-3756, 2005.

[8] M. Suzuki, H. Anzai, S. Oguro, and T. Ono, "Performance evaluation of a three dimensional intensity probe," *J. Acoust. Soc. Jpn (E).,* vol. 16, pp. 233-238, 1995.

[9] B. S. Cazzolato and C. H. Hansen, "Errors arising from three-dimensional acoustic energy density in one-dimensional sound fields," *J. Sound Vib.*, vol. 238, pp. 375-400, 2000.

[10] M. Schumacher, "*A transducer and processing system for acoustic energy density sensing in one-dimensional sound fields*," Master's thesis, The University of Texas at Austin, 1984.

Chapter 2: Previous Work

2.0 2-D PROBES AND THEIR LIMITATIONS

The main objective of this dissertation report is to develop a probe that can be used to measure the sound intensity vectors, given a sound source. The two-microphone intensity probes have been around for the past few decades, and are very useful in measuring sound intensity vectors in a sound field [1, 2] . The main drawback of any two-microphone intensity probe is its limitation in characterizing sound fields in a three-dimensional space. The two-microphone systems are inherently one-dimensional in nature. These systems require physical scanning (or rotating) around the source to estimate sound fields and to map vector intensity fields in a three-dimensional space. This scanning process requires additional hardware and software, and is not always feasible considering some difficult to reach sound sources in a 3-D space. As an example, different industrial machines placed on a manufacturing floor have different acoustic signatures. Identifying those signatures in the presence of other acoustic sources using only a two-microphone intensity measuring device is very difficult and often unreliable.

To address this limitation in the intensity measurement, a sound intensity probe for the direct measurement of acoustical properties in the 3-D sound fields have been investigated in this report.

2.1 3-D INTENSITY PROBES AND THEIRS LIMITATIONS

Sound intensity is a vector quantity with a magnitude and a direction. The intensity vectors in a three-dimensional space can provide very useful information of a sound field. The multi-dimensional vector intensity measurements not only provide relatively accurate magnitude information but also directions to the radiating sound source in a sound field regardless of its direction. One dimensional probe can only calculate intensity if it is pointed toward the source and still can not provide useful information about the source direction. This is one of the major advantages of a 3-D intensity probe over a two-microphone system. Due to this advantage, different three-dimensional intensity probes have been developed and used in sound source localization applications [11]. The sensitivity mismatch error and the phase mismatch error are inherent to every acoustic intensity measuring system, regardless of their dimensions (2-D or 3-D), and the number of microphones in the system [3, 4, 5, 6, 7].

Multi-microphone three-dimensional intensity probes of different sizes, orientations, and measurement techniques have been developed over the past two decades. All of them focus on various applications and have various limitations. One common requirement of these devices is the adjustment of the microphone spacing relative to each other for measurements in a wide band sound field.

One of the widely used commercial three-dimensional intensity probes was developed and manufactured by Brüel & Kjaer [8]. This intensity probe has six microphones arranged in an orthogonal configuration and are connected to each other through spacers for efficient frequency ranges. In this probe, the sound pressure at the center is estimated from the surrounding microphones. In this design, the spacers, the microphones, and the supporting structure can have potential adverse effects on

measurements due to diffractions and reflections, which can limit the useful maximum frequency up to about 5.0 kHz.

The estimated center pressure from the surrounding microphones could add additional error in the calculations of the particle velocity, intensity, and related acoustic quantities. Another commercial 3-D six-microphone intensity probe developed by GRAS [9] has the similar design and limitations as the B&K. Illustrations of these probes are shown in the Figure 2.1.

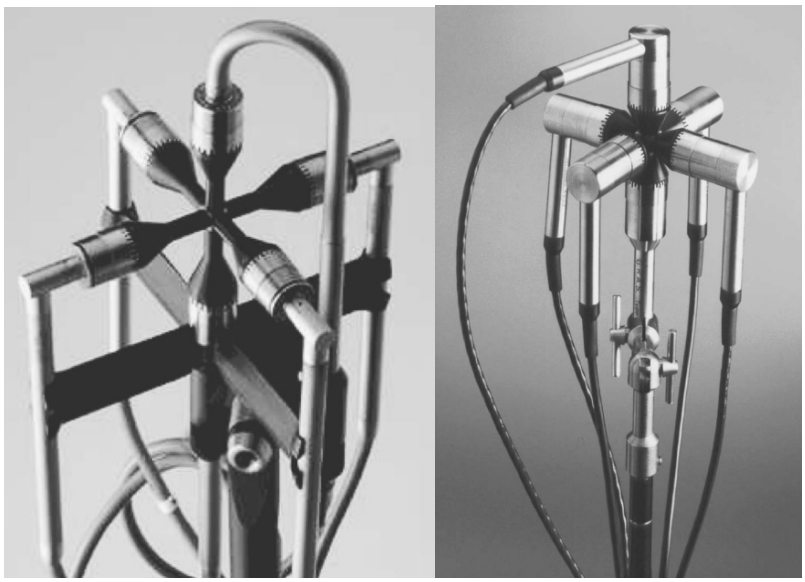

(a) (b)

Figure 2.1: (a) B&K Type 5356 six-microphone 3-D Intensity probe [8], (b) GRAS 3-D six-microphone intensity probe [9].

A 3-D intensity probe has four microphones in a side-by-side tetrahedral array arrangement with one microphone is located at the center of the probe. This four-microphone intensity probe system was first developed by Dr. Elmer L. Hixson and used by his then graduate students from the University of Texas at Austin. [10, 12, 13]. Several upgrades in the data acquisition and in the measurement techniques were made in that four-microphone probe for improved performance. Later, a Japanese Company, *Ono Sokki* has developed a similar four-microphone 3-D intensity probe for the commercial purpose (see Figure 2.2) [10, 11]. One of the benefits of this four-microphone configuration is the presence of a center microphone to measure center pressure directly. Like the other 3-D probes discussed earlier, one of the disadvantages of this four-microphone probe is the need to adjust microphone spacing to accommodate a wide band sound field. In addition, each microphone of the probe needs to be calibrated separately.

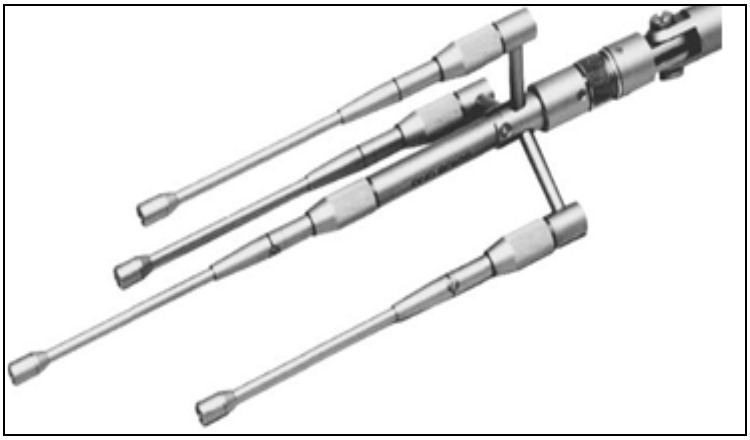

Figure 2.2: *Ono Sokki* four-microphone three-dimensional intensity probe [11].

The seven-microphone 3-D intensity probe designed and developed in this dissertation research is similar to the four-microphone configuration discussed in the previous paragraph. The main difference between the newly developed intensity probe and the existing probes is the arrangement of the microphones in a two-concentric array in the probe. This arrangement can cover a sound field of a wide frequency band (200 Hz – 6.5 kHz) without the need of any spacing adjustment between the microphones during measurements (see Figure D.1 in the Appendix). A calibration technique for simultaneous calibration of the microphones in the probe is also discussed in this report.

References

[1] F. J. Fahy, "Measurements of acoustic intensity using the cross-spectral density of two microphone signals," *J. Acoust. Soc. Am.,* vol. 62, pp. 1057-1059, 1977.

[2] M. P. Waser and M. J. Crocker, "Introduction to the two-microphones cross-spectral method of determining sound intensity," *Noise Control Eng. J.,* vol. 22, pp. 76-85, 1984.

[3] P. S. Watkinson, "The practical assessment of errors in sound intensity measurement," *J. Sound Vib.,* vol. 105, pp. 255-263, 1986.

[4] J. Y. Chung, "Cross-spectral method of measuring acoustic intensity without error caused by instrument phase mismatch," *J. Acoust. Soc. Am.,* vol. 64, pp. 1613-1616, 1978.

[5] G. Krishnappa, "Cross-spectral method of measuring acoustic intensity by correcting phase and gain mismatch errors by microphone calibration," *J. Acoust. Soc. Am.,* vol. 69, pp. 307-310, 1981.

[6] T. Yanagisawa and N. Koike, "Cancellation of both phase mismatch and position errors with rotating microphones in sound intensity measurements," *J. Sound Vib.,* vol., 113, pp. 117-126, 1987.

[7] J. K. Thompson and D. R. Tree, "Finite Difference approximation errors in acoustic intensity measurements," *J. Sound Vib.,* vol. 75, pp. 229-238, 1981.

[8] E. Fredriksen and O. Schultz, "*Pressure microphones for intensity measurement with significantly improved phase properties*," In Brüel & Kjaer Technical Review, no. 4-1986, Brüel & Kjaer, Naeurm, Denmark, pp. 11-23, 1986.

[9] G.R.A.S. Sound & Vibration, "*Vector Intensity Probe Type 50VT*", Product Data and Specification sheet, Holte, Denmark, 2002.

[10] J. A. Moryl and E. L. Hixson, "A total acoustic energy density sensor with applications to energy density measurement in a reverberation room," *Proceedings of Inter-Noise,* vol. 87, pp. 1195-1198, 1987.

[11] M. Suzuki, H. Anzai, S. Oguro, and T. Ono, "Performance evaluation of a three-dimensional intensity probe," *J. Acoust. Soc. Jpn (E),* vol. 16, pp. 233-238, 1995.

[12] M. Schumacher, "*A transducer and processing system for acoustic energy density sensing in one-dimensional sound fields*," Master's thesis, The University of Texas at Austin, 1984.

[13] T. J. Poterek, "*Energy density analysis of acoustic intensity*," Master's thesis, The University of Texas at Austin, 2001.

Chapter 3: Design of the Intensity Measuring System

3.0 PHYSICAL DESIGN OF THE PROBE

The acoustic intensity measuring system discussed in this report is developed in the Acoustics Research Laboratory at the University of Texas at Austin. This system has three major components: a microphone array with an interface analog circuit, a data acquisition device, and a personal computer with a custom signal processing software. A block diagram of the system is shown in Figure 3.1.

3.1 MICROPHONE SPACING AND ORIENTATION

3.1.1 Microphone Spacing

The three-dimensional intensity probe developed in this dissertation research consists of seven microphones. Six microphones are arranged in a two-concentric array (Figure 3.2) with one microphone located at the center of the probe. The center microphone is used as the reference microphone of the system. The inner array is for the high-frequency (1.0 kHz − 6.5 kHz) measurements, with an effective spacing between the reference and each of the three microphones is 18 mm. The outer array is for the low-frequency (200 Hz − 1.0 kHz) measurements, with an effective spacing between the reference microphone and each of the three microphones is 80 mm. The reference microphone can be moved either in forward or in backward direction along the probe axis by adjusting a screw. Microphone effective distances were selected to keep finite-

difference approximation error to a minimum. The relationship between the microphone effective spacing and the finite-difference approximation error of the probe is discussed later in this chapter. The center reference microphone can be adjusted to any of the three different positions: measurement position, low-frequency calibration position, and high-frequency calibration position (see Figure 3.7). The purpose of the center microphone adjustment for calibrations positions is to place all the microphones of each array in a plane for calibration in an anechoic chamber.

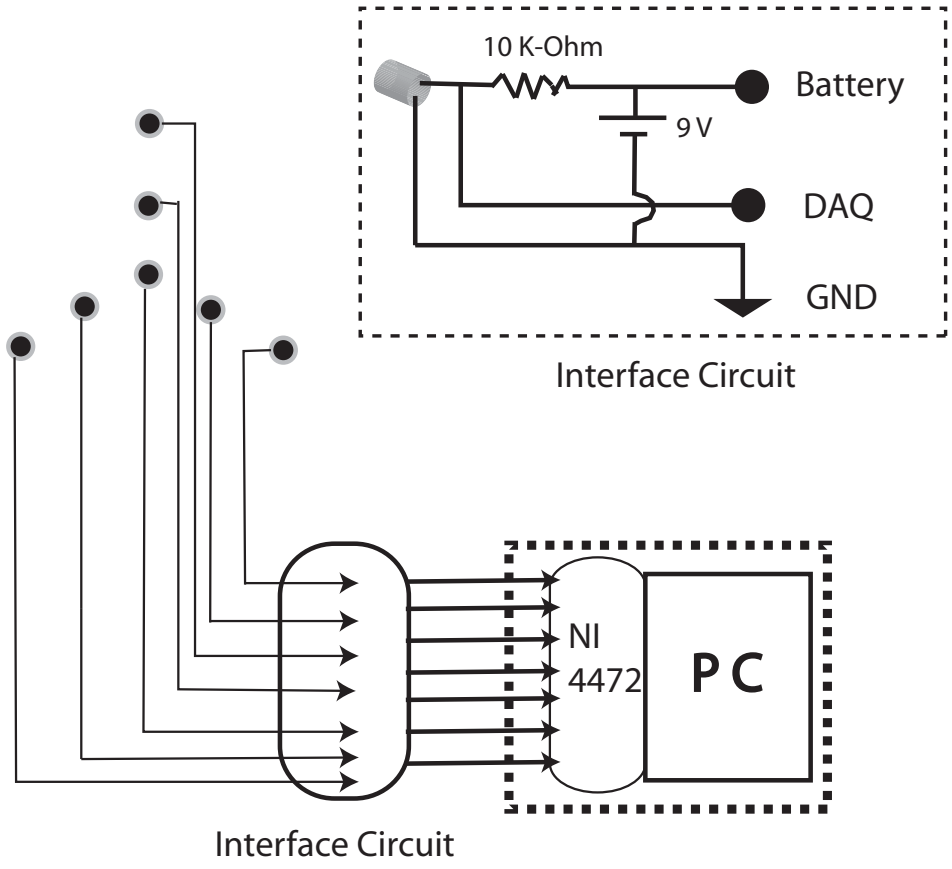

Figure 3.1: A block diagram of the seven-microphone intensity probe system.

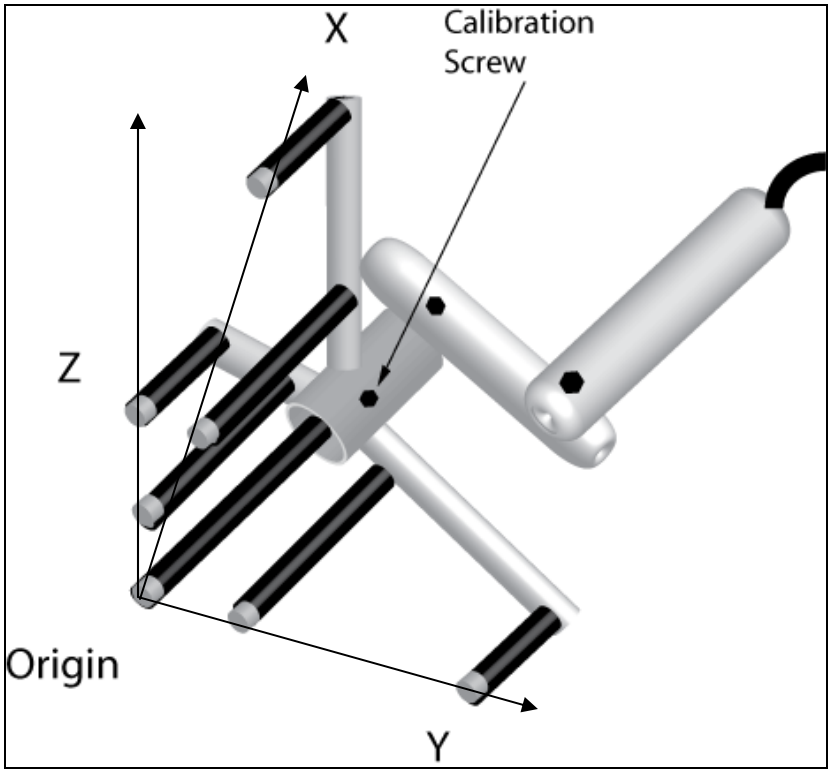

Figure 3.2: Intensity probe: seven microphones arranged in a two-concentric array along the three axes (x, y, and z) with a reference microphone at origin of the coordinate system (not in scale).

3.1.2 Microphone Orientation

A side-by-side microphone configuration (Figure 3.2) was chosen for the seven-microphone intensity probe design to minimize diffractions and reflections off the structures.

3.1.3 Microphone Selection

Each microphone of the probe is an omnidirectional Electret condenser microphone cartridge (Panasonic model, WM - 61A) with the sensitivity of -30.0 dB (0 dB = 1 V/Pa) with the standard operation voltage (9.0 volt) with the load impedance, 10.0 k-ohm. Each microphone has a diameter of 6.0 mm and a height of 3.4 mm. The frequency response of each of these microphones is nearly flat (+/- 2 dB) for frequencies from 50 Hz to 7 kHz. The interface circuit is shown in Figure 3.1.

3.2 DATA ACQUISITION

An eight-channel analog input data acquisition device (Model: PCI-4472, manufactured by National Instrument) was used to acquire microphone signals for the post processing. This data acquisition device (DAQ) has input channels with the maximum simultaneous sampling rate of 102.4 KS/s, 24-bit resolution, and multiple triggering modes including one external digital triggering. The simultaneous signal acquisition from all seven microphones using one DAQ card was used to prevent any potential time-delay mismatch. A LabView version 8.2 was used as the data acquisition software. Individual microphone calibration, and pre-filtering software were also developed in the LabView programming environment. The acquired signal data was then saved in the TXT format for subsequent post processing in MATLAB. Signal conditioning, filtering, the intensity, and the energy density calculations were also done in MATLAB.

3.3 MICROPHONE SPACING DETERMINATION

The spacing between a surrounding microphone and the center (reference) microphone has great impact on both the high-frequency and the low-frequency measurement errors. The finite-difference approximation error at high frequencies, and the phase mismatch error at low frequencies are greatly affected by the microphone spacing.

The finite-difference approximation error affects both the mean pressure and the particle velocity calculations. Thus, it affects the overall intensity measurement, and subsequent parameter estimations. The finite-difference approximation error originates from the pressure estimation at the midpoint between the two microphones. In this estimation, the midpoint pressure is the average value of pressures measured at each

microphone in a two-microphone pair. The second error arises from the approximation, which estimates a pressure gradient at the midpoint of a two-microphone pair as the slope of pressures across the two microphones [1]:

$$\frac{\partial P}{\partial x}(x,t) \cong \frac{P_m - P_o}{\Delta r_{mo}}, \tag{3.1}$$

where P_m is the pressure at one of the six microphones in the array, P_O is the pressure at the origin microphone, and Δr_{mo} is the effective distance between the center microphone and any of the six microphones in the probe. The "effective" distance is defined as the actual center-to-center distance between the two microphones. Graphical depiction of the finite-difference approximation error (in the extreme case) is shown in Figure 3.3.

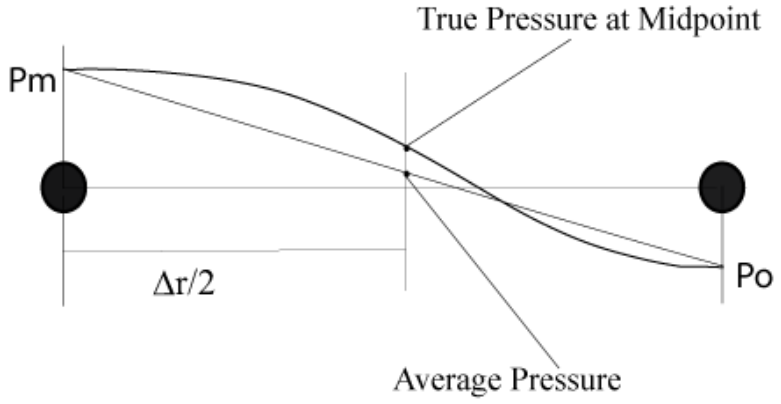

Figure 3.3: Mid-point pressure estimation, which causes the finite-difference approximation error in the mean pressure measurement.

The permissible frequency range for a specified spacing between the two microphones can be determined using the following formula [1]:

$$error_{probe} = 10\log\left(\frac{\sin\left(2\pi\frac{\Delta r}{\lambda}\right)}{2\pi\frac{\Delta r}{\lambda}}\right) \tag{3.2}$$

where λ is the wavelength, and Δr is the effective distance between the two microphones. The term on the right hand side of the Equation 3.2 is the ratio of the two intensities, thus the ($10\ \log_{10}$) is used to express the probe error in dB. Based on this equation, the impact of microphone spacing on the finite-difference approximation error for different frequencies is shown in the Figure 3.4. This figure was used as a guide in selecting the effective spacing between the two microphones.

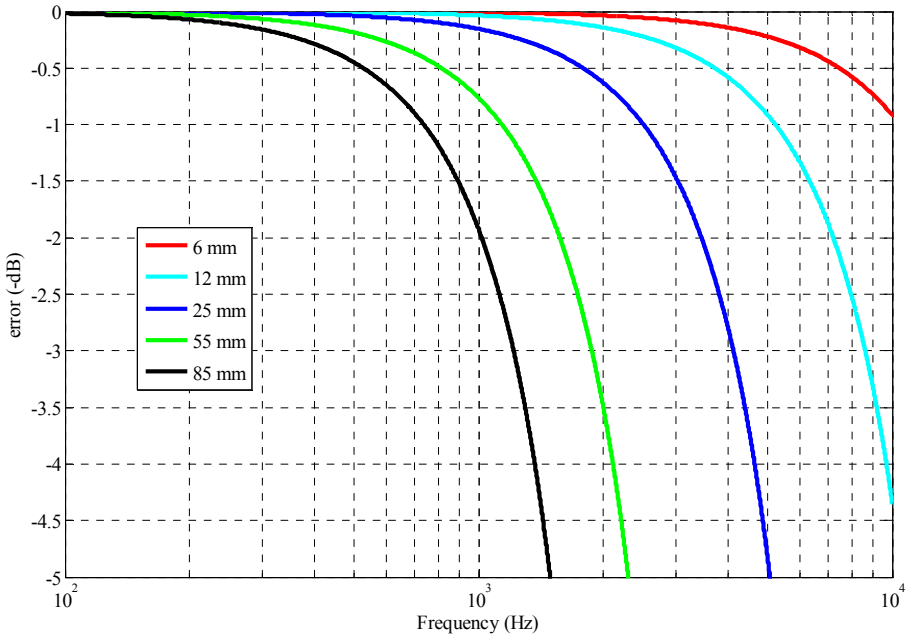

Figure 3.4: Impact of microphone spacing on the finite-difference approximation error in the intensity measurements (excluding other effects).

It is seen in the above Figure that as a spacing between the two microphones increases, the probe error increases, and vice versa. For example, at 85 mm spacing the probe error at 1.0 kHz is -2 dB. At another extreme, the probe error is -0.5 dB at 7.0 kHz for the spacing of 6 mm between the microphones. So, to keep the probe error at a minimum, a small spacing between the microphones is desirable. Another factor that affects the probe error is the phase mismatch between the microphones. This error is also related to the spacing between the microphones. The relationship between the microphone spacing and the probe error due to the phase mismatch between the microphones is discussed in the following paragraph.

Another potential error that was considered while selecting the microphone spacing for each array is the phase mismatch between the microphones in the probe. The microphones in each array were placed in an equal distance from the center (origin) microphone. Ideally, if these microphones are subject to a plane wave, then the phase differences among the microphones would be zero. From measurement standpoint, these phase differences are rarely zero, and can be termed as phase mismatch among the microphones. This phase mismatch error has the major effect in low frequencies where the signal wavelength is very large in compare to the spacing between the two microphones. If the spacing between the microphones is very small, then the physical phase difference (due to the physical separation of the microphones from each other) could be masked by the phase mismatch error introduced by instrumentation. The phase error in the probe can be related to the phase mismatch in the microphones due to their spacing can be related by this equation [1]:

$$error_{phase} = 10\log\left(1+\frac{\Delta\alpha}{\Delta\phi}\right), \tag{3.3}$$

where $\Delta\alpha$ is the phase mismatch introduced by the instrumentation, and $\Delta\phi$ is the actual physical phase difference due to the physical separation of the two microphones. It can be seen in this above equation, if the physical phase difference is small compared to the instrumentation phase mismatch then the probe error will be large. So, to keep this error smaller for a fixed instrumentation, the physical phase difference needs to be large. The large physical phase difference can be achieved by increasing the spacing between the microphones. So, to keep the probe error due to the phase mismatch at a minimum, large microphone spacing is preferred. Now, it is to be remembered that as the microphone spacing becomes large, so thus the finite-difference error.

In the intensity probe developed in this dissertation, the effective distance between the two microphones was selected to be 18 mm and 80 mm for the inner and the outer array, respectively. Since a small spacing between the two microphones causes a large phase mismatch error, and a large spacing causes bigger finite-difference approximation error at high frequencies, there was a tradeoff in selecting the microphone spacing to keep both the errors at a minimum. The probe error related to the sensor spacing is shown in the Figure 3.5.

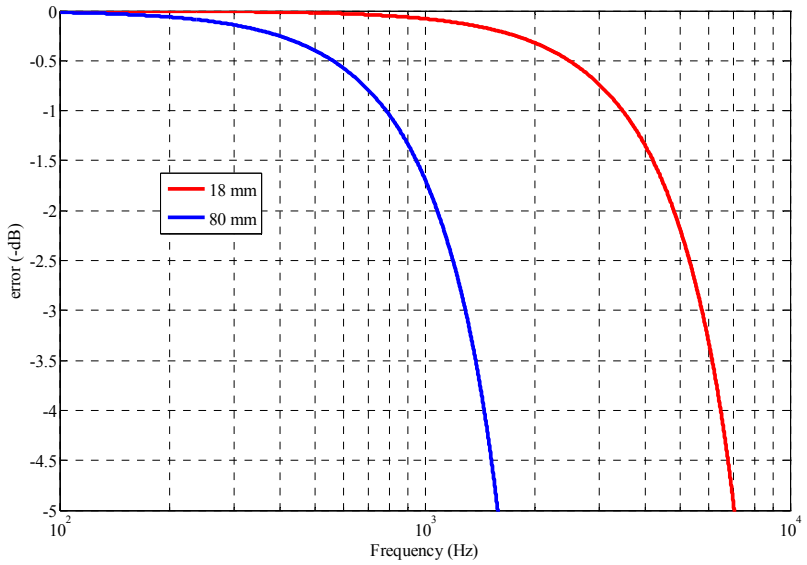

Figure 3.5: Probe error due to the finite-difference approximation dependent on the microphone spacing within the array.

It can be seen in the above plot that the outer low-frequency array spacing has an error of about -2.0 dB at 1000 Hz, while the inner high-frequency array has an error of about -4.0 dB at 6.5 kHz. This intrinsic error is considered large for the accurate measurements of different acoustical parameters, and needs to be minimized for the intensity calculations. Different microphone spacing for the different probe modes (high-frequency calibration, low-frequency calibration, and measurement) is listed in the Table 3.1.

Table 3.1: Microphone Effective spacing from the center microphone for the different probe modes.

Probe Mode	Effective distance from the center microphone (mm)					
	X-low	Y-low	Z-low	X-high	Y-high	Z-high
High-frequency calibration position	Fixed	Fixed	Fixed	15	15	15
Low-frequency calibration position	70.4	70.4	70.4	Fixed	Fixed	Fixed
Measurement position	80	80	80	18	18	18

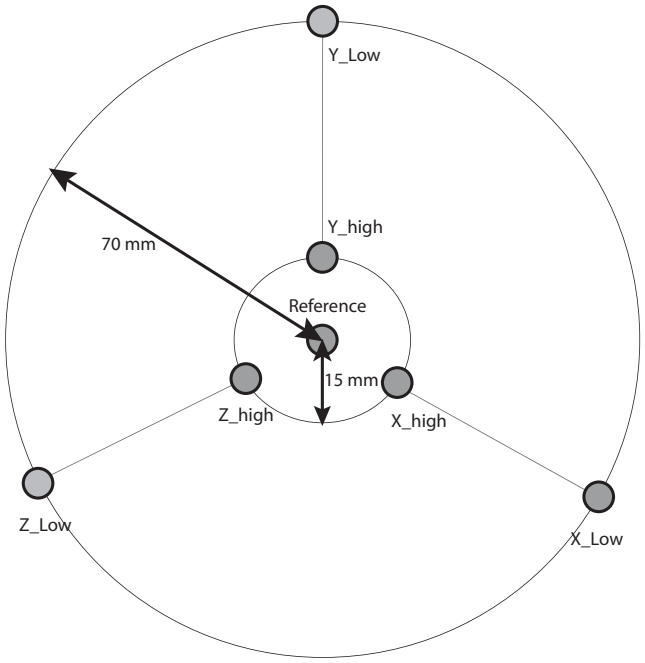

Figure 3.6 : A schematic showing horizontal spacing between the microphones in the calibrate position.

3.4 MICROPHONE CALIBRATION

Microphone calibration is an important step in designing a reliable acoustic intensity measuring system. A good calibration technique uses a standard measuring system for repeatability. Several studies have addressed some critical issues related to the microphone calibration, and related system errors [2, 3, 4].

The sensitivity of the standard reference microphone used in the probe microphone calibration was itself being calibrated by using a standard reference sound source (QUEST ELECTRONICS model: QC-20 microphone calibrator), and a sound level meter. The calibrator produced a 1 kHz tone of 94 dB SPL (ref. to 20 μPa) for the standard reference microphone calibration. The calibration positions of the reference microphone are referenced in the Table 3.1, and shown in Figure 3.7. The calibrated standard reference microphone was then placed inside an anechoic chamber to calibrate the origin microphone of the intensity probe. The calibrated origin microphone was then used for simultaneous calibration of the other microphones of the probe. The calibration techniques and procedures are discussed in the Chapter 4 of this report.

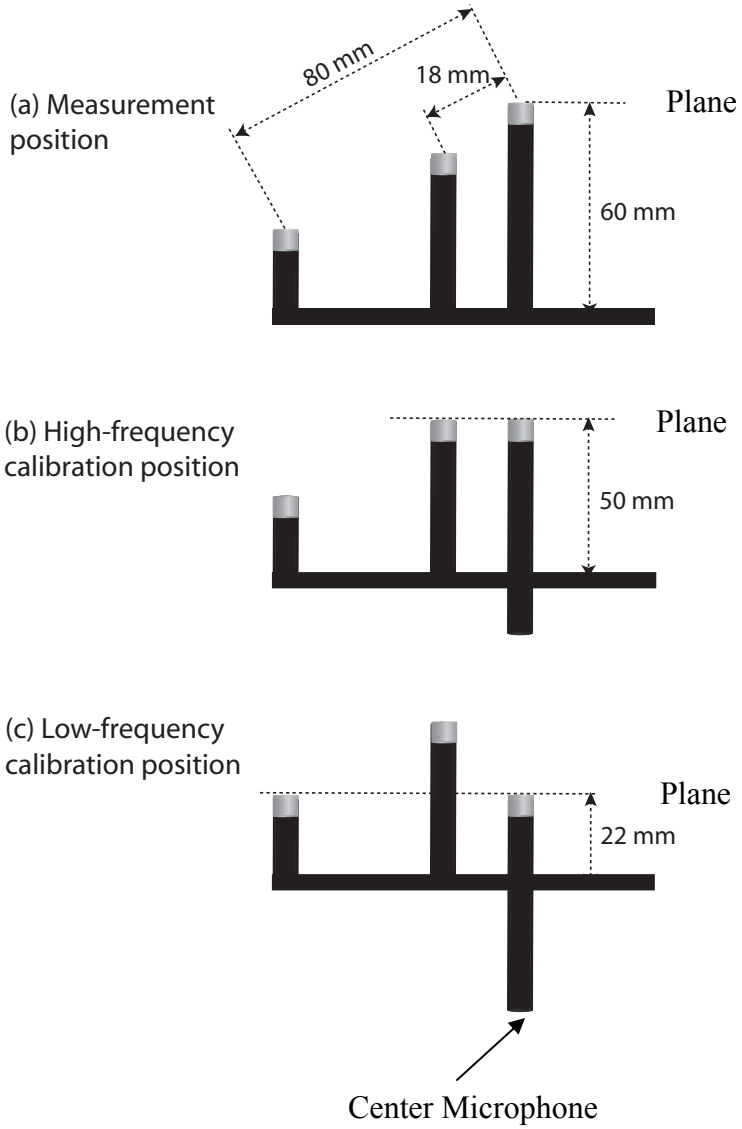

Figure 3.7: A schematic depicting microphone spacing with an adjustable center microphone in the measurement position, the high-frequency calibration position, and the low-frequency calibration position (not in scale).

References

[1] H. P. Corporation, "*Application Note 1230: Sound Power Measurements*," Hewlett-Packard Co., Singapore, 1992.

[2] J. Y. Chung, "Cross-spectral method of measuring acoustic intensity without error caused by instrument phase mismatch," *J. Acoust. Soc. Am.,* vol. 64, pp. 1613-1616, 1978.

[3] G. Krishnappa, "Cross-spectral method of measuring acoustic intensity by correcting phase and gain mismatch errors by microphone calibration," *J. Acoust. Soc. Am.*, vol. 69, pp. 307-310, 1981.

[4] A. J. Zuckerwar and G. C. Herring, "Calibration method of the pressure sensitivity of microphones by a far-field method at frequencies up to 80 kHz," *J. Acoust. Soc. Am.,* vol. 119, pp. 320-329, 2006.

Chapter 4: Measurement Errors Analysis

4.0 INHERENT SYSTEMATIC ERRORS IN THE PROBE

There are two different techniques widely used in the measurement of the pressure and the particle velocity vectors in an intensity probe. One of them is the pressure-pressure (*p-p*) technique that uses two pressure sensitive transducers (microphones). The other one is pressure-particle velocity (*p-v*) technique that uses a pressure transducer (microphone) and a direct particle-velocity sensor. The particle-velocity sensor uses the acoustic transduction principle, which is based on the convection of an ultrasonic beam by the audio-frequency particle flow [1]. A particle-velocity sensor is much more expensive than a pressure transducer (microphone). The overall complexity of a direct particle-velocity sensor implementation in an intensity probe out-weights potential benefits. So, I have chosen the *p-p* (pressure-pressure) technique over the *p-v* technique to develop the intensity probe in this report.

Inherent systematic errors can be explained as errors from the imperfections of the probe design and construction, and not from the direct results of an intensity measurement technique. Inherent errors are functions of the wavefield under investigation, and of the orientation of microphones in the probe. So, a precise estimation of these errors in an arbitrary sound field can be very difficult, or nearly impossible. Several studies [1, 2, 3, 4] were done in the past using different idealized and well understood models of a sound field to estimate these errors.

Inherent errors associated with the *p-p* technique used in the probe design, can be attributed the finite-difference approximations of the pressure and the particle velocity vectors. These errors are analyzed in reference to a spatial distribution of a sound field in the direction of the probe axis. These inherent errors can be quantified as the normalized

errors in pressure and particle velocity estimations. Pressure estimates is denoted as p_e, where as v_e is denoted as the particle velocity estimated. Normalized errors in the pressure, p and the particle velocity, v, estimates along the probe axis (microphone axis) due to the inaccuracies in the half distance between the two microphones are as follows [1] :

$$error_P = \frac{(p_e - p)}{p} = \left[\left(\frac{d^2}{2}\right)p''(t) + \left(\frac{d^4}{24}\right)p^{iv}(t) + \cdots\cdots\right]\frac{1}{p(t)}, \tag{4.1}$$

$$error_v = \frac{(v_e - v)}{v} = \frac{\int_{-\infty}^{t}\left[\left(\frac{d^2}{6}\right)p'''(\tau) + \left(\frac{d^4}{120}\right)p^{v}(\tau) + \cdots\cdots\right]d\tau}{\int_{-\infty}^{T} p'(\tau)d\tau}, \tag{4.2}$$

For the above errors analysis, a plane progressive sound wave model was used. For this sound field, Equations 4.1, 4.2, and subsequent normalized errors associated with the intensity are given by the following equations [1]:

$$error_p = \cos(kd) - 1 \approx -\frac{(kd)^2}{2} + \frac{(kd)^4}{24} - \frac{(kd)^6}{720} + \cdots\cdots \tag{4.3}$$

$$error_v = \left[\frac{\sin(kd)}{kd}\right] - 1 \approx -\frac{(kd)^2}{6} + \frac{(kd)^4}{120} - \frac{(kd)^6}{5040} + \cdots\cdots \tag{4.4}$$

$$error_{Intensity} = \frac{I_e - I}{I} \approx -\left(\frac{2}{3}\right)(kd)^2 + \left(\frac{2}{15}\right)(kd)^4 \tag{4.5}$$

In the above equations, k is the wave number, and d is half of the distance between the two microphones. Superscript on p in Equation 4.1 and 4.2 indicates spatial derivatives of the pressures. Normalized errors (for extreme case) for the pressure, particle velocity, and intensity at different fd (where f is the frequency), for both the inner and the outer arrays of the probe are plotted in the Figure 4.1.

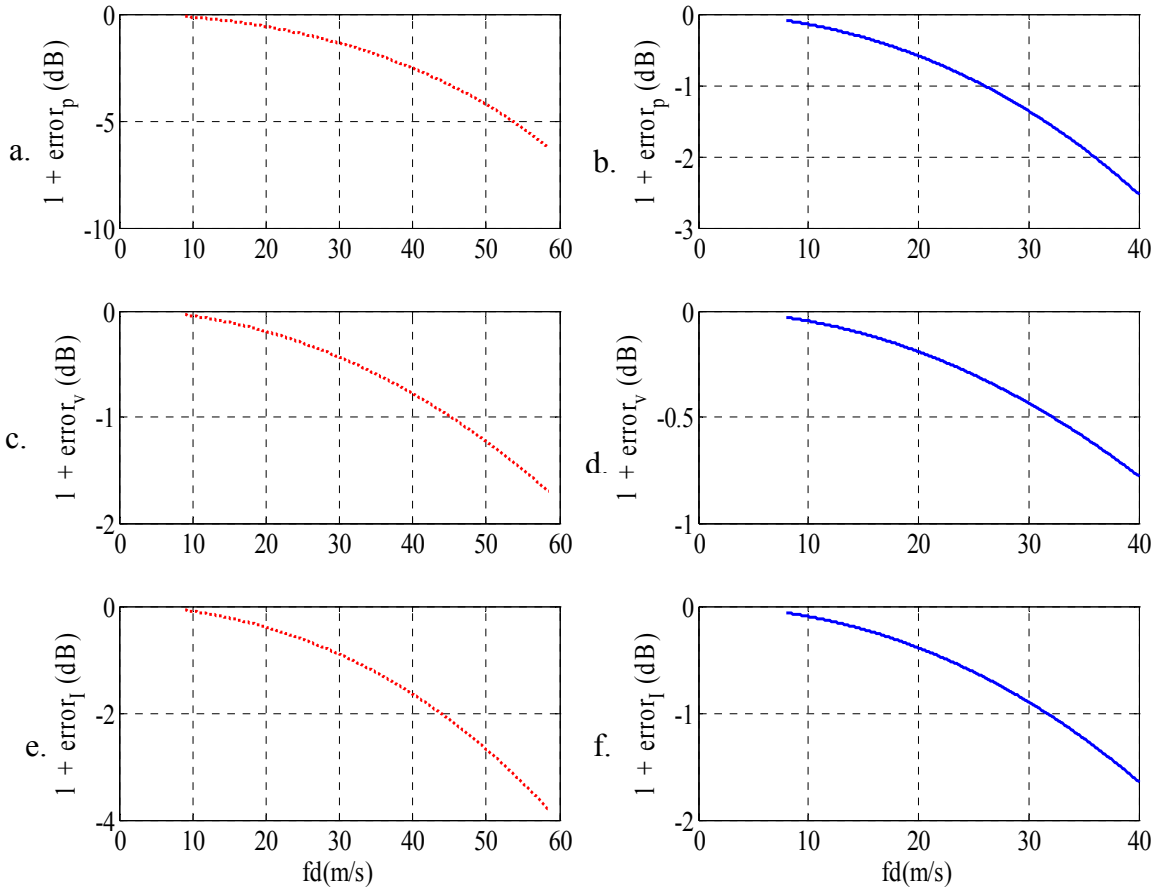

Figure 4.1: Systematic p-p errors as a function of frequency (f) and separation distance (d): (a) pressure error (high-freq.); (b) pressure error (low-freq.); (c) particle velocity error (high-freq.); (d) particle velocity error (low-freq.); (e) Intensity error (high-freq.); and (f) Intensity error (high-freq.). (**extreme case**).

In Figure 4.1, the plots on the left are for the high frequency array and the ones on the right are for the low-frequency array of the probe. For the high frequency array, the half of the effective spacing is 9 mm. At this spacing and at the frequency of 6.5 kHz, the normalized pressure error in air is -6.0 dB, the normalized particle velocity error is -1.5 dB, and the normalized intensity error is -3.75 dB. Similarly, for the low-frequency array, the half of the effective spacing is 40 mm. At this spacing and at the frequency of 1.0 kHz, the normalized errors for the pressure, particle velocity, and intensity are -2.6 dB, -0.8 dB, and -1.65 dB, respectively. The large errors in the high-frequency plots can be attributed to the finite-difference approximation error discussed in the Chapter 3 of this report.

The plots in Figure 4.1 were used as a guide to understand systematic errors introduced in the measurements due to the selection of a particular microphone spacing and the type of transducers chosen for the intensity probe design. It is important to remember that these errors are the maximum potential errors that can be caused due to the change of spacing. If the spacing error between the microphones is zero, then these errors will also be zero.

4.1 MICROPHONE CALIBRATION TECHNIQUES

In this section, the center (origin) microphone was calibrated using a standard reference microphone. The calibration of the standard reference microphone was discussed in the Section 3.4. The effect of the diffractions and reflections on the center microphone is also analyzed in this section. Once the center microphone is calibrated, it was used as the reference microphone to simultaneously calibrate the three microphones of each array, separately. For the calibration of the array microphones in the anechoic chamber, it was assumed that if all the microphones are placed in the same plane and are subject to a plane wave, then all the microphones will have the same pressure amplitude, and their corresponding phase difference would be zero. In the anechoic chamber, a point source radiates spherical waves. If the distance of the probe is far enough from the source, then the microphones of probe would experience a plane wave. This plane wave justification in the anechoic chamber is discussed in the following section.

4.1.1 Plane wave justification in the anechoic chamber

If the center of the probe and the center of the sound source are both in the same axis, and the distance from the center microphone to any of the surrounding microphones is small, then the arc of the spherical wave between the center and a surrounding microphone can be considered close to a straight line. This straight line approximation is illustrated in the following schematic:

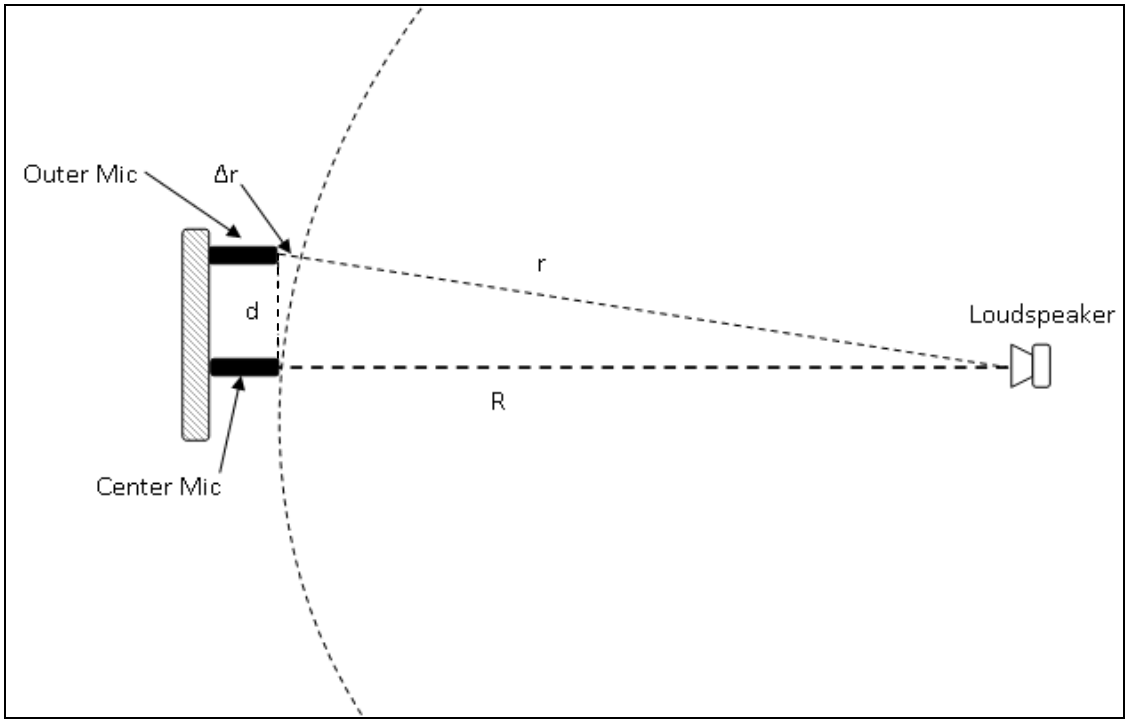

Figure 4.2: A schematic of the plane wave justification of the spherical progressive wave.

In the above schematic, r is the distance from the loudspeaker to the outer array microphone, R is the distance from the loudspeaker center to the center (origin) microphone, d is the effective distance (the distance between the center of the origin and one of the microphones in the array), and is perpendicular to the R. Δr is the distance from the center of the surrounding microphone to the crossing point between the arc and the hypotenuse. The r forms the hypotenuse of the right triangle formed by d, R, and r. So, for a given R and d, the r can be calculated as:

$$r = \sqrt{d^2 + R^2}\ , \tag{4.6}$$

$$\Delta r = \sqrt{d^2 + R^2} - R\,, \tag{4.7}$$

Now, using the Binomial expansion, Δr can be approximated as,

$$\Delta r \approx \frac{d^2}{2R}. \tag{4.8}$$

Now, knowing *R*, given *d*, the effect of the plane wave assumption on the amplitude deviation can be calculated:

$$E_{|P|} \approx \frac{1}{1+\frac{1}{2}\frac{d^2}{R^2}}, \tag{4.9}$$

$$\left(E_{|p|}\right)_{dB} = -20\log_{10}\left(1+\frac{d^2}{2R^2}\right), \tag{4.10}$$

Similarly, the phase deviation (in degree) due to the plane wave assumption can be calculated as:

$$E_{\angle P} = \frac{\Delta r}{\lambda} * 360\,, \tag{4.11}$$

where λ is the signal wavelength.

Now, for measurements in the anechoic chamber, the distance between the source and the center (origin) microphone, R = 2 m, and the distance between the center and the surrounding microphone, d = 70 mm for the outer (low-frequency) array, and 15 mm for the inner array (high-frequency), respectively. Based on these parameters, the amplitude deviation at the inner microphones is calculated (using equations 4.8, 4.9, and 4.10) to be 0.0002 dB, and for the outer array is 0.005 dB. Now the effect of the plane wave justification on the phase deviation at 1 kHz is 1.2 degrees at the outer array microphone, and at 6.5 kHz the phase deviation is 0.38 degree at the inner array microphone. The average of the maximum phase deviation is 0.79 degree. The equation 4.11 is used to calculate the phase deviations at the arrays. These deviations are small and were neglected for the subsequent measurements in this report. A discussion of near-field and far-field from the source in relation to the wavelength and distance from the source are discussed in the Appendix C.

4.1.2 The center (origin) microphone calibration

The center (origin) microphone was calibrated using the standard reference microphone in the anechoic chamber. In this measurement, a 1 kHz sine wave of 84 dB SPL was used as the excitation signal. First, the standard reference microphone was placed in the anechoic chamber without the intensity probe. The sound pressure level in dB was recorded using a sound level meter. Then the intensity probe was placed inside the anechoic chamber. The center microphone was placed exactly at the same position as the standard reference microphone. The measured SPL of the center microphone was then adjusted to the SPL of the standard reference microphone. Then the frequency response of the center microphone was calculated for the frequency range of 200 Hz to

7.0 kHz. Before the center microphone frequency response measurements, the frequency response of the two different sizes (3 inch and 6 inch) loudspeakers was calculated as a precaution, and to check any diffractions effects of the loudspeaker housing on the measurements. The frequency response of the two loudspeakers is plotted in Figure 4.3 and 4.4.

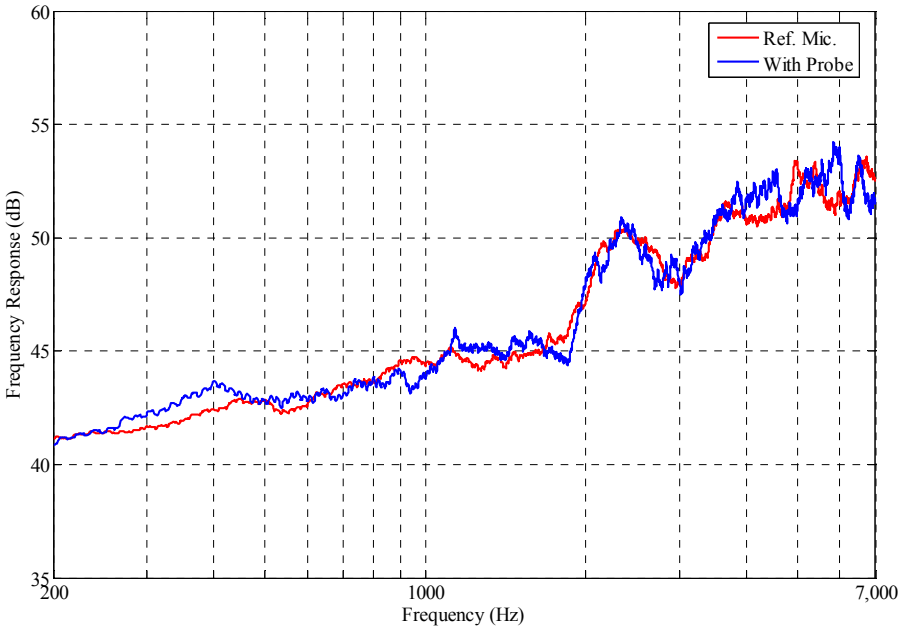

Figure 4.3: The comparison of the **3 inch** loudspeaker frequency response using the standard reference microphone (**red**) and the center microphone (**blue**).

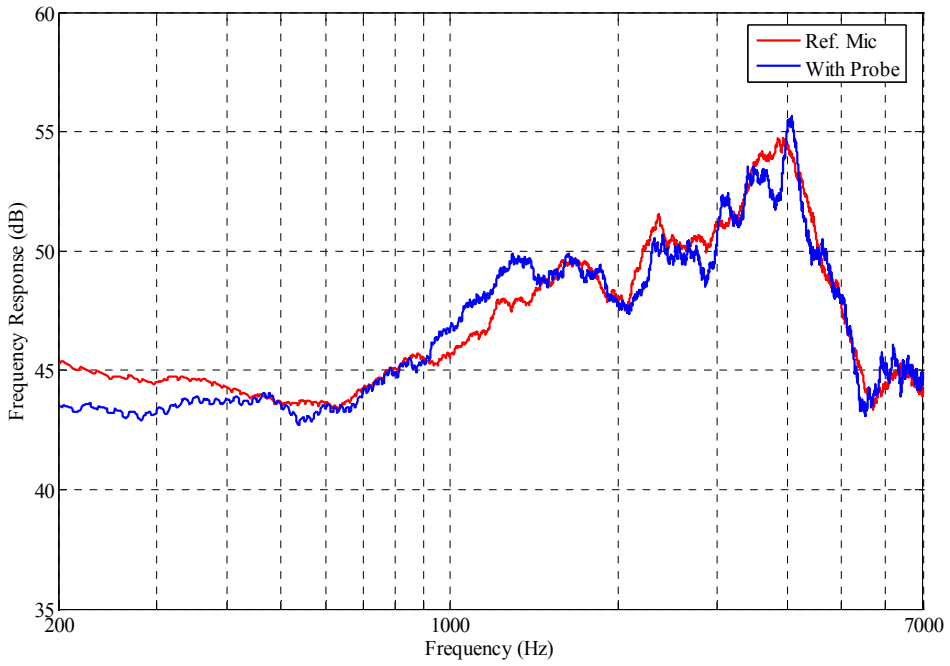

Figure 4.4: The comparison of the **6 inch** loudspeaker frequency response using the standard reference microphone (**red**) and the center microphone (**blue**).

The diffraction and reflection effects on the loudspeaker frequency response is overall random, but in some frequency regions the deviations were about 1 dB. It is to be noted that both the small and the large loudspeakers were covered with sound absorbing materials (Fiber Glass) to minimize any potential effect due to diffractions off the speaker housing.

The frequency response of the center (origin) microphone using both the 3 inch and the 6 inch loudspeaker was measured. Then the overall frequency response was calculated by combining the responses from the two loudspeakers. The frequency response for these two cases is shown Figure 4.5 and 4.6.

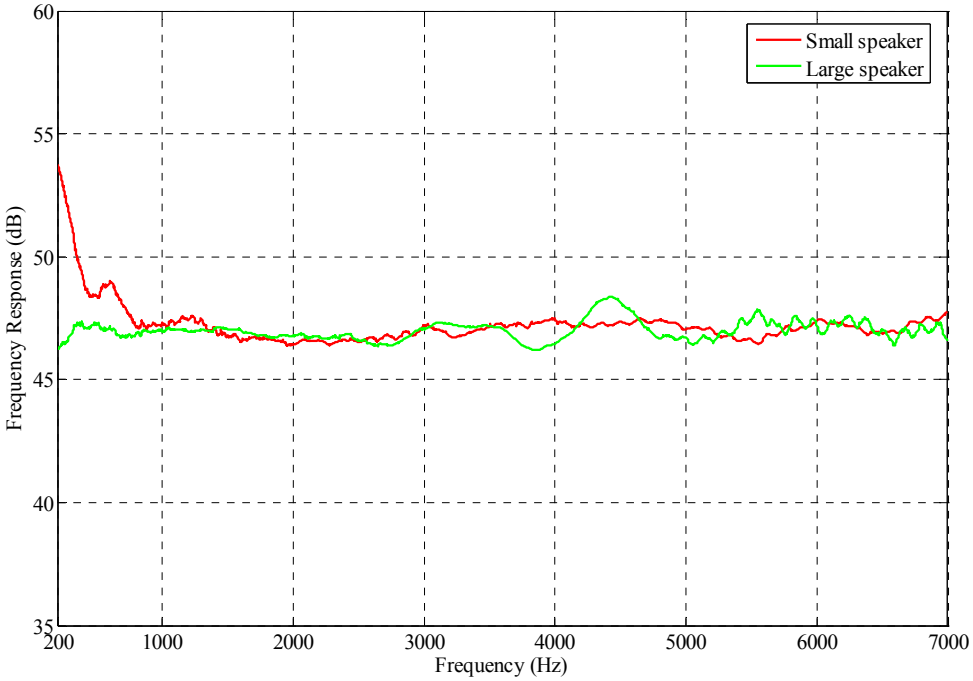

Figure 4.5: Frequency response of the **center (origin)** microphone for both the small (**red**) and the large (**green**) loudspeaker for the frequency range of 200 Hz to 7.0 kHz.

The response using the small speaker was about 5 dB (maximum) off from the mean at frequencies below 800 Hz. The response using the large speaker was about +/- 1.0 dB from the mean for high frequencies (above around 3 kHz). This observation verifies the known fact that the small size loudspeaker fairs well in generating high frequency sound, while loudspeakers with large diameter works well in generating low frequency sounds.

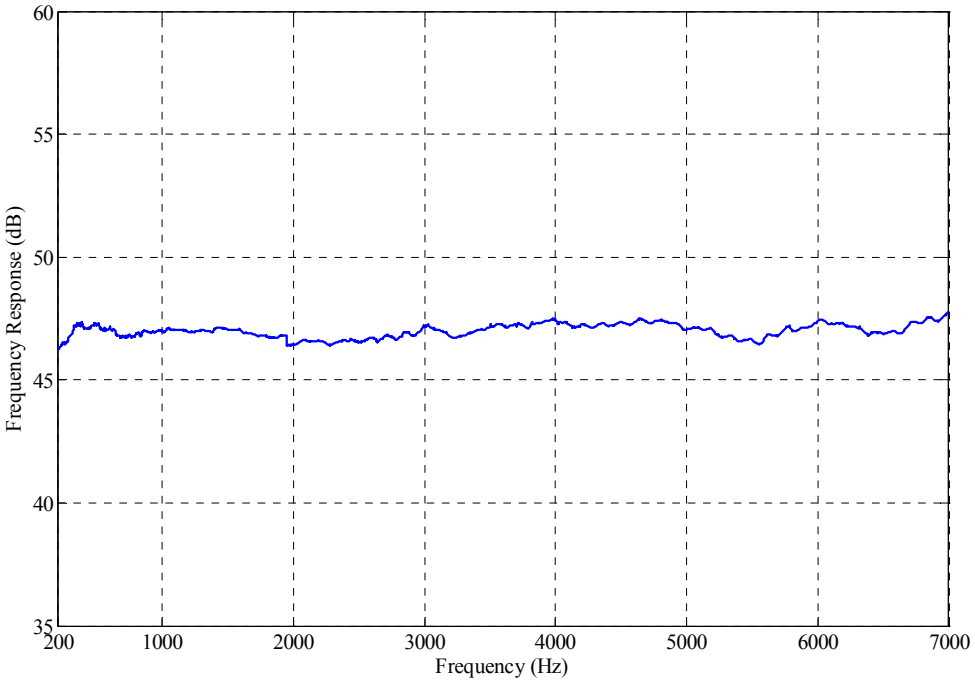

Figure 4.6 (a): The overall frequency response of the **center (origin)** microphone for the frequency range of 200 Hz to 7.0 kHz. The **linear scale** was used in the horizontal direction to even out the display of the response.

From the Figure 4.6(a), the frequency response of the center (origin) microphone (linear frequency scale) is nearly flat (+/- 0.5 dB) for the frequency range of 200 Hz to 7.0 kHz. This frequency response is used to compare any diffractions and reflections effects of the probe microphones, and the supporting structures.

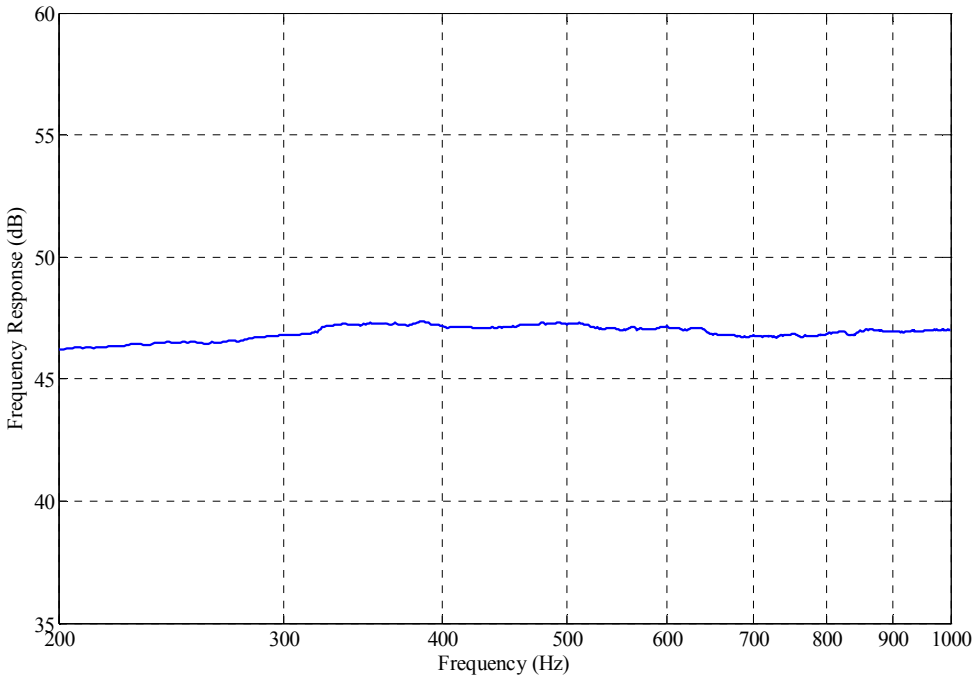

Figure 4.6 (b): The low frequency response of the **center (origin)** microphone. The **log scale** was used in the horizontal axis to clearly show the response at the low frequency range (200 Hz – 1.0 kHz).

To understand and quantify diffraction and reflection effects on the center (origin) microphone due to the presence of the standard reference microphone and the probe structure, the probe was placed in the three different positions around the standard reference microphone in the anechoic chamber. First, the low-frequency array microphone of the probe was placed in the same plane as the standard reference microphone along the perimeter of the array (Figure 4.7). In this setup, the microphones were facing directly the sound source where the probe structure can cause reflections. Second, the probe position was reversed and was facing the standard reference microphone (Figure 4.9) where the probe structure can cause diffractions. Third, the probe origin microphone was placed in the same plane as the standard reference microphone but was facing perpendicular to the reference microphone axis (Figure 4.11). The frequency response of the center (origin) microphone for these three positions around the standard reference microphone are plotted and compared with the response of the center microphone calculated using only the reference microphone in the Figures 4.8, 4.10, and 4.12.

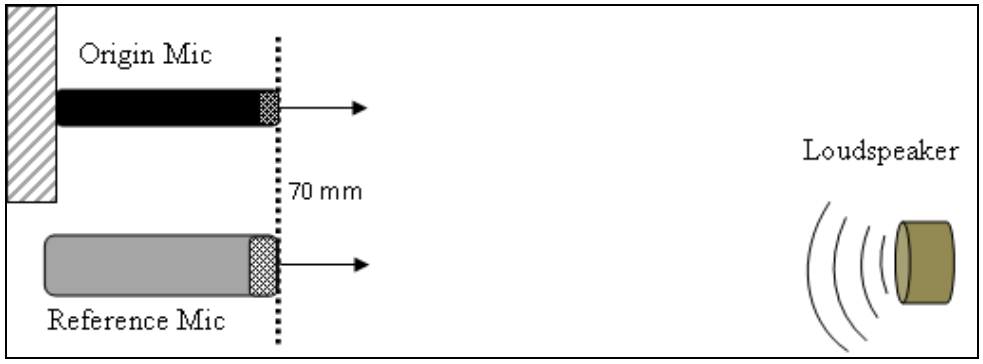

Figure 4.7: The probe is placed in the same plane as the standard reference microphone, and facing directly to the loudspeaker.

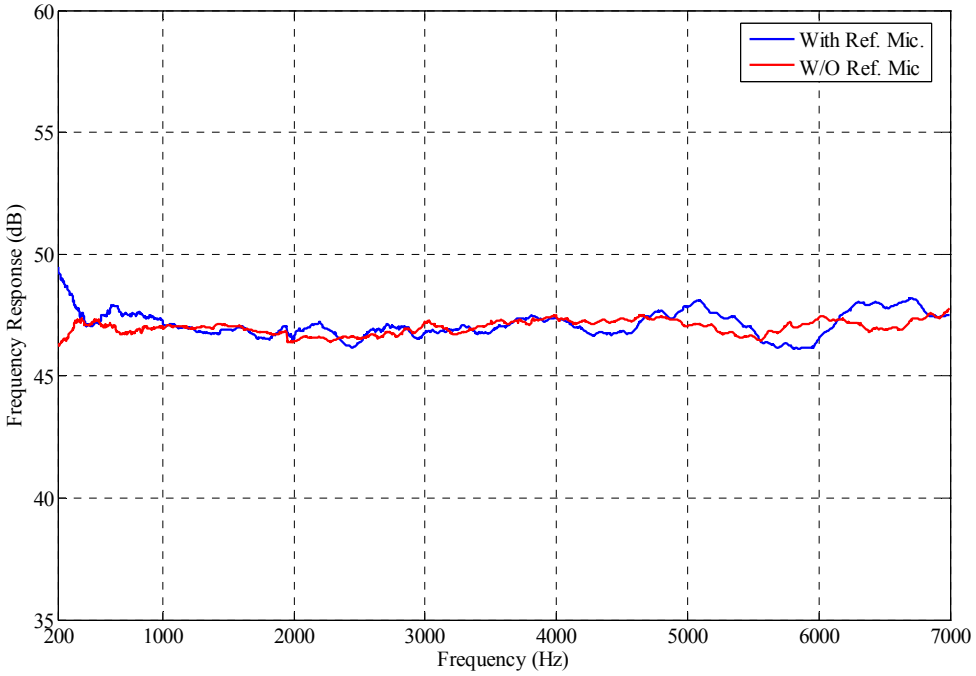

Figure 4.8: Frequency response of the center (origin) microphone (The probe is placed in the same plane as the standard reference microphone, and facing directly to the loudspeaker).

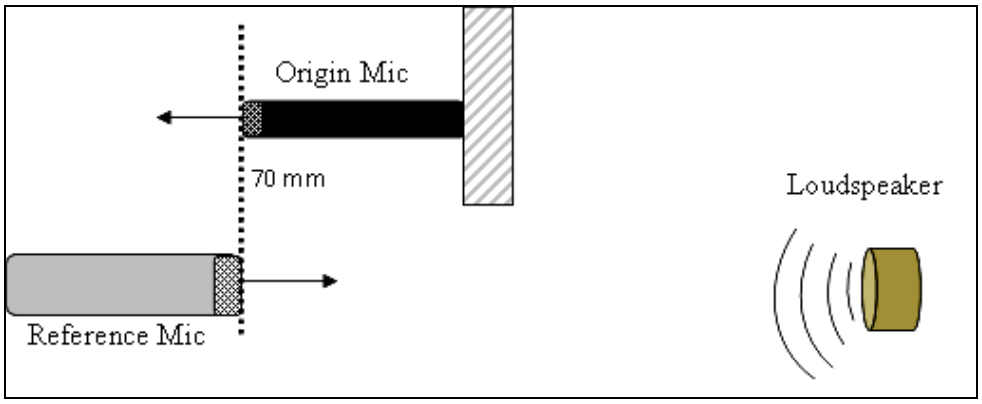

Figure 4.9: The probe is placed in the same plane as the standard reference microphone, but facing directly opposite to the loudspeaker.

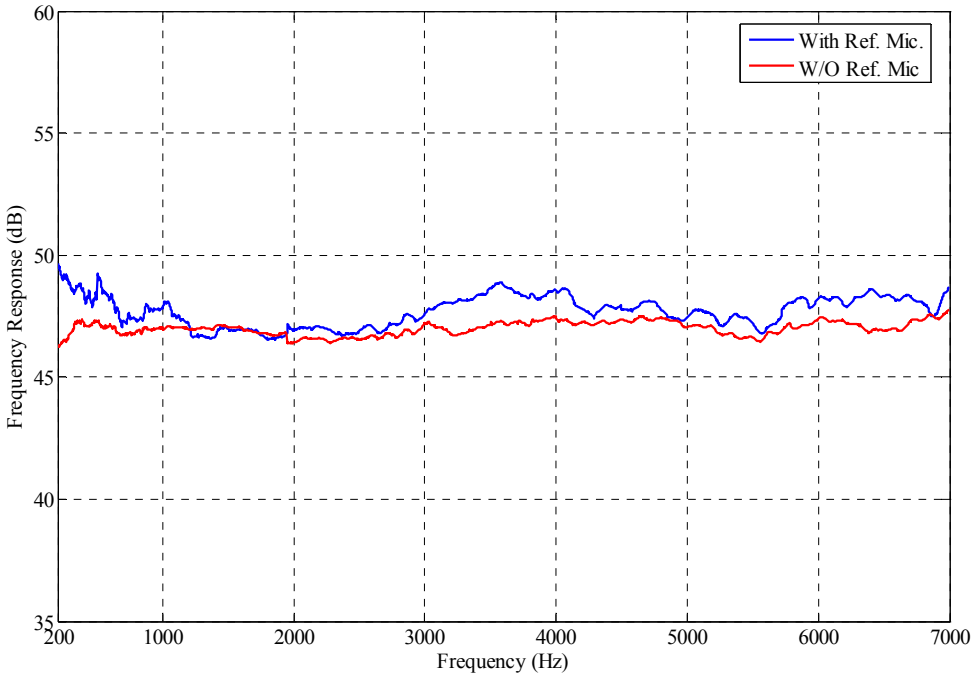

Figure 4.10: Frequency response of the center (origin) microphone (The probe is placed in the same plane as the standard reference microphone, but facing directly opposite to the loudspeaker).

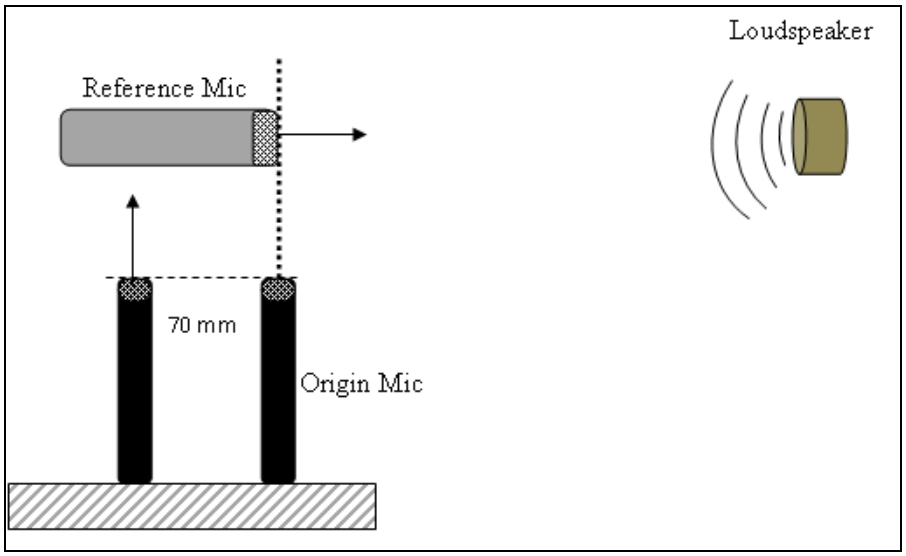

Figure 4.11: The probe is placed in the same plane as the standard reference microphone, but facing perpendicular to standard reference microphone axis.

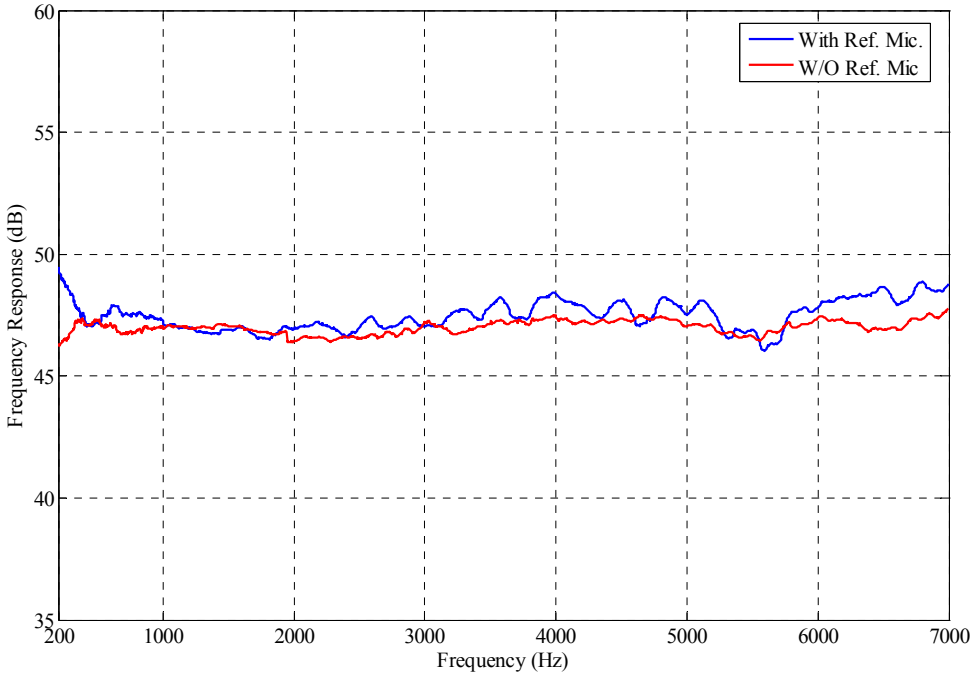

Figure 4.12: Frequency response of the center (origin) microphone (The standard reference microphone is placed in the same plane as the outer array microphone but facing perpendicular to the microphone axis).

The frequency response plots of the center (origin) microphone in Figure 4.8, 4.10, and 4.12 shows the diffraction and reflection effects due to the presence of the probe structure. The overall pattern of the deviation from the response without the probe is somewhat random, but varied +/- 0.5 dB over the frequency band. The presence of the standard reference microphone at different locations in relation to the probe did not make any coherent impact on the center (origin) microphone frequency response.

A single tone (1 kHz) sine wave of 84 Db SPL was used to quantify the effects of the probe presence on the standard reference microphone SPL. The 1 kHz tone (sine wave) was later used to calculate the intensity and energy density for comparison with their corresponding ideal values. Deviation in SPL measurements for the three probe positions around the reference microphone is listed in the following table:

Table 4.1: A list of SPL deviations due to the presence of the probe in different positions in relation to the standard reference microphone.

Probe Location	Measured SPL (dB)	Deviation (dB)
Next to Ref. Mic.	84.12	**0.12**
Opposite to Ref. Mic.	84.31	**0.31**
Side of the Ref. Mic.	84.14	**0.14**

From the above table, the average deviation in SPL measurements from the reference microphone due to the presence of the probe is 0.19 dB. This value is lower than +/- 0.5 dB deviation over the desired frequency band (200 Hz – 6.5 kHz) shown in the previous plots (Figure 4.8, 4.10 and 4.12).

4.1.3 The surrounding microphones calibration

The already calibrated center (origin) microphone is now used in calibrating the other microphones of the probe. All (three) microphones of the inner (or outer) array were placed in the same plane as the center microphone. In this configuration, each microphone of the array should experience the same sound pressure amplitude, and have zero phase difference between the microphones considering the microphones plane is perpendicular to the incoming plane wave direction. Thus, the three microphones of the probe can be calibrated simultaneously using the origin microphone. The other array of the probe was then calibrated similarly. This calibration method uses the plane wave justification made in the Subsection 4.1.1.

As for measurements, 1 kHz sine wave of 84 dB SPL measured by the center (origin) microphone was used as the sound source. Then, the measured SPL from the three microphones (inner array or outer array) were adjusted to the center microphone SPL. Then a broadband random noise was used to calibrate the frequency response of the surrounding microphones of each of the two arrays. The magnitude and phase response of the center microphone was used as the reference values to calibrate the other microphone of the probe. Thus, each microphone of the probe was calibrated using the already calibrated center (origin) microphone. In the calibration procedure, even though the SPL for each microphone were adjusted with the SPL of the center microphone using a 1.0 kHz sine wave, the sensitivity plots over the frequency range of each array shows a very small deviation in SPL at 1.0 kHz among the microphone dues to random diffraction and reflections effects off the microphones and the supporting structure. Sensitivity and phase offsets of the microphones before and after calibration for both the outer (low-frequency) array and the inner (high-frequency) are plotted in the following figures.

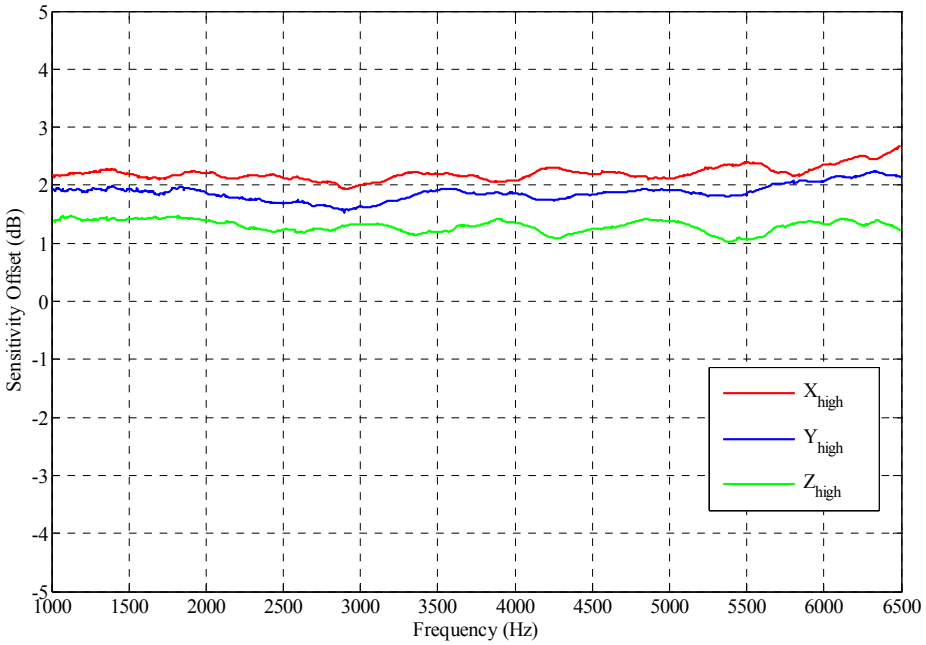

Figure 4.13: Sensitivity offset plots of the inner (**high-frequency**) array microphones (**before calibration)**.

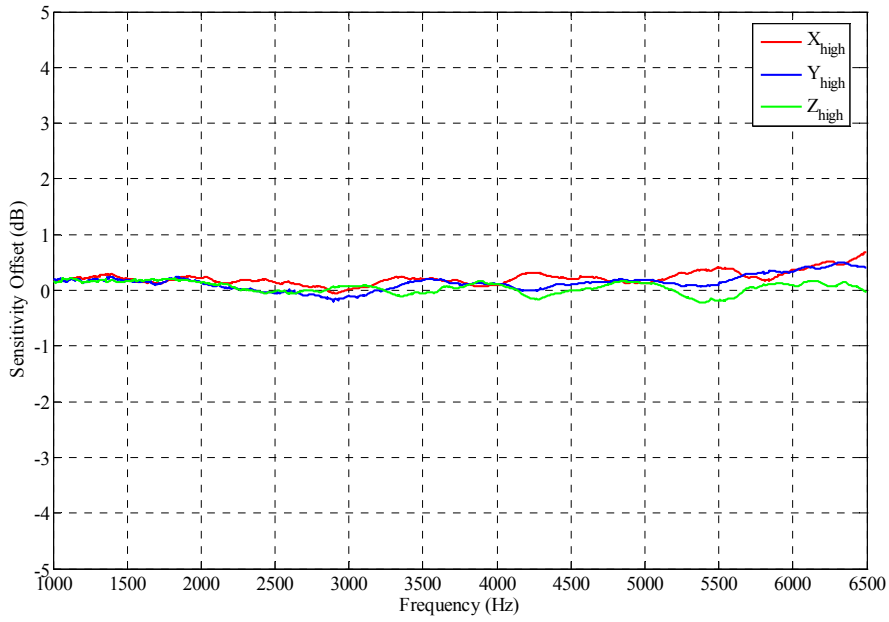

Figure 4.14: Sensitivity offset plots of the inner (**high-frequency**) array microphones (**after calibration)**.

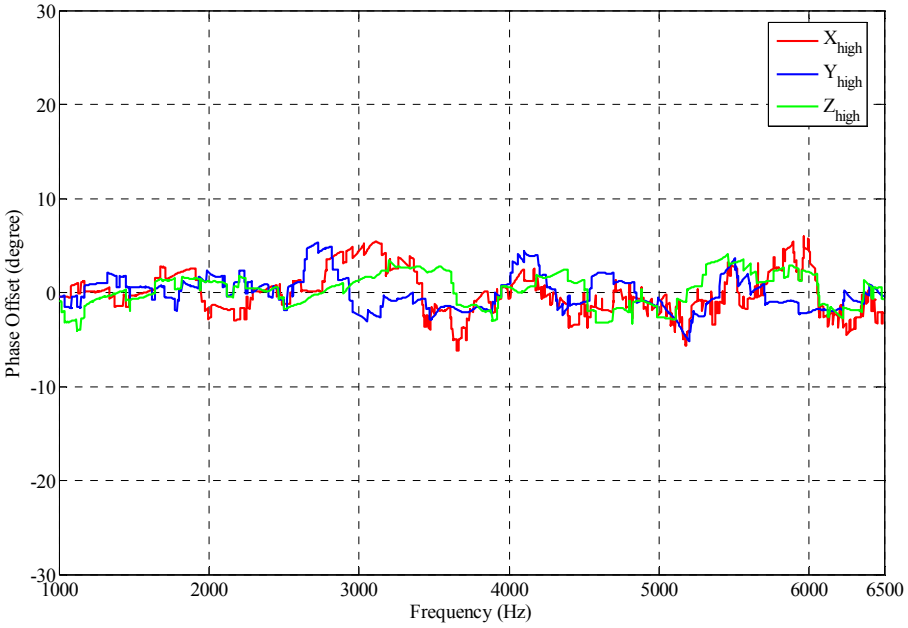

Figure 4.15: Phase offset plots of the inner (**high-frequency**) array microphones (**before calibration)**.

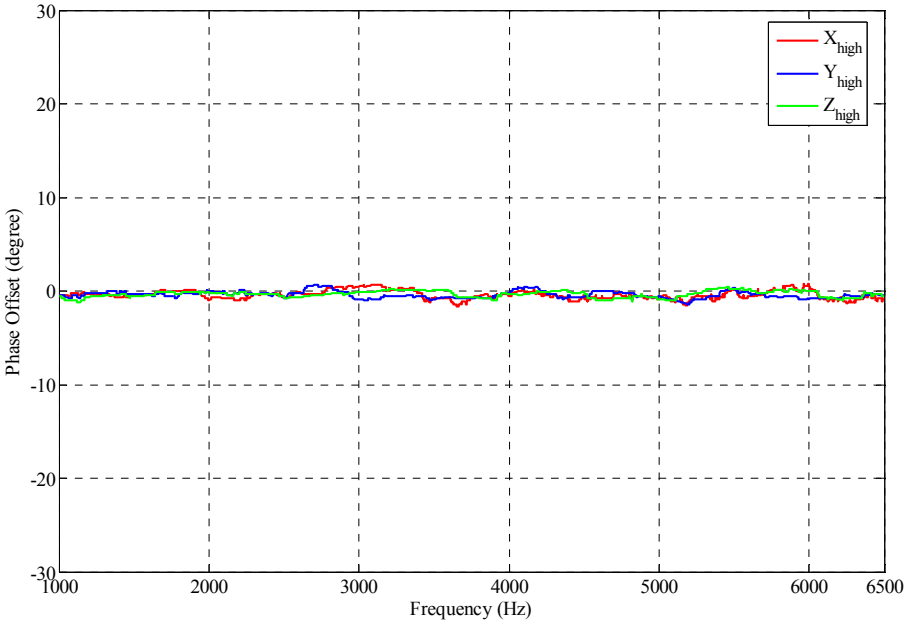

Figure 4.16: Phase offset plots of the inner (**high-frequency**) array microphones (**after calibration)**.

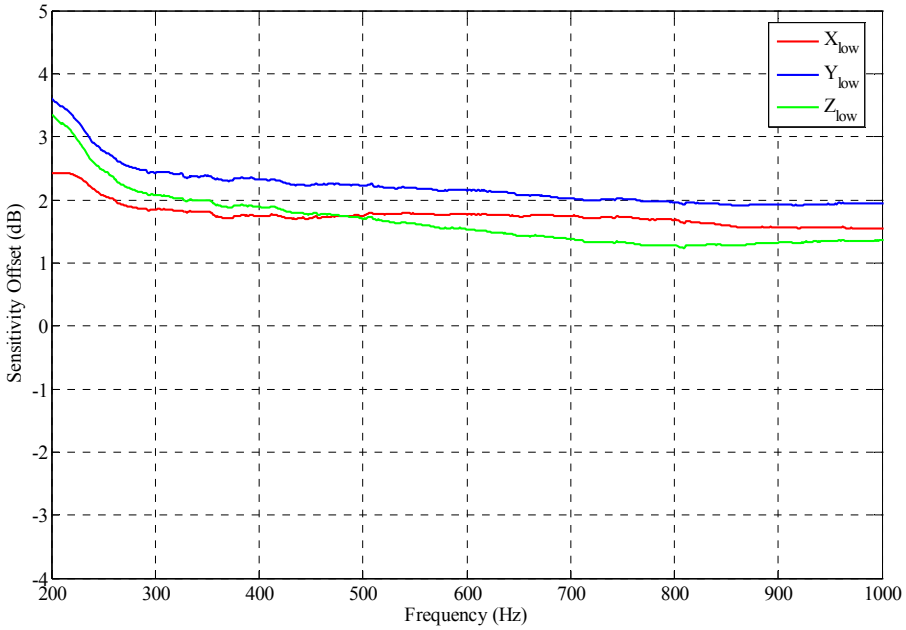

Figure 4.17: Sensitivity offset plots of the outer (**low-frequency**) array microphones (**before calibration)**.

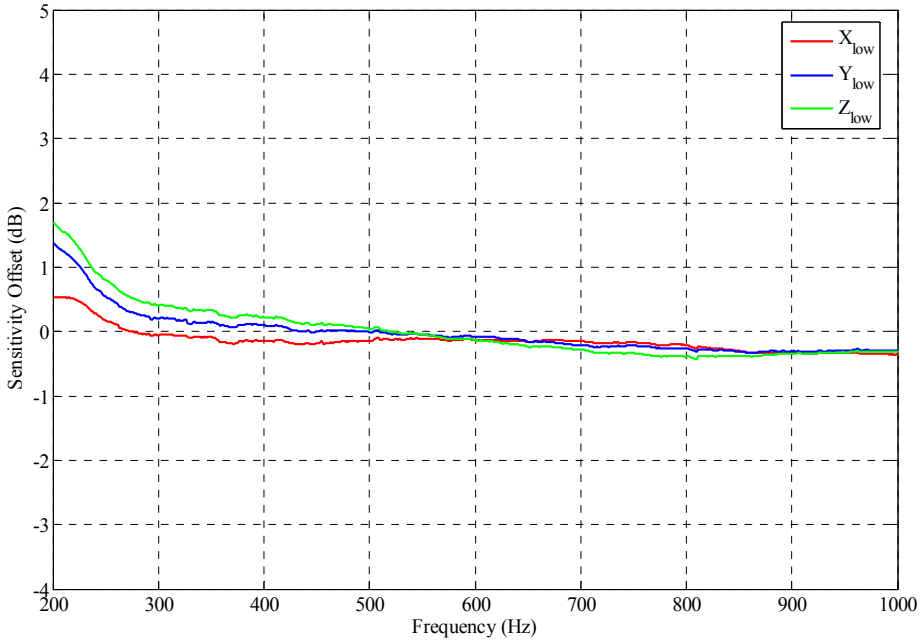

Figure 4.18: Sensitivity offset plots of the outer (**low-frequency**) array microphones (**after calibration)**.

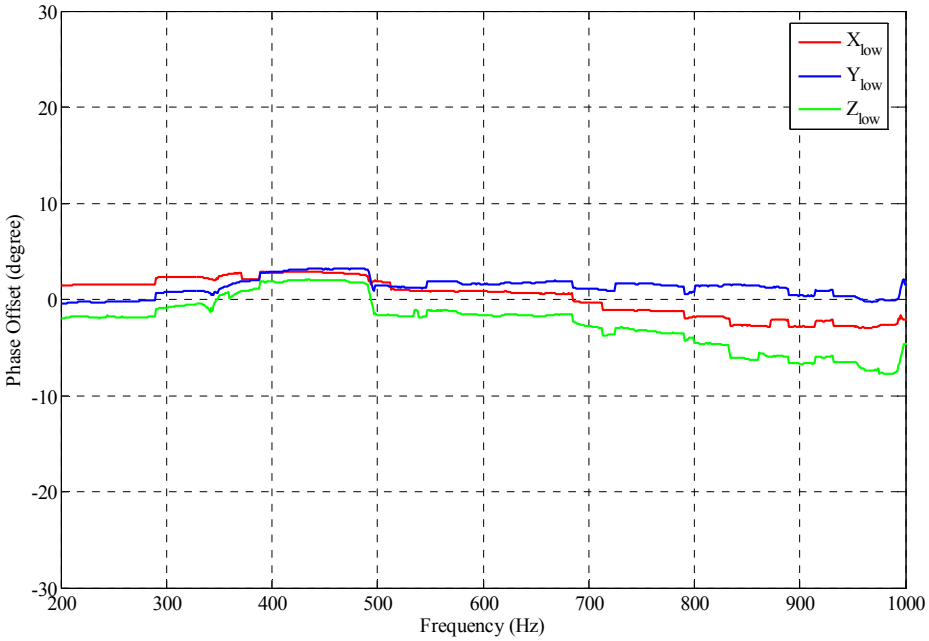

Figure 4.19: Phase offset plots of the outer (**low-frequency**) array microphones (**before calibration)**.

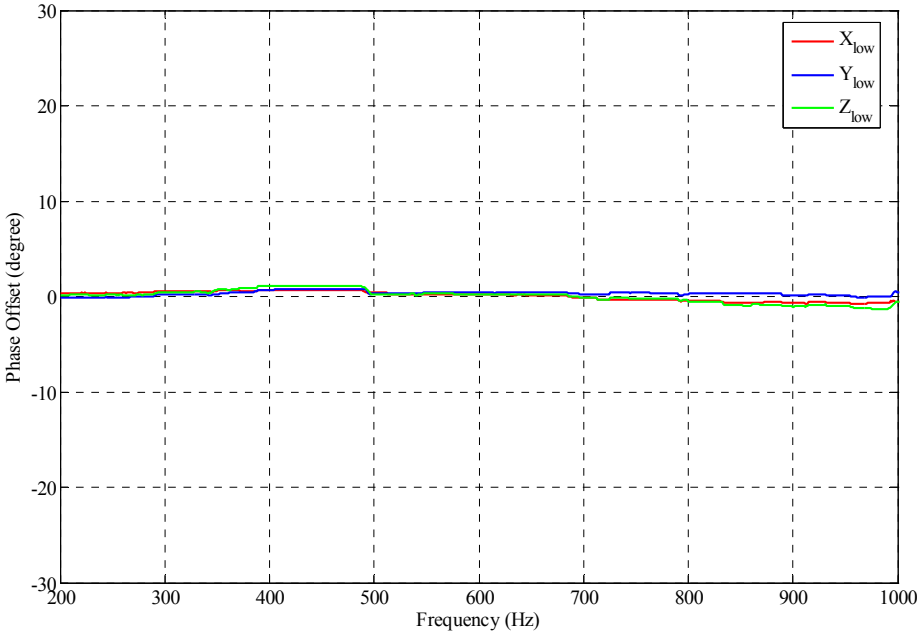

Figure 4.20: Phase offset plots of the outer (**low-frequency**) array microphones (**after calibration)**.

From Figure 4.14, the calibrated microphones of the inner array has overall sensitivity offset of +/- 0.3 dB for the frequency range of 200 Hz to 6.5 kHz. From Figure 4.16, the overall phase offset for the same array is about +/- 0.6 degree. From Figure 4.18, the calibrated microphones of the outer (low-frequency) array has overall sensitivity offset of +/- 1.0 dB for the frequency range of 200 Hz to 6.5 kHz. From Figure 4.20, the overall phase offset for the same array is about +/- 1.1 degrees. For the low-frequency array, the useful frequency range is from 200 Hz to 1.0 kHz. For the high-frequency array, the useful frequency range is from 1.0 kHz to 6.5 kHz. So, the sensitivity and phase offsets outside their respective range were not considered for the measurements. The calibration has greatly improved both the sensitivity offset and phase offset for two arrays.

4.1.4 Comparisons of the average pressure to the origin pressure for the different probe orientations

In the measurement position, the microphones in the probe were adjusted to the measurement position as illustrated in Figure 3.7 and also referenced in Table 3.1. If the probe is placed in the anechoic chamber with its axis pointed toward the plane wave propagation direction, then the theoretical amplitude and phase offset measured from the surrounding microphones can be related to the center microphone using the following relationships. Two different probe scenarios were considered. First, the probe was facing directly the incoming plane wave (Figure 4.21). Second, the probe was rotated in 180 degrees in the horizontal direction, and was facing opposite to the incoming plane wave (Figure 4.22). The theoretical values were first calculated and then compared with the measured values (Table 4.2 and 4.3)

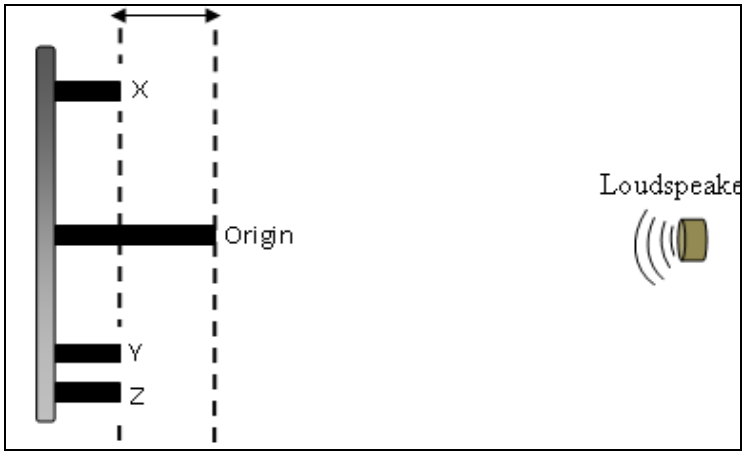

Figure 4.21: The probe is in the measurement position and facing directly the loudspeaker.

In this position (Figure 4.21), the average sound pressure of the three microphones will be smaller than the Origin microphone for being further from the source. The average pressure of the outer array will be smaller than the average pressure of the inner array. The average pressures of the both arrays will be smaller than the Origin microphone. This relationship can be formulated as:

$$\frac{\left(P_{xl}+P_{yl}+P_{zl}\right)}{3} < \frac{\left(P_{xh}+P_{yh}+P_{zh}\right)}{3} < P_{origin} \ , \tag{4.12}$$

where P_{xl}, P_{yl}, and P_{zl} are the pressure measured from the outer (low-frequency) array microphones; P_{xh}, P_{yh}, and P_{zh} are the pressure measured from the inner (high-frequency) array microphones; and P_{origin} is the measured center (origin) microphone pressure.

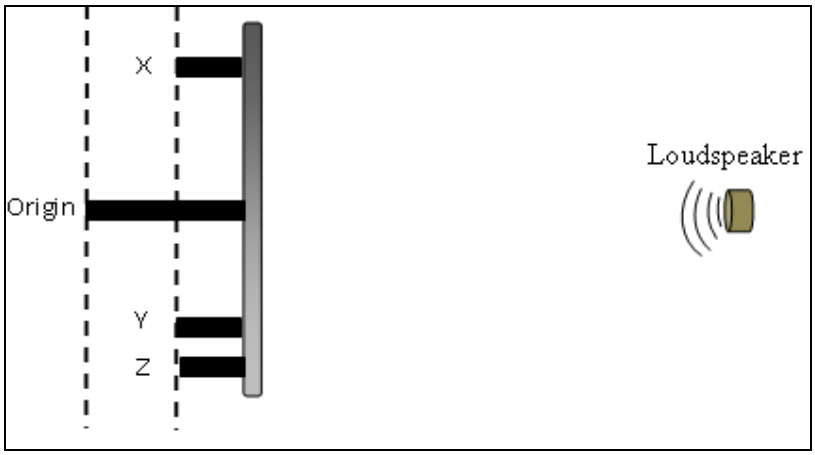

Figure 4.22: The probe is in the measurement position and facing opposite the loudspeaker.

Similarly for the reversed microphone position, the relationship can be written as

$$\frac{\left(P_{xl}+P_{yl}+P_{zl}\right)}{3} > \frac{\left(P_{xh}+P_{yh}+P_{zh}\right)}{3} > P_{origin}\,. \tag{4.13}$$

Table 4.2: The relationship of the Equation 4.12 and 4.13 are shown based on the measured values.

Front facing probe	SPL (dB)
Origin Microphone	**84.07**
Outer array average	**83.95**
Inner array average	**83.82**
Opposite facing probe	SPL (dB)
Origin Microphone	**83.38**
Outer array average	**83.36**
Inner array average	**83.27**

It can be seen in the above table that the relationship in the Equation (4.13) is violated. It is due to the diffractions effects of the microphones and the supporting structures.

Now, the phase differences due to the microphone horizontal spacing for the two cases (the probe facing directly and opposite of the sound source) is calculated and compared with the measured values in the following the Table. A 1000 Hz sine wave of 84 dB SPL was used for the measurements.

Table 4.3: Calculated and measured phase difference due to microphone horizontal spacing for the two cases.

Front facing probe	Calculated (deg)	Measured (deg)
Outer array average	40	**38.2**
Inner array average	11	**11.6**
Opposite facing probe		
Outer array average	-40	**-36.8**
Inner array average	-11	**-11.8**

The measured values for the physical phase differences matched well with their corresponding theoretical values. Also, the polarity changes are due to the shift of the probe direction. These above tables and the Equations 4.12 and 4.13 are discussed here to cement the validity of the anechoic chamber measurements.

4.2 SUMMARY OF THE CHAPTER

Inherent systematic errors due to the imperfections in the probe design and construction was discussed. Potential normalized errors in the pressure, particle velocity, and intensity measurement due to changes in distance between the microphones were calculated and plotted in Figure 4.1. These plots were used as a reference in the design process.

Microphone calibration techniques were then discussed. First the center microphone was calibrated using a standard reference microphone in the anechoic room. The justification of the plane wave in the anechoic chamber was established with formulas and calculations. Different aspects of diffractions and reflections effects on the center microphone were analyzed by changing the probe location around the standard microphone. The overall effect of the diffractions on the microphone calibration was less than 0.5 dB. Loudspeakers of two different sizes were used to measure frequency response of the center microphone. The calibrated center microphone was then used to calibrate microphones of each array of the probe. Sensitivity offset and phase offset both before and after calibration were plotted and compared for each microphone. The overall sensitivity offset was about 1.0 dB, and the phase offset was about 1.0 degree. These small offsets showed the effectiveness of the microphone calibration techniques used in the design of the probe.

Then the probe microphones were adjusted in the measurement positions and were subject to an incoming plane wave. The amplitude and phase relations among the microphones were calculated from the measured data, and compared to cement the plane wave assumption used for calibrations in the anechoic chamber.

Reference

[1] F. J. Fahy, "*Sound Intensity*," second edition, E & FN SPON, London, sec 6.2, pp. 98-114, 1995.

[2] G. Pavic, "Measurement of sound intensity," *J. Sound Vib.,* vol. 51, pp. 533-546, 1977.

[3] F. J. Fahy, "Measurements of acoustic intensity using the cross-spectral density of two microphone signals," *J. Acoust. Soc. Am.,* vol. 62, pp. 1057-1059, 1977.

[4] J. Y. Chung, "Cross-spectral method of measuring acoustic intensity without error caused by instrument phase mismatch," *J. Acoust. Soc. Am.,* vol. 64, pp. 1613-1616, 1978.

Chapter 5: Intensity and Energy Density Formulations

5.0 INTENSITY CALCULATIONS

Measuring acoustic intensity in the frequency-domain requires the knowledge of pressure amplitudes and their phase relations between the two microphones. Based on the Chung [2], Fahy [1], and Krishnappa [3], an expression for the acoustic intensity for a closely spaced microphone-pair in any given direction is given by,

$$I(f) = \frac{\mathrm{Im}(D_{xy})}{2\rho\Delta r\omega}, \tag{5.1}$$

where the angular frequency $\omega = 2\pi f$, f is the frequency. The cross-spectral density,

$$D_{xy} = P_x(f)P_y^*(y), \tag{5.2}$$

where $P_x(f)$ and $P_y(f)$ are the Fourier transforms of the two time-domain pressure signals sensed by the two microphones (the center microphone and one of the microphones along the axis of the coordinate system), ρ is the density of the medium, and Δr is the effective distance between the two sensing microphones. " * " in the above equation denotes the complex conjugate and can be shown that,

$$P_x(f)P_y^*(f) = \left[P_y(f)P_x^*(f)\right]^* \ . \tag{5.3}$$

Now, the equations for x, y, and z components of intensity for the inner and the outer array can be written as followings:

$$I_{lx}(f) = \frac{\mathrm{Im}\left(P_0(f)P_{lx}^*(f)\right)}{2\rho\Delta r_l \omega} \tag{5.4}$$

$$I_{ly}(f) = \frac{\mathrm{Im}\left(P_0(f)P_{ly}^*(f)\right)}{2\rho\Delta r_l \omega} \tag{5.5}$$

$$I_{lz}(f) = \frac{\mathrm{Im}\left(P_0(f)P_{lz}^*(f)\right)}{2\rho\Delta r_l \omega} \tag{5.6}$$

$$I_{hx}(f) = \frac{\mathrm{Im}\left(P_0(f)P_{hx}^*(f)\right)}{2\rho\Delta r_h \omega} \tag{5.7}$$

$$I_{hy}(f) = \frac{\mathrm{Im}\left(P_0(f)P_{hy}^*(f)\right)}{2\rho\Delta r_h \omega} \tag{5.8}$$

$$I_{hz}(f) = \frac{\mathrm{Im}\left(P_0(f)P_{hz}^*(f)\right)}{2\rho\Delta r_h \omega} \tag{5.9}$$

Where Δr_l and Δr_h are the effective microphone spacing between the two microphones in the outer array and the inner array, respectively. Now, the low-frequency and the high-frequency components of the intensity for each axis are combined to form the overall intensity components for frequencies from 200 Hz to 6.5 kHz. For the low-frequency components, the frequency range is 200 Hz to 1.0 kHz. For the high-frequency components, the frequency range is 1.0 kHz to 6.5 kHz.

The following expression summarized the overall intensity in the all three axes:

$$I_{x,y,z}(f) = \begin{cases} \dfrac{\mathrm{Im}\left(P_0(f)P^*_{lx,ly,lz}(f)\right)}{2\rho\Delta r_l \omega}, & \text{for } f = 200 \text{ Hz to } fl - df \\ \dfrac{\mathrm{Im}\left(P_0(f)P^*_{hx,hy,hz}(f)\right)}{2\rho\Delta r_h \omega}, & \text{for } f = fl + df \text{ to } 6500 \text{ Hz} \\ \dfrac{1}{2}\left(\dfrac{\mathrm{Im}\left(P_0(f)P^*_{lx,ly,lz}(f)\right)}{2\rho\Delta r_l \omega} + \dfrac{\mathrm{Im}\left(P_0(f)P^*_{hx,hy,hz}(f)\right)}{2\rho\Delta r_h \omega}\right), & \text{for } fl - df < f < fl + df \end{cases} \quad (5.10)$$

Where *fl* is the high end of the low-frequency range, while *df* is the length of a frequency band over which an averaging is done to smooth out the transition zone between the high-frequency and the low-frequency components of the intensity vectors.

In the above, cross-correlations between sound pressures of the two microphones (the center and along an axis) were used to calculate the sound intensity. Then the individual intensity vector components along the three axes were combined to form the total intensity. The total sound intensity at the probe center can be calculated from the surrounding microphone pressures using the Equation 5.10.

5.1 ENERGY DENSITY CALCULATIONS

Research in active noise control (ANC) systems led scientists to investigate the importance of different acoustic parameters in a representing sound field. Several research articles [4, 5, 6, 7, 8] have indicated that the total energy density measurements can be an effective tool for many ANC applications. Energy density is the measure of the total energy at a point in space. Acoustic energy density is the sum of the acoustic potential energy density and the acoustic kinetic energy density. It was concluded in Cook & Schade's article [9] that the total energy density estimates an enclosed sound field better than that of the potential energy density measurements alone.

In the past, the acoustic energy density estimation was done in the time-domain with the time-averaged pressure and the particle velocity measurements using a two-microphone sensor. An equivalent approach in the frequency-domain uses the weighted sum of auto-spectral densities of the pressure and the particle velocity. Like the intensity measurement, this approach is inherently one-dimensional in nature. Ben Cazzolato [11] and others derived an expression for the time-averaged energy density estimates for a two-microphone system using a purely frequency-domain expression [10, 11]. This frequency-domain expression suits well for the experiments and for the numerical calculations. Before discussing the frequency-domain expressions, analytical expressions for the instantaneous energy density in the time-domain are introduced.

5.1.1 Time-domain Energy density expressions

The instantaneous energy density at any given time in space is given by [12]

$$W_T(t) = \frac{p^2(t)}{2\rho c^2} + \frac{\rho |\mathbf{v}(t)|^2}{2}, \tag{5.11}$$

where ρ is the density, c is the sound speed of the medium, $|\mathbf{v}(t)|$ is the magnitude of particle velocity vector along the three axes, and $p(t)$ is the instantaneous sound pressure. An equivalent expression for the two-concentric array probe designed in this report can be written as,

$$W_T(t) = \frac{p^2(t)}{2\rho c^2} + \left(\sum_{nl=x_L, y_L, z_L} \frac{\rho v_{nl}^2(t)}{2} + \sum_{nh=x_H, y_H, z_H} \frac{\rho v_{nh}^2(t)}{2} \right), \tag{5.12}$$

where $v_{nl}(t)$ and $v_{nh}(t)$ are the magnitude of particle velocity component for the low-frequency and the high-frequency array, respectively.

The pressure is estimated using an average of the microphone pressures and can be written as,

$$p(t) \approx \frac{1}{m} \sum_{n=1}^{m} p_n(t), \tag{5.13}$$

where m is the number of microphones within the probe. The particle velocity components along the probe axes can be estimated using the finite-difference approximations of pressures between the two microphones as,

$$v_n(t) \approx \frac{1}{\rho \Delta r} \int_{-\infty}^{t} [p_0(\tau) - p_n(\tau)] d\tau, \tag{5.14}$$

where $p_0(\tau)$ is the pressure of the center microphone, $p_n(\tau)$ is the pressure of a microphone along an axis, and Δr is the effective distance between these two microphones. Now, substituting Equations 5.13 and 5.14 into the Equation 5.12 gives an

expression of the instantaneous acoustic energy density estimates in pressure for the seven-microphone probe designed in this report. The seven-microphone probe designed in this report consists of a two-concentric array with two different effective spacing (Δr_L and Δr_H) between the microphones.

$$W_T(t) \approx \frac{\left[\frac{1}{7}\left(p_0(t)+p_{x_L}(t)+p_{y_L}(t)+p_{z_L}(t)+p_{x_H}(t)+p_{y_H}(t)+p_{z_H}(t)\right)\right]^2}{2\rho c^2} + \sum_{nl=x_L,y_L,z_L} \frac{\rho}{2}\left[\frac{1}{\rho\Delta r_L}\int_{-\infty}^{t}\left[p_0(\tau)-p_{nl}(\tau)\right]d\tau\right]^2 + \sum_{nh=x_H,y_H,z_H} \frac{\rho}{2}\left[\frac{1}{\rho\Delta r_H}\int_{-\infty}^{t}\left[p_0(\tau)-p_{nh}(\tau)\right]d\tau\right]^2 \tag{5.15}$$

where p_0, p_{nl}, and p_{nh} are the center, outer-array and inner-array microphone pressure, respectively. This equation is used later in Chapter 6 to calculate the total energy density.

5.1.2 Frequency-domain expressions

Frequency-domain expressions for the total energy density are useful in applications where spectral content is an integral part of the measurements. Frequency-domain expressions for the potential energy density and the kinetic energy density estimates were investigated by Elko [13], and later were corrected by Ghan *et. al*. [10]. In this subsection, expressions developed by Elko [13] and Cazzolato [11] are extended for this particular (seven-microphone two-concentric array) probe configuration. Using the Parseval's theorem [14], the double-sided time-averaged acoustic energy density spectral density is given as,

$$\hat{W}_{total}(\omega) = \lim_{T\to\infty} \frac{1}{T} \cdot E\left\{ \frac{1}{2\rho c^2} \left|P(\omega,T)\right|^2 + \frac{\rho}{2} \left|V\ (\omega,T)\right|^2 \right\}, \tag{5.16}$$

where $P(\omega,T)$ and $V(\omega,T)$ are the Fourier transforms of the acoustic pressure and the particle velocity between the two microphones, respectively. Subscripts on V in the subsequent equations indicate components of the particle velocity along the three axes. In the frequency-domain,

$$P(\omega,T) \approx \frac{1}{2}\left[P_0(\omega,T) + P_n(\omega,T)\right] \text{ and} \tag{5.17}$$

$$V(\omega,T) \approx \frac{1}{\rho\Delta r} \cdot \left[\frac{P_0(\omega,T) - P_n(\omega,T)}{j\omega} \right]. \tag{5.18}$$

Now, the Equation 5.16 can be rewritten as,

$$\hat{W}_{total}(\omega) \approx \lim_{T\to\infty} \frac{1}{T} \cdot E\left\{ \begin{array}{l} \frac{1}{2\rho c^2} \cdot \left[\frac{P_0(\omega,T) + P_n(\omega,T)}{2} \right] \times \left[\frac{P_0(\omega,T) + P_n(\omega,T)}{2} \right]^* + \\ \frac{1}{2\rho\Delta r^2} \cdot \left[\frac{P_0(\omega,T) - P_n(\omega,T)}{j\omega} \right] \times \cdot \left[\frac{P_0(\omega,T) - P_n(\omega,T)}{j\omega} \right]^* \end{array} \right\}. \tag{5.19}$$

$$\hat{W}_{total}(\omega) \approx \left(\frac{1}{8\rho c^2} + \frac{1}{2\rho \Delta r^2}\right)\left(R_{P_0P_0}(\omega) + R_{P_nP_n}(\omega)\right) + \left(\frac{1}{8\rho c^2} - \frac{1}{2\rho \Delta r^2}\right)\left(R_{P_0P_n}(\omega) + R_{P_nP_0}(\omega)\right) \quad . \tag{5.20}$$

In the above equation, $R_{P_XP_X}(\omega)$ is the double-sided auto-spectral density of P_x, and is written as,

$$R_{P_XP_X}(\omega) = \lim_{T\to\infty} \frac{1}{T} \cdot E\left[P_x(\omega,T)P_x(\omega,T)^*\right], \tag{5.21}$$

where E is the expected value over a finite number of samples.

5.2 ENERGY DENSITY EQUATIONS FOR THE SEVEN-MICROPHONE PROBE

In terms of components of the particle velocity in the three axes (x, y, and z), the frequency-domain energy density can be written as,

$$\hat{W}_{total}(\omega) = \lim_{T\to\infty} \frac{1}{T} \cdot E\left\{\begin{array}{l} \frac{1}{2\rho c^2}\left|P(\omega,T)\right|^2 + \frac{\rho}{2}\left|V_x(\omega,T)\right|^2 \\ + \frac{\rho}{2}\left|V_y(\omega,T)\right|^2 + \frac{\rho}{2}\left|V_z(\omega,T)\right|^2 \end{array}\right\}, \tag{5.22}$$

where

$$P(\omega,T) \approx \frac{1}{7} \cdot \left[\begin{array}{l} P_0(\omega,T) + P_{x_L}(\omega,T) + P_{y_L}(\omega,T) + P_{z_L}(\omega,T) \\ + P_{x_H}(\omega,T) + P_{y_H}(\omega,T) + P_{z_H}(\omega,T) \end{array}\right], \tag{5.23}$$

$$\left|V_x(\omega,T)\right| \approx \frac{1}{\rho\Delta r_L}\cdot\left[\frac{P_0(\omega,T)-P_{x_L}(\omega,T)}{j\omega}\right]+\frac{1}{\rho\Delta r_H}\cdot\left[\frac{P_0(\omega,T)-P_{x_H}(\omega,T)}{j\omega}\right], \quad (5.24)$$

$$\left|V_y(\omega,T)\right| \approx \frac{1}{\rho\Delta r_L}\cdot\left[\frac{P_0(\omega,T)-P_{y_L}(\omega,T)}{j\omega}\right]+\frac{1}{\rho\Delta r_H}\cdot\left[\frac{P_0(\omega,T)-P_{y_H}(\omega,T)}{j\omega}\right], \quad (5.25)$$

$$\left|V_z(\omega,T)\right| \approx \frac{1}{\rho\Delta r_L}\cdot\left[\frac{P_0(\omega,T)-P_{z_L}(\omega,T)}{j\omega}\right]+\frac{1}{\rho\Delta r_H}\cdot\left[\frac{P_0(\omega,T)-P_{z_H}(\omega,T)}{j\omega}\right]. \quad (5.26)$$

Now, substituting the Equations 5.23, 5.24, 5.25, and 5.26 into the Equation 5.22, and reducing cross-correlations terms between any two axis, an expression for the double-sided time-averaged acoustic energy spectral density estimates can be written as,

$$\begin{aligned}\hat{W}_{total}(\omega) \approx & \left(\frac{1}{98\rho c^2}-\frac{3}{\rho^2\omega^2\Delta r_L^2}-\frac{3}{\rho^2\omega^2\Delta r_H^2}-\frac{6}{\rho^2\omega^2\Delta r_L\Delta r_H}\right)\cdot R_{00}(\omega)+ \\ & \left(\frac{1}{98\rho c^2}-\frac{1}{\rho^2\omega^2\Delta r_L^2}-\frac{1}{\rho^2\omega^2\Delta r_L\Delta r_H}\right)\cdot\left[R_{0x_L}(\omega)+R_{0y_L}(\omega)+R_{0z_L}(\omega)\right]+ \\ & \left(\frac{1}{98\rho c^2}-\frac{1}{\rho^2\omega^2\Delta r_H^2}-\frac{1}{\rho^2\omega^2\Delta r_L\Delta r_H}\right)\cdot\left[R_{0x_H}(\omega)+R_{0y_H}(\omega)+R_{0z_H}(\omega)\right].\end{aligned} \quad (5.27)$$

This derived frequency-domain formula for calculating the total energy density can be used in applications where spectral analysis of different acoustical parameters is necessary for the measurements. However, an application of this equation is the subject of the future work.

References

[1] F. J. Fahy, "Measurements of acoustic intensity using the cross-spectral density of two microphone signals," *J. Acoust. Soc. Am.,* vol. 62, pp. 1057-1059, 1977.

[2] J. Y. Chung, "Cross-spectral method of measuring acoustic intensity without error caused by instrument phase mismatch," *J. Acoust. Soc. Am.,* vol. 64, pp. 1613-1616, 1978.

[3] G. Krishnappa, "Cross-spectral method of measuring acoustic intensity by correcting phase and gain mismatch errors by microphone calibration," *J. Acoust. Soc. Am.*, vol. 69, pp. 307-310, 1981.

[4] S. D. Sommerfeldt and P. J. Nashif, "A comparison of control strategies for minimising the sound field in enclosures," *Proceedings of Noise-Con.,* vol. 91, pp. 299-306, 1991.

[5] P. J. Nashif and S. D. Sommerfeldt, "An active control strategies for minimising the energy densities in enclosures," *Proceedings of Inter Noise*, vol. 92, pp. 357-361, 1992.

[6] S. D. Sommerfeldt and J. W. Perkins, "Active control of energy density in three dimensional enclosures," *J. Acoustic. Soc. Am.,* vol. 95, pp. 2989, 1994.

[7] W. Shen and J. Q. Sun, "A study of shell interior noise control," *SPIE*, vol. 3041, pp. 812-818, 1997.

[8] Y. C. Park and S. D. Sommerfeldt, "Global attenuation of broadband noise fields using energy density controls," *J. Acoust. Soc. Am.,* vol. 101, pp. 350-359, 1997.

[9] R. K. Cook and P. A. Schade, "New method for the measurement of the total energy density of sound waves," *Proceedings of Inter-Noise*, vol. 74, pp. 101-106, 1974.

[10] J. Ghan, B. S. Cazzolato and S. D. Snyder, "Expression for the estimation of time-averaged acoustic energy density using the two-microphone method (L)," *J. Acoust. Soc. Am.,* vol. 113, pp. 2404-2407, 2003.

[11] B. S. Cazzolato and J. Ghan, "Frequency domain expressions for the estimation of time-averaged acoustic energy density," *J. Acoust. Soc. Am.,* vol. 117, pp. 3750-3756, 2005.

[12] F. J. Fahy, "*Sound Intensity*," second edition, E & FN SPON (Chapman & Hall), London, 1995.

[13] G. W. Elko, "*Frequency domain estimation of the complex acoustic intensity and acoustic energy density*," Ph.D. thesis, The Pennsylvania State University, 1984.

[14] E. C. Ifeachor and B. W. Jervis, "*Digital Signal Processing – A Practical Approach,*" ADDISON-WESLEY, Wokingham, England, pp. 62, 1995.

Chapter 6: Probe Evaluation and Analysis

6.0 CHAPTER OUTLINE

The center (origin) microphone was first calibrated using a standard reference microphone. Then the calibrated center microphone was used to calibrate the other microphones of the probe. The calibration process was discussed in Chapter 4 of this report.

In this Chapter, the particle velocity vectors were calculated using the pressure difference between the microphones and were compared with the ideal value (Table 6.1). The ideal value was determined using Equation 6.1, and the calculated value was determined using Equation 5.14. The intensity components using Equations 6.2 and 6.3 were also calculated and compared (Table 6.2). Then the total energy density components were also calculated using Equations 6.4 and 5.15, and were also compared with each other (Table 6.3). Ideal and calculated acoustic impedance from the anechoic room measurements was also calculated and compared (Table 6.4). For all these measurements, the intensity probe was positioned in the measurement position and the probe axis (the support of the origin microphone) was aligned to the center of the sound source (loudspeaker). Now, the effectiveness of the seven-microphone probe in measuring the sound intensity of a broadband (200 Hz – 6.5 kHz) sound field is quantified, by calculating the intensity at each array of the probe (using equation 5.10), and then compared it with the overall probe. The sound intensity calculated from the center (origin) microphone was used as the reference intensity.

To verify the omnidirectional characteristic of the intensity probe, directivity patterns of the probe intensity measurements for different single tone sine waves were plotted in X-Y, X-Z, and Y-Z plane (Figure 6.4, 6.5, and 6.6). Then the directivity patterns of intensity along different planes were compared with each other (Figure 6.7, 6.8, and 6.9). A small loudspeaker with 2.0 kHz sine wave was used to estimate the source direction (azimuth and elevations angles) in reference to the probe. Deviations in source direction estimation from the reference (the probe) is plotted in Figure 6.11.

The characteristics of a reverberation sound field were also analyzed using the intensity probe. Since in a reverberation room, the sound field is diffuse and intensity measurements require multiple microphones, the newly developed intensity probe was used for that purpose. The characterization of the reverberation field with a single microphone will be incomplete considering its inability to measure intensity in a diffuse sound field. This chapter is concluded with a discussion of the different measurements.

6.1 ACOUSTICAL PARAMETER MEASUREMENTS

In this section, the particle velocity, intensity, impedance and total energy density is calculated and compared with the determined corresponding ideal values.

6.1.1 Particle Velocity

In this section, the particle velocity is calculated from the sound pressure measured from each of the microphones using the following equation [1]:

$$V = \frac{P}{\rho c} , \tag{6.1}$$

Where P is the measured sound pressure at each microphone, ρ is the density of the medium, and c is the sound speed at the measurement temperature. The calculated particle velocity from the Equation 6.1 is listed in the Table below as the **Ideal** value, while the calculated particle velocity from the Equation 5.14 is listed as the **Calculated** value in the same Table. At the measurement temperature (25°C), ρ = 1.184 kg/m^3 and c = 346.1 m/s. A 1.0 kHz sine wave was used as the source excitation signal.

Table 6.1: Comparison between the **Ideal** and **Calculated** values of the **particle velocity** components.

Component	**Ideal** (m/s)	**Calculated** (m/s)	Deviation (m/s)
X_Low	1.53E-03	1.62E-03	0.09E-03
Y_Low	1.53E-03	1.40E-03	0.13E-03
Z_Low	1.53E-03	1.60E-03	0.07E-03
X_High	1.53E-03	1.58E-03	0.05E-03
Y_High	1.53E-03	1.52E-03	0.01E-03
Z_High	1.53E-03	1.54E-03	0.01E-03

In the above Table, the differences between the ideal and calculated values among the microphones of each array, and even between the two arrays are very small. The velocity magnitude for each array can be determined by taking the square-root of the sum of the squares of the three components with the probe axis pointing at the source. For the high-frequency array, the particle velocity magnitude is 2.65E-03 m/s (ideal), and 2.67E-03 m/s (calculated). For the low-frequency array, the particle velocity magnitude is 2.65E-03 m/s (ideal), and 2.67E-03 m/s (calculated). The average deviation (average from all the microphones) from the ideal value is about 4 %.

6.1.2 Acoustic Intensity

The time-averaged intensity was first calculated using ideal values of the sound pressure using the following equation:

$$I = PV = \frac{P^2}{\rho c}. \tag{6.2}$$

The time-averaged intensity was then calculated using the following pressure gradient relationship:

$$I = \frac{P_0 + P_n}{2}.\frac{1}{\rho \Delta r}\int_{-\infty}^{t}(P_0 - P_n)dt\,, \tag{6.3}$$

where P_0 is the center microphone pressure, P_n is the pressure of any of the surrounding microphones, and Δr is the effective distance between the two microphones.

Table 6.2: Comparison between the **Ideal** and **Calculated** values of the **Intensity** components (at 1.0 kHz sine wave).

Component	**Ideal** (W/m^2)	**Calculated** (W/m^2)	Deviation (W/m^2)
X_Low	9.61E-04	10.17E-04	0.56E-04
Y_Low	9.62E-04	8.81E-04	0.81E-04
Z_Low	9.64E-04	10.06E-04	0.32E-04
X_High	9.62E-04	9.92E-04	0.30E-04
Y_High	9.63E-04	9.55E-04	0.08E-04
Z_High	9.66E-04	9.70E-04	0.04E-04

From the above table, the total intensity magnitude for the high-frequency array is 1.67E-03 W/m^2 (ideal), and 1.68E-03 W/m^2 (calculated). For the low-frequency array, the

total intensity magnitude is 1.67E-03 W/m^2 (ideal), and 1.68E-04 W/m^2 (calculated). The average deviation (average from all the microphones) from the ideal value is 3.65 %.

6.1.3 Total Energy density

The time-averaged total energy density was first calculated using ideal values of the pressure and the particle velocity using the following equation:

$$W_{total} = \frac{P^2}{2\rho c^2} + \frac{\rho|\mathbf{V}|^2}{2}, \tag{6.4}$$

where P^2 is the time averaged square pressure of the average of the all the microphones of the probe, and $\boldsymbol{V}$ is the vector velocity. The time-averaged total energy density was then calculated using the pressure gradient between the two microphones using the Equation 5.15.

Table 6.3: Comparison between the **Ideal** and **Calculated** values of the **Total Energy Density of the overall probe** (at 1.0 kHz sine wave).

	N/m^2
Ideal Total Energy Density	8.31E-06
Calculated Total Energy Density	8.44E-06
Deviation	**0.13E-06**

Total energy density information is very useful in sound fields characterization than the individual energy density components of each microphone of the probe. The deviation between from the ideal value was about ~2 percent.

6.1.4 Acoustic Impedance

Acoustic impedance is the ratio of the sound pressure and the particle velocity of a sound field at a point in space. Acoustic Impedance is a frequency dependent quantity, and vector natured since the particle velocity is a vector. The impedance component normal to the surface relates the sound pressure at the surface of a material body with its particle velocity vector component normal to the surface. The reflective and absorptive properties of a material can be measured from impedance measurements. The general equation for the acoustic impedance can be written as,

$$|Z| = \frac{P}{|V|} \ , \tag{6.5}$$

where $|Z|$ is the magnitude of the acoustic impedance, $|V|$ is the magnitude of the particle velocity component, and P is the sound pressure.

Table 6.4: Comparison between the **Ideal** and **Calculated Acoustic Impedance** values of a 1.0 kHz sine wave.

Component	Ideal (MKS Rayls)	Calculated (MKS Rayls)	Deviation (MKS Rayls)
X_Low	410.26	387.47	22.79
Y_Low	410.39	448.51	38.12
Z_Low	410.78	392.82	17.94
X_High	410.19	397.21	12.98
Y_High	410.52	413.22	02.70
Z_High	411.37	408.70	02.67

The average deviation in impedance calculation from the ideal values was about 4 percent.

6.2 PROBE PERFORMANCE IN THE INTENSITY MEASUREMENTS

Now, the overall probe intensity as a function of frequency is calculated and compared with each of the two arrays of the probe. The intensity from the origin microphone was calculated using mean-squared pressure and was used as the reference intensity. The measurements were done in the anechoic chamber using the small loudspeaker as the sound source. A broadband (200 Hz – 7.0 kHz) noise signal was used as the excitation source.

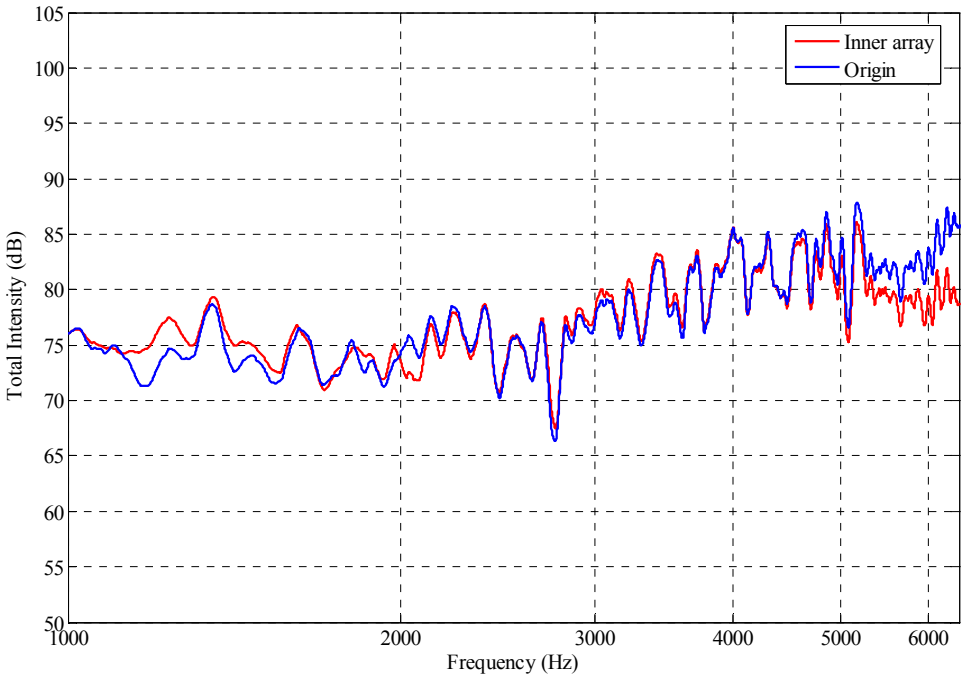

Figure 6.1: Total Intensity plots of the small loudspeaker from the **Origin microphone** and from the **inner array**.

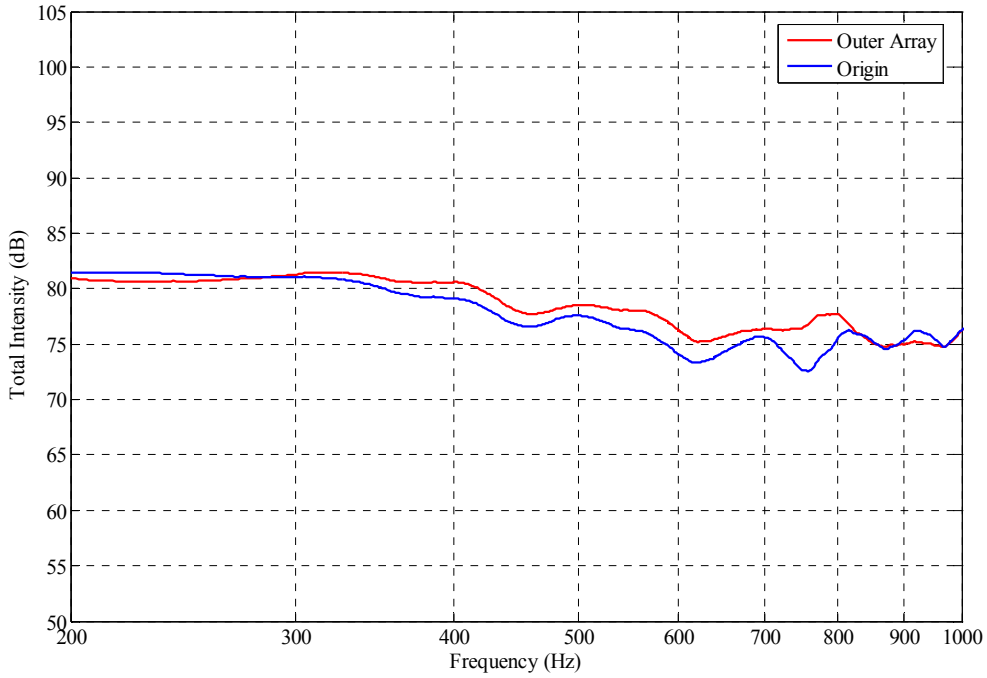

Figure 6.2: Total Intensity plots of the small loudspeaker from the **Origin microphone** and from the **outer array**.

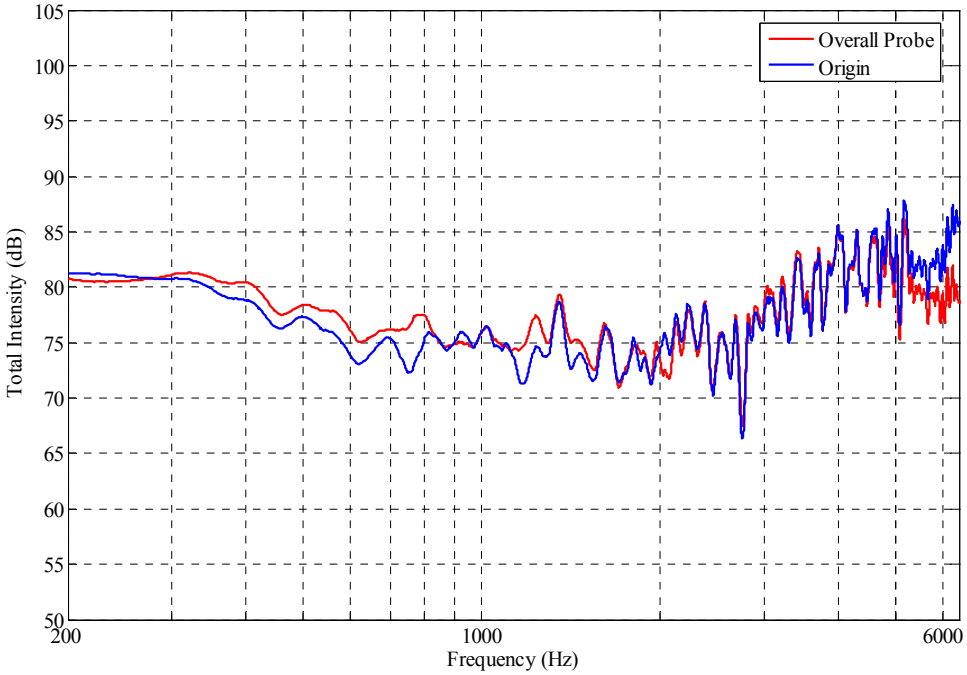

Figure 6.3: Total Intensity plots of the small loudspeaker of the **overall probe** (compared with the measured intensity of the Origin microphone).

In the Figures 6.1, 6.2, and 6.3, the inner array, outer array, and the overall probe intensity were compared with the intensity measured from the origin (reference) microphone. The maximum deviation from the reference microphone intensity was +/- 1.5 dB over the frequency range of 200 Hz to 6.5 kHz. The overall probe intensity was calculated by combining the low-frequency components (200 Hz – 1.0 kHz) of the outer array, and the high frequency components (1.0 kHz – 6.5 kHz) of the inner array. The ~3 dB oscillations resulted from diffractions off the small speaker enclosure.

6.3 DIRECTIVITY PATTERN OF THE PROBE

To understand the directional characteristic of the probe, intensity levels were calculated at each plane. Three different (500 Hz, 2 kHz, and 4 kHz) single tone sine waves were used as the excitation signal for these measurements. To measure intensity in the reference X-Y plane (Figure D.9), the center microphone axis (reference Z-axis) of the probe was first aligned along the center of the sound source (loudspeaker). Then the probe was rotated around that axis to cover the entire plane. Measurements in the other two reference planes were made similarly by rotating the probe around the reference X and Y axis, separately. Polar plots of the directivity patterns are shown in the following Figures:

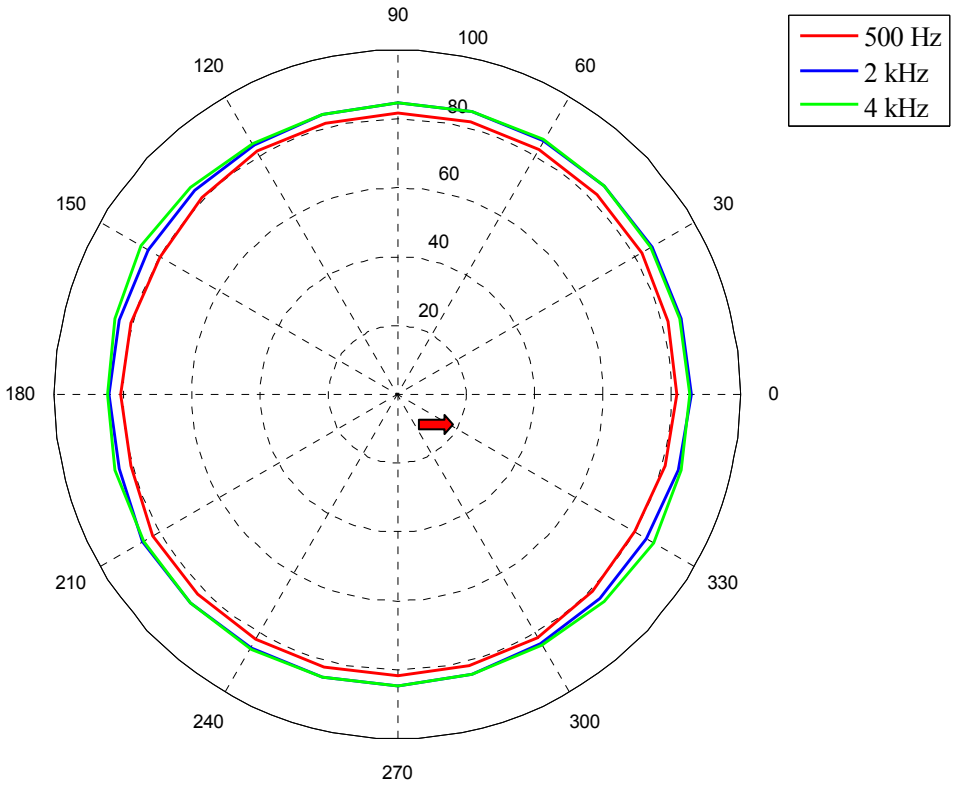

Figure 6.4: Directivity patterns of the overall probe intensity (dB) (along the reference X-Y plane).

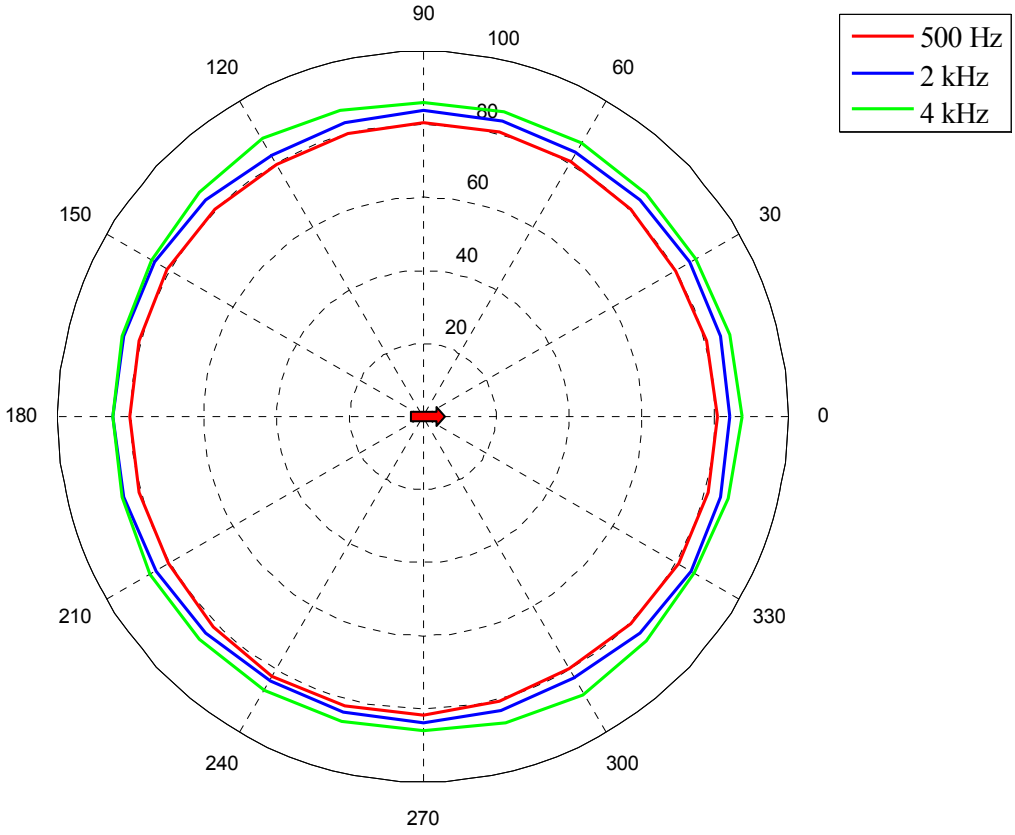

Figure 6.5: Directivity patterns of the probe intensity (dB) (along the reference X-Z plane).

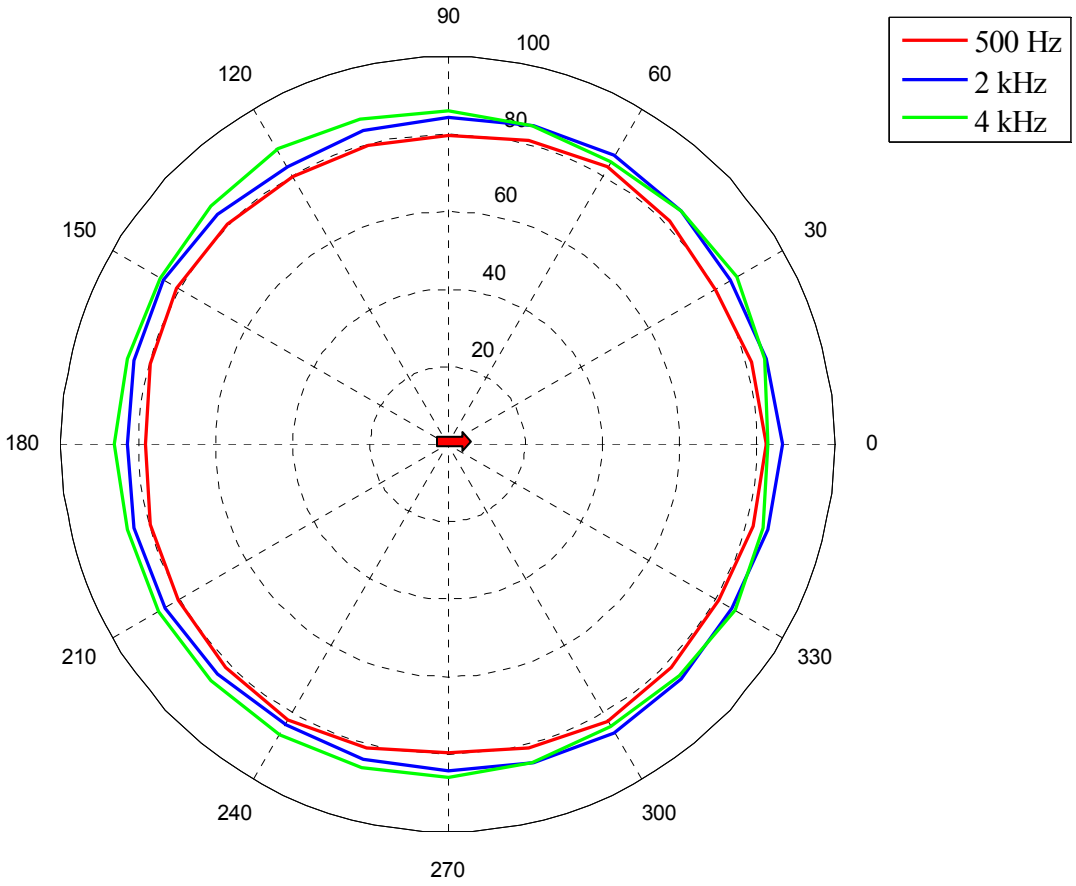

Figure 6.6: Directivity patterns of the probe intensity (dB) (along the reference Y-Z plane).

Difference in the intensity level among different frequencies was +/- 3 dB. The red arrow in the above figures (6.4, 6.5, and 6.6) indicates the source direction. Variations in the intensity measurements when the probe was facing opposite the sound was about +/- 1.5 dB in compare to the probe facing the sound source directly. This variation can be attributed to the diffractions effect of the microphones, and the supporting structures. Next, directivity patterns are compared among different axes at different frequencies in the following three figures.

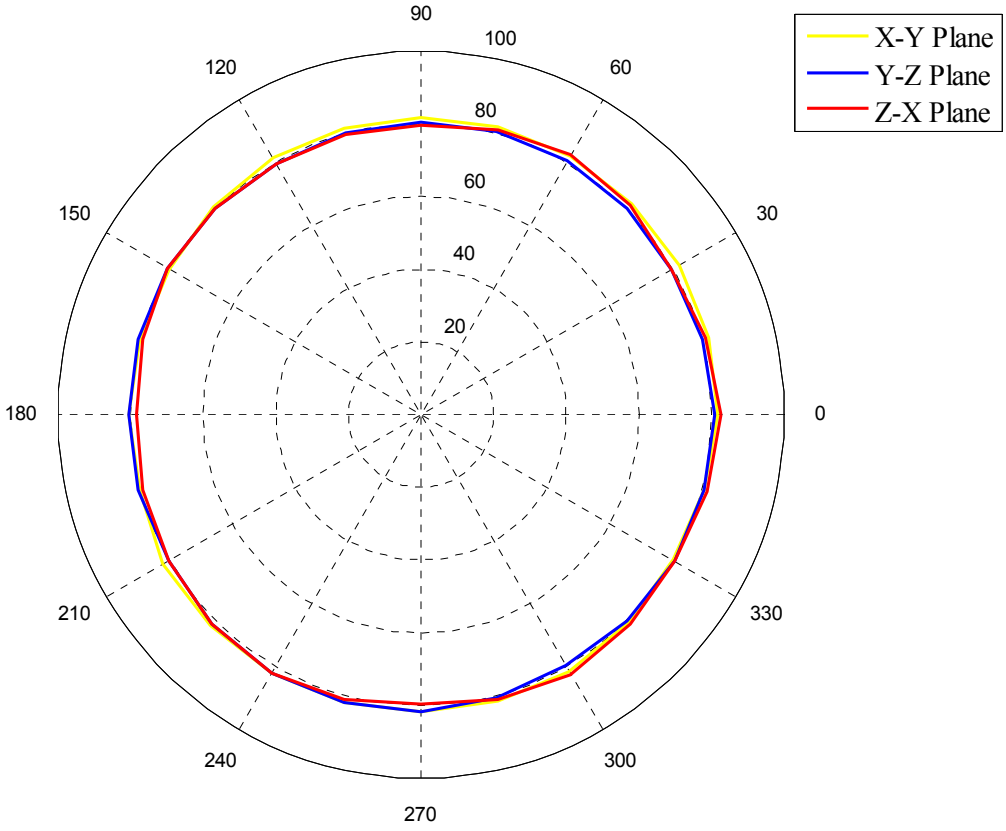

Figure 6.7: Directivity patterns of the probe intensity (dB) at **500 Hz** (along the reference X - Y, Y - Z, and Z - X plane).

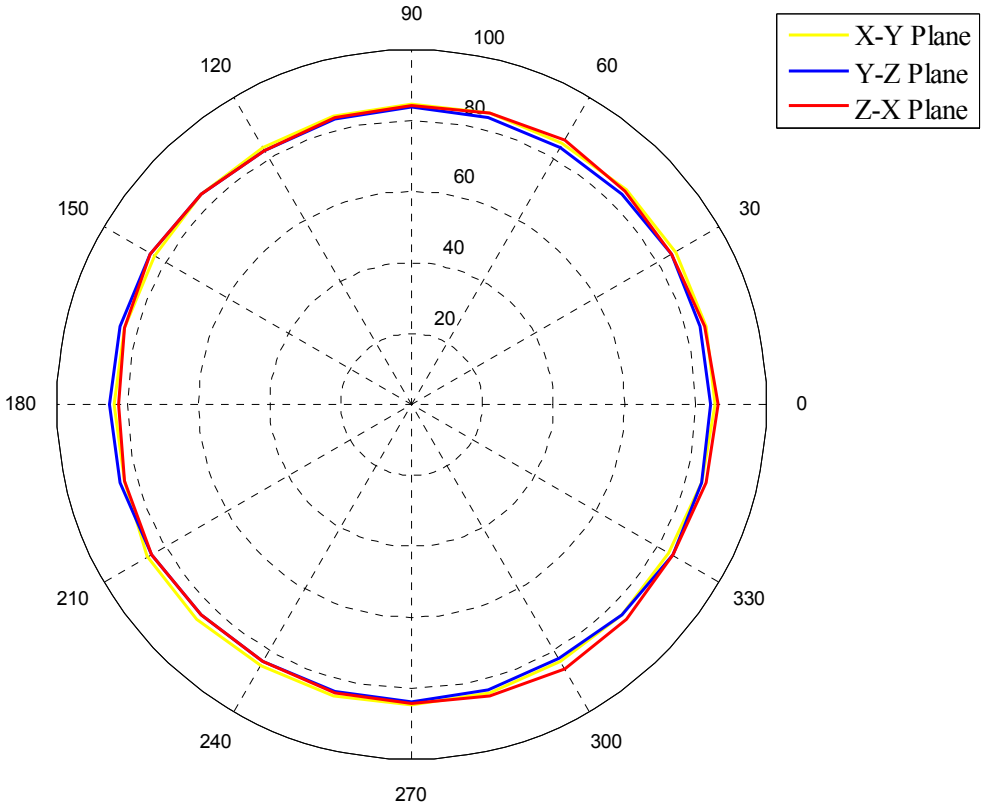

Figure 6.8: Directivity patterns of the probe intensity (dB) at **2 kHz** (along the reference X - Y, Y - Z, and Z - X plane).

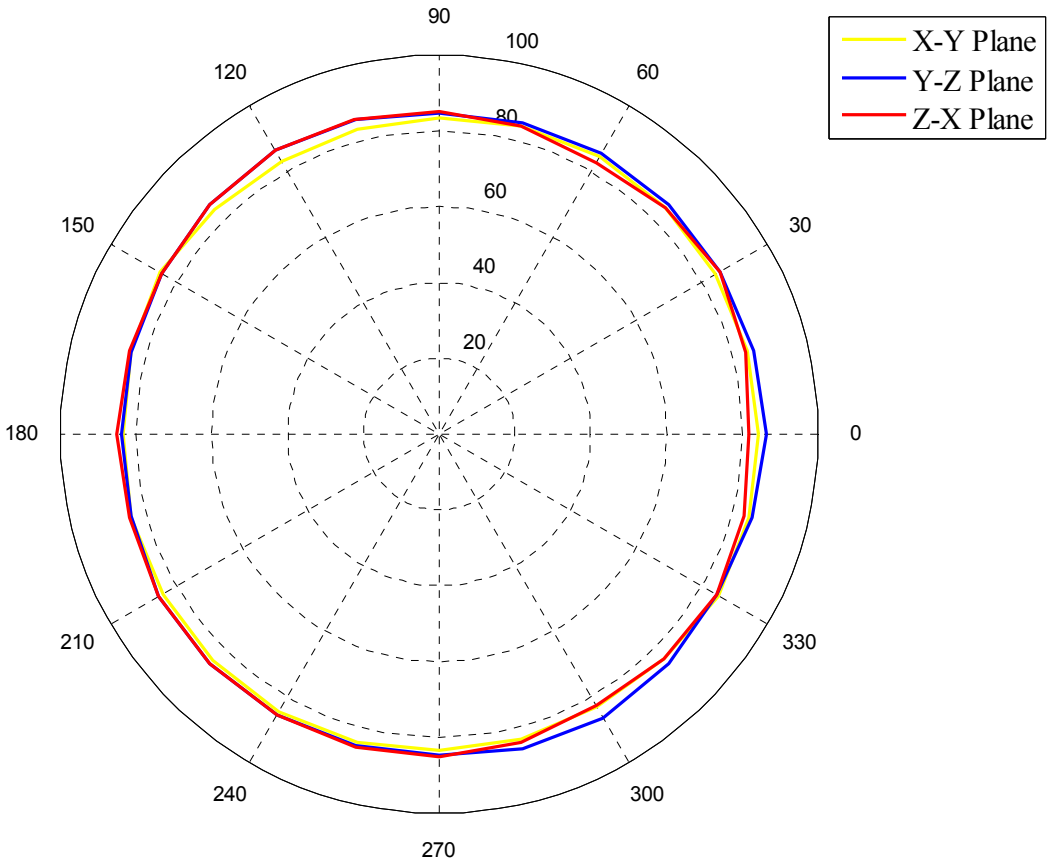

Figure 6.9: Directivity patterns of the probe intensity (dB) at **4 kHz** (along the reference X - Y, Y - Z, and Z - X plane).

Directivity patterns of the probe intensity at a single frequency along different plane were compared in Figures 6.7, 6.8, and 6.9 for **500 Hz**, **2 kH**z and **4 kHz** sine wave, respectively. The average variations among different planes were less than +/- 1.0 dB. This variation can be related to the reflection and diffraction effects of the probe, the supporting structure, and the tripod used to mount the probe for measurements. Overall, the performance in the intensity measurement shows the omnidirectional nature of the probe.

Next, the z-axis of the probe was positioned perpendicular to the direction of the incoming plane waves. Thus, the x-y plane was parallel to the plane wave. Also, the x-axis of the probe was pointed perpendicular to the direction of the center of the source. In this arrangement, the particle velocity directivity plot of the two microphones (the center and the inner array x direction microphone) is shown in the Figure below:

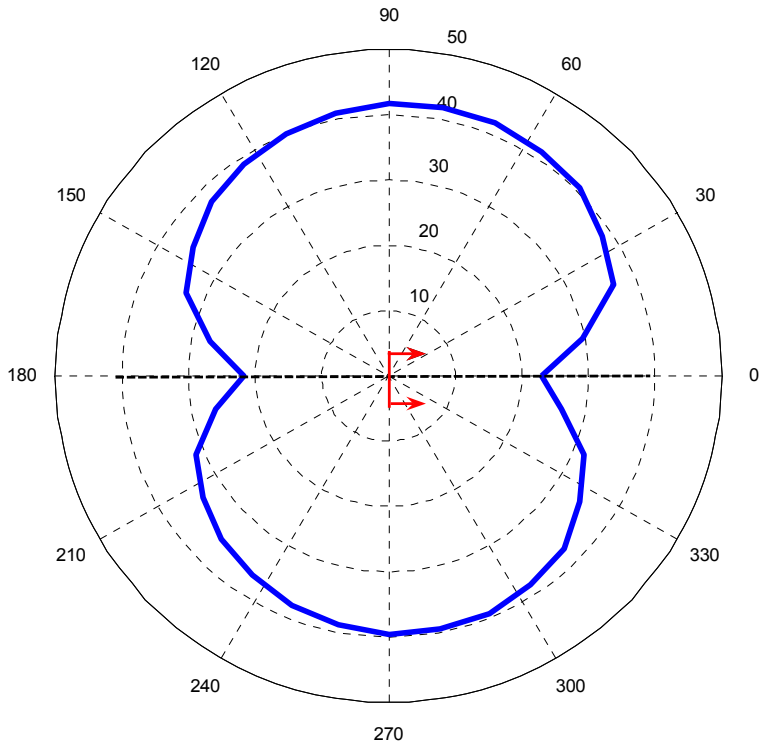

Figure 6.10: Velocity directivity plot in the x-direction of the probe using a 2 kHz sine wave (directions of the two microphones are shown by the two arrows).

From Figure 6.10, the overall cardioid shape of the directivity plot of the velocity component in the x-direction was in general agreement with the theory. This observation bodes well with the plane wave response of the two microphones facing in the direction of the incoming plane waves.

6.4 SOUND SOURCE DIRECTION ESTIMATION

In this section, a small (3-inch) loudspeaker with a 2 kHz sine wave is used for the source direction measurement using the intensity probe. Particle velocity vectors along the three axes and the overall particle velocity magnitude was used to calculate the azimuth and elevation angles of the source in relation to the probe. In these measurements, one of the probe axes was positioned perpendicular to the incoming plane wave (see Figure 3.2 for axis orientation). Since the microphones in that axis are in the same plane, the particle velocity measured from the sound pressures of the center and the one of the array microphones should ideally be zero. Now, the direction of the source in the plane comprised by the other two probe axes can be calculated as:

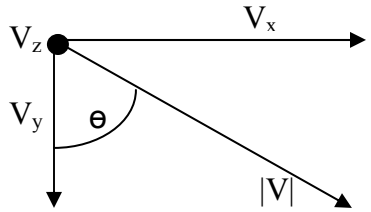

Figure 6.11: Schematic of the Particle velocity components and the particle velocity magnitude relationship.

$$V_z \approx 0$$
$$\cos\theta = \frac{V_y}{|V|} \tag{6.5}$$

In the above diagram and in Equation 6.5, the z-axis of the probe is perpendicular and pointed to the center of the sound source, θ, is the angle between the source and the probe in the x-y plane, and $|V|$ is the particle velocity magnitude. Subscript in V indicates particle velocity vectors in along different axis. The deviations in the angles from the measured position are shown in Table 6.5 From this table, the average deviation from the measured was about $4^{\circ} \pm 3^{\circ}$. The 3° is the possible error in the geometrical measured angle due to inaccuracies of the probe rotation around the tripod.

Table 6.5: Deviations (difference between the geometrical measured angle and acoustical measured angle) of the source position from the probe (reference) in the x-y plane.

theta	Acoustical measured angle	Geometrical measured angle	Deviation (degree)
83.7	6.3	0	**6.3**
61.7	28.3	22.5	**5.8**
47.1	42.9	45	**2.1**
24.3	65.7	67.5	**1.8**
6.35	83.65	90	**6.35**
23.94	113.94	112.5	**1.44**
42.6	132.6	135	**2.4**
70.6	160.6	157.5	**3.1**
83.46	173.46	180	**6.54**

Deviations in the angle measurements can be improved by using a precision rotating device to rotate the probe from the initial location to the different positions.

6.5 CHARACTERIZATION OF A REVERBERATION SOUND FIELD

Most practical sound measuring environments are considered reverberant. The concept of reverberation is more statistical than deterministic, and is little useful itself in most noise reduction and control applications [7, 8, 9]. In a reverberant sound field, there is a considerable fluctuation in sound pressures due to random superimposition of incident and reflected waves from the boundaries. In a diffuse sound field, measuring the sound intensity at a point using a single microphone with mean-squared pressure would present little useful information. The energy density is useful in reverberation room measurements. A multi-microphone intensity probe would be a better tool to characterize the direct field and to measure the energy density of the sound field. A proper understanding of a reverberant sound field is very useful in understanding the acoustic signature and the behavior of different sound sources in an enclosed space, and their effects on environments where measurements are taken.

In a reverberant sound field, the direct radiated (free-field) sound pressure diminishes as one move farther away from the source. However, after a certain distance from the source, the reverberant sound field dominates the sound field. The location of the transition point (zone) between the free-field and the reverberant field largely depends on the volume of the enclosed space and on the overall absorption properties of the materials enclosing the space [8]. The knowledge of the location of the transition zone in an enclosed space enables proper measurement of the sound level, sound intensity, and other key acoustic parameters. This concept is very useful in noise control in a large room or in the office space environment where few noise sources (such as copier/fax machine, computer server, loud speaker, etc) are sparsely scattered around the room.

This concept of sound pressure field in the reverberant space is illustrated in the Figure 6.12.

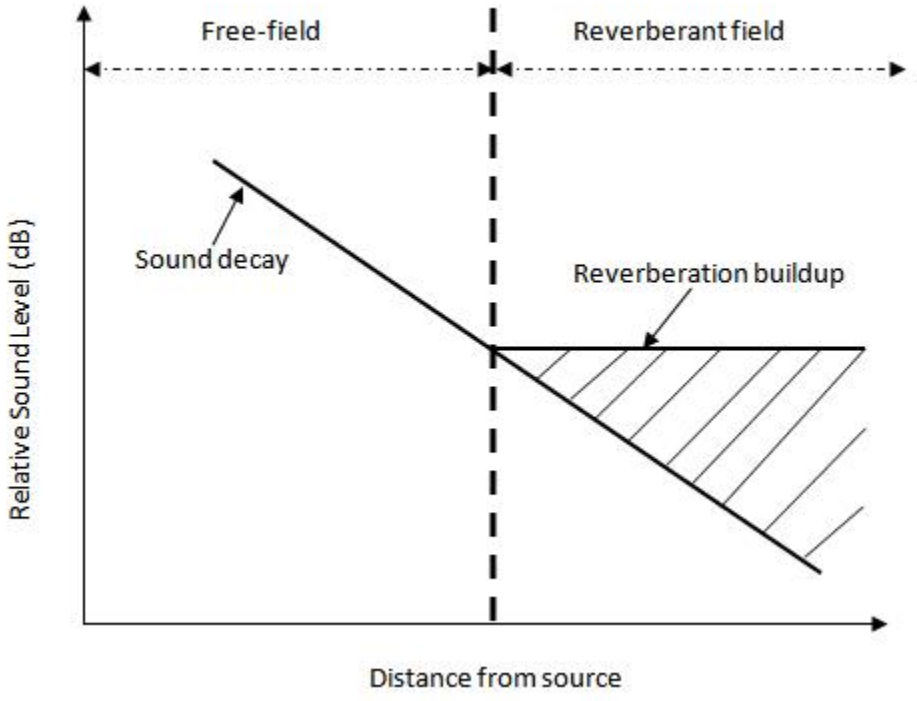

Figure 6.12: A schematic of sound field in a reverberant enclosed space [8].

In a reverberant space, the mean-square sound pressure at any particular distance from the source can be written as

$$P^2 = W\rho c\left[\frac{Q_\theta}{4\pi r^2} + \frac{4}{R}\right], \qquad (6.6)[8]$$

where P^2 is the mean-square pressure (unit: Pa^2), W is the source acoustic power (unit: Watt), ρc is the characteristic impedance of the medium (unit: MKS Rayls), Q_θ is the

source directivity factor (unitless), *r* is the distance from the source (unit: m), and *R* is the room constant (unit: m^2).

One of the important parameters in the above equation is the room constant, R and is defined as,

$$R = \frac{S\overline{\alpha}}{1-\overline{\alpha}}, \tag{6.7}$$

where $\overline{\alpha}$ is the average absorption coefficient of the material of the enclosed space, and S is the total surface area (unit: m^2). The Equation 6.6 can also be written in a useful logarithmic form as,

$$L_p = L_W + 10\log_{10}\left[\frac{Q_\theta}{4\pi r^2} + \frac{4}{R}\right], , \tag{6.8}[8]$$

where L_p is the sound pressure (unit: dB), and L_w is the source acoustic power level (unit: dB).

It can be said from Equations 6.6, 6.7, and 6.8 that the reverberation sound field is accounted for by the inclusion of the term *4/R*, where *R* is the measure of the total absorption in the enclosed space. It can also be said that for a very large average absorption coefficient, $\overline{\alpha}$, the room constant *R* becomes very large. Thus, for a very large room constant, the sound field approaches the free-field conditions [8]. For better understanding, a numerical simulation was done, and the difference between sound pressure level and source acoustic power level were plotted for different room constants at varying distance from the source (Figure 6.13). Note that the sound pressure level continues to decrease to zero with no reverberation.

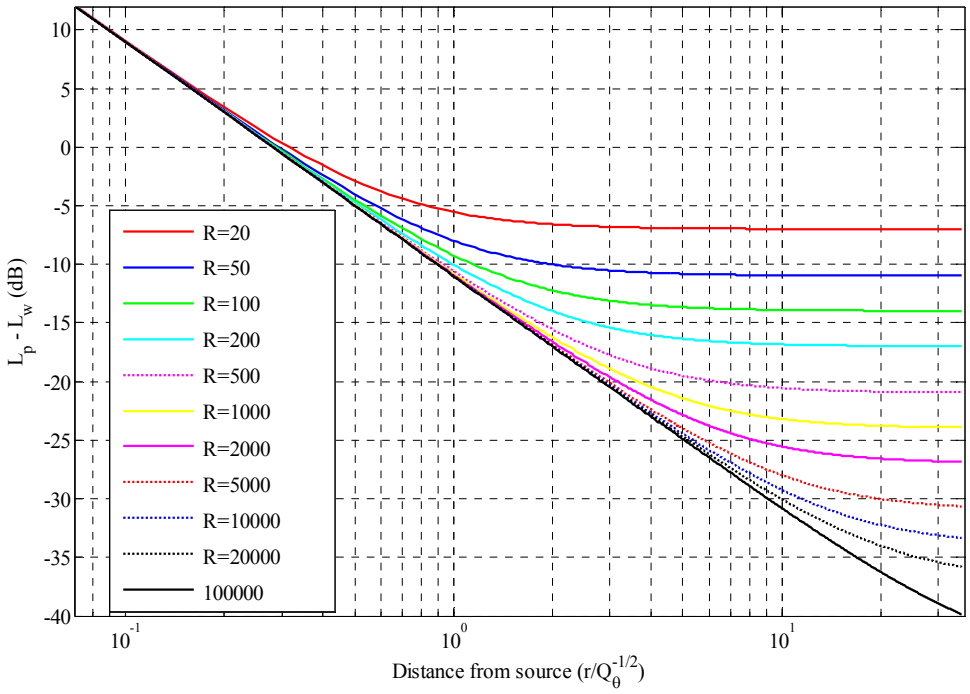

Figure 6.13: Chart to determine the sound pressure level at a distance r (0.2 m to 100 m) from the sound source for Q_θ of 8, with a varying room constant, R from 20 to 100000 (simulation).

6.5.1 Reverberation Chamber Measurements

An experiment (Figure 6.14) to demonstrate the concept of sound fields in an enclosed reverberation space was performed in the reverberation chamber located in the Acoustic Research Laboratory at the University of Texas at Austin. Sound intensities were measured using the broadband intensity probe designed in this report. Sound pressure were measured by the origin microphone. Some key parameters used in the intensity level measurement in this experiment are shown in the Table 6.6. An octave band noise centered around 1 kHz was used as the source excitation signal.

Table 6.6: A list of parameters used in the reverberation chamber measurements.

Volume, V (m^3)	**260**
Total surface area, S (m^2)	**250**
Average absorption coefficient, $\overline{\alpha}$	**0.0338**
Room constant, R (m^2)	**8.74**
Characteristic impedance, ρc (MKS Rayls)	**413**
Source directivity factor, Q_θ	**8**
Distance from the source, r (m)	**0.5, 1.5, 3.0, 5.0, & 6.0**

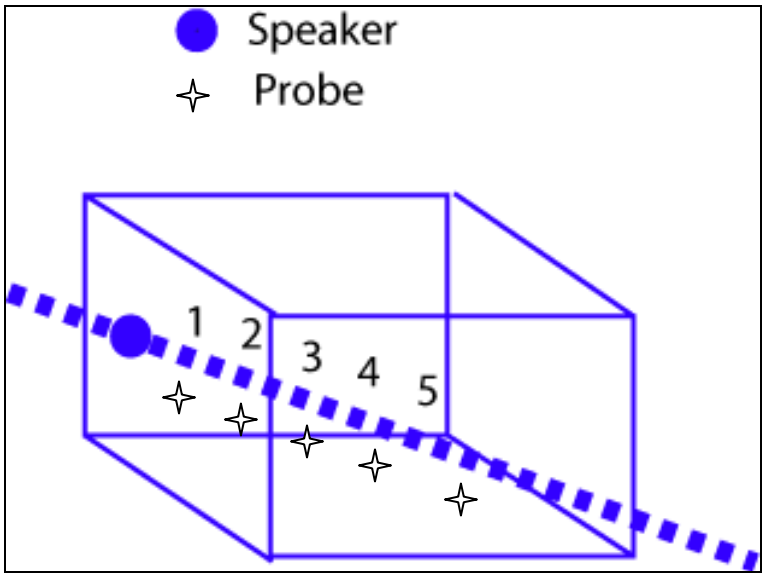

Figure 6.14: A schematic of the source and the probe locations inside the reverberation chamber.

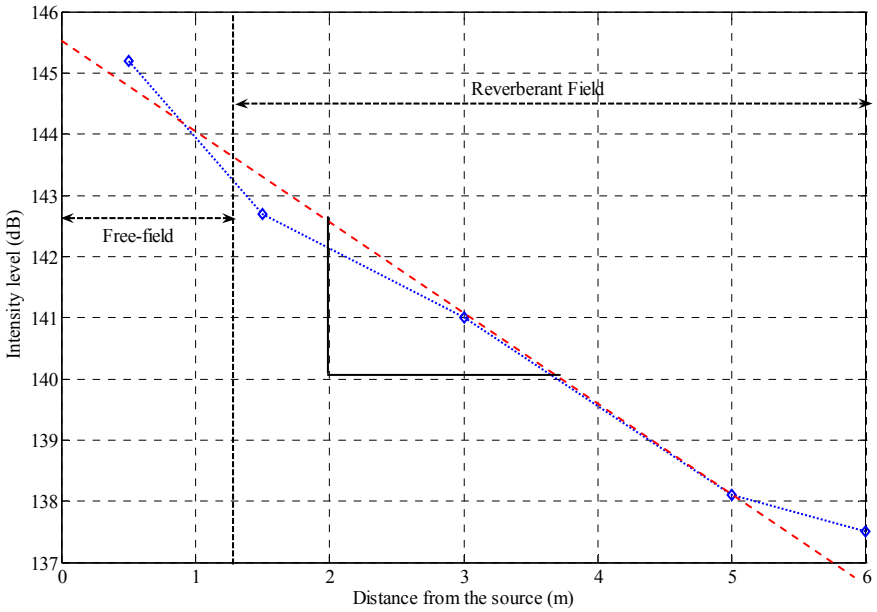

Figure 6.15: Intensity level measured in the reverberation chamber with a stationary source and the moving probe along a straight line.

From the above intensity plot (Figure 6.15), it can be said that the intensity level drops approximately logarithmic as we move the probe farther away from the source. The intensity decays toward the steady state system noise level. The intensity measurement defines the source even in the reverberant field. The theoretical transition point is calculated using Equation 6.8. At the transition point,

$$\frac{Q_\theta}{4\pi r^2} = \frac{4}{R}, \tag{6.9}$$

From Equation 6.9, the distance of the transition point, r can be calculated by the known values of the room constant, R, and the source directivity factor, Q_θ. The 1.2 m theoretical transition point was calculated using Equation 6.9 and Table 6.4.

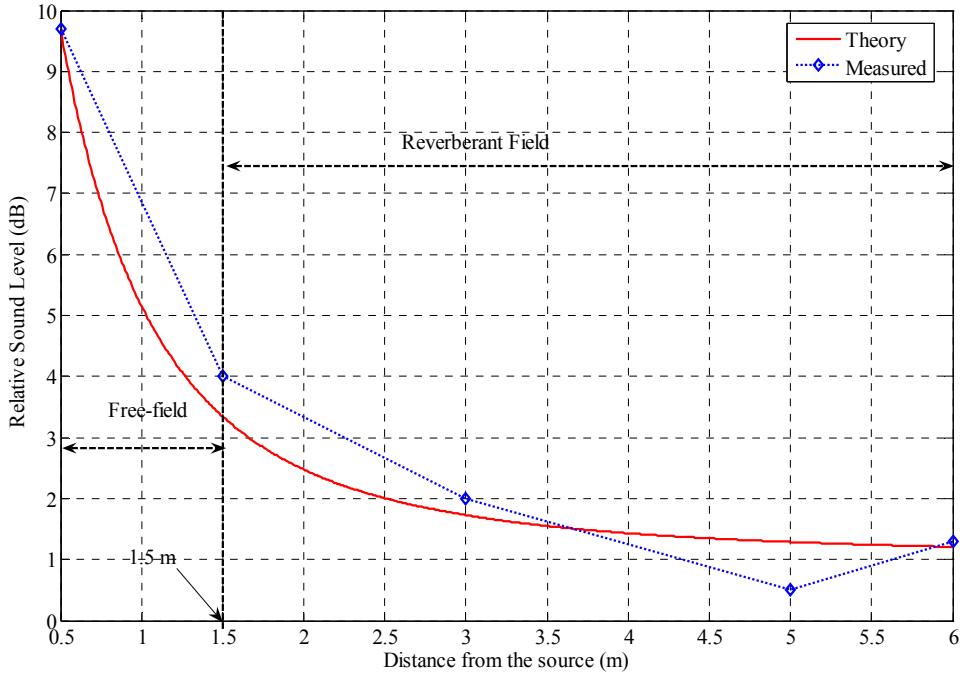

Figure 6.16: Sound Pressure Level (SPL) of the reverberation sound field depicting different sound fields. The transition zone is around 1.5 +/- 0.25 m from the source.

Although very few data points were recorded, the sound pressures plot of Figure 6.16 indicates a transition distance at around 1.5 +/ 0.25 m. In the free-field, the sound pressure level drop is inversely proportional the distance from the source. Beyond the transition zone, the reverberant field dominates as the steady state noise approaches the diffuse reverberant field. The level of the steady state SPL depends on the volume of the enclosed space and the overall absorptive properties of the surrounding materials.

6.6 SUMMARY

In this chapter, particle velocity vectors for the different microphones were calculated and compared with ideal values. Then intensity level was also calculated and compared with the ideal values. Accuracy of these calculated quantities were within 4 percent. Then total energy density was calculate for the overall probe and compared with the ideal value. The accuracy of the total energy density calculations were within 2 percent of the ideal value. The accuracy of the acoustic impedance calculations were within 4 percent of the ideal value.

Then intensity plots for the overall probe was plotted over the desired frequency range (200 Hz – 6.5 kHz) and compared with intensity level calculated from the center reference microphone. The maximum deviation of the calculated intensity from the reference intensity over the desired frequency range (200 Hz – 6.5 kHz) was +/- 1.5 dB. The random peaks and troughs in the intensity plots can be attributed to the diffractions off the sound source (loudspeaker) enclosures.

Directivity patterns were plotted using the intensity level measurements, and these plots confirms the omnidirectional nature of the probe with an error of +/- 1.5 dB. Diffraction and reflection effects due on the probe directivity due to the microphones and the supporting structure was negligible. Symmetry on both sides of the probe axis was observed (Figure 6.4, 6.5, 6.6, 6.7, 6.8, and 6.9). A 2 kHz sine wave was used in the anechoic chamber as the source of the sound source direction estimation measurements. From the Table 6.5, the average deviation error of the source direction from in relation to the probe in the x-y plane was about ~ 4°.

Then sound field in the reverberation room was characterized using the probe. SPL and intensity level were calculated by moving the probe away from the sound source. The transition zone between the free-field and reverberation field was in general agreement with theoretical calculations. The location of the exact transition point was not clear due to small number of measurements, but the overall concept of the sound field was understandable from the plots (Figure 6.15 and 6.16). It can be concluded from the measurements and results discussed in this chapter that the newly developed probe can be used to measure key acoustic parameters (particle velocity, intensity, impedance, and energy densities), and can also be used in applications where the radiating pattern of a sound source is an integral part of the measurements.

References

[1] M. Möser, "*Engineering Acoustics-An Introduction to Noise Control*," second edition, Springer, Berlin, 2004.

[2] J. B. Allen and D. A. Berkley, "Image method for efficiently simulating small-room acoustics," *J. Acoust. Soc. Am.,* vol. 65, pp. 943-950, 1979.

[3] B. Champagne, M. Eizenman, and S. Pasupathy, "Exact maximum likelihood time delay estimation for short observation intervals," *IEEE Trans. Signal Processing*, vol. 39, pp. 1245-1257, June, 1991.

[4] Y. T. Chen and K. C. Ho, "A simple and efficient estimator for hyperbolic location," *IEEE Trans. Signal Processing*, vol. 42, pp. 1905-1915, Aug., 1994.

[5] Y. T. Chen and K. C. Ho, "An efficient closed-form localization solution from time difference of arrival measurements," *in Proc. IEEE Int. Conf. Acoust., Speech, Signal Processing*, vol. II, pp. 393-396, 1994.

[6] Y. Huang, J. Benesty, and J. Chen, "*Acoustic MIMO Signal Processing*," Springer-Verlag, Berlin, 2006.

[7] L. E. Kinsler, A. R. Frey, A. B. Coppens, and J. V. Sanders, "*Fundamentals of Acoustics*," 3rd edition, John Wiley, New York, 1982.

[8] P. M. Morse and K. U. Ingard, "*Theoretical Acoustics*," McGraw-Hill, New York, 1968.

[9] L. H. Bell and D. H. Bell, "*Industrial Noise Control: Fundamentals and Applications*," 2nd edition, Marcel Dekker, New York, 1994.

Chapter 7: Conclusion and Future Work

7.0 CONCLUSION

The main motivation behind this dissertation research was to develop an acoustical probe system to measure key acoustical parameters that can be used for some practical applications. Specific goals were to measure the sound intensity level, total energy density, and directivity patterns of the probe in a three-dimensional space. Accurate measurements of these key parameters are very useful in acoustic noise control and improving the sound quality of various sources in different environments.

Two-microphone intensity probe systems, and related parameter measurement techniques have been available for decades. The main limitation and the possible source of errors of these systems and techniques lie in measuring the inherent three-dimensional parameters with one-dimensional measurements. Even though some techniques physically scan around the source for the three-dimensional coverage, the need of extra hardware and resources put constraints on many applications. In the recent decades, several three-dimensional intensity measuring systems have been developed. These systems use multiple microphones (sensors) in different array configurations for various applications. Some limitations of these systems become very apparent when the sound source has a broad frequency range (200 Hz – 6.5 kHz). At this frequency range, the finite-difference error, and the phase mismatch error adds inaccuracy to the measurements. Some of the systems address this issue by adjusting the distance and/or changing the microphones arrangement within the probe. This extra step in the measurement adds inconvenience and in some cases measurements may not be feasible.

The intensity probe system designed and tested in this report eliminates this narrowband constraint by combining the two different arrays in the same probe. This new design also resolves the finite-difference and the phase mismatch errors associated with the broadband measurements.

A seven-microphone two-concentric array three-dimensional probe design was considered in this report. The outer array covers the low-frequency (200Hz – 1.0 kHz) components while the inner array covers the high-frequency (1.0 kHz – 6.5 kHz) components of the sound field. Each array consists of three microphones and forms a tetrahedron with the center microphone. Each microphone in the array is arranged along the three axes with one microphone located at the origin. The center reference microphone lies at the origin of the coordinate system. The screw adjustable center microphone was used to calibrate the other microphones of the probe, and to calculate the average pressure and the pressure difference between the two microphones. The average and differential pressure estimates were then used to calculate the particle velocity and the intensity vectors. Each microphone used in this probe is an Electret condenser microphone with a flat (+/- 2 dB) magnitude response in the frequency range of 200 Hz to 7 kHz.

Microphones and the overall probe calibration techniques and procedures were important in designing the intensity probe. In the calibration process, the center (origin) microphone of the probe was first calibrated using a standard reference microphone in the anechoic chamber. It was assumed that if the probe is placed far from the sound source in an anechoic room, then all the microphones in the same plane would experience incoming plane waves of the same amplitude. The merit of this assumption was justified with measurements. After the center (origin) microphone was calibrated, microphones of each of the two arrays were calibrated simultaneously. The diffraction and reflection

effects due to the probe supporting structures and the other microphones were also investigated in this report.

Theories and mathematical formulas for calculating the intensity, potential energy density, and kinetic energy density vectors for the seven-microphone probe were extended from the formulas developed for the four-microphone tetrahedron configuration described by Cazzolato *et. al.* [1].

Different measurements in the anechoic chamber were made to evaluate the probe performance. The overall frequency response of the probe was calculated by combining the low-frequency (200Hz – 1.0 kHz) and the high-frequency (1.0 kHz – 6.5 kHz) responses of the outer and the inner array, respectively. The transition zone was set between the high-end of the low-frequency cutoff and the low-end of the high-frequency cutoff. The bandwidth of the transition zone was 200 Hz (from 900 Hz to 1.1 kHz).

Results of the intensity level measurements of the overall probe showed significant improvements over either the outer or the inner array measurements, separately. The overall calculated intensity of the probe was +/- 1.5 dB within the reference value calculated using the center (origin) microphone.

The characterization of sound fields in a reverberation room, and identification of a source direction in an anechoic chamber were two applications where the newly developed three-dimensional intensity probe was used. Results of the different measurements in the anechoic room showed effectiveness of the probe as a tool to measure key acoustical properties in most practical environments. The scope of the future work is discussed in the following section.

7.1 FUTURE WORK

Though results of the different measurements showed improved performance of the newly designed probe over the narrowband probes, the commercial use of this probe as it is will require a fine tuning in different aspects of the probe, and the signal processing software. Fluctuations in the microphones sensitivity; inherent measurement and signal processing noises; imperfections in the mechanical design of the probe; and improvements in the calibration techniques are some open areas that can be considered in the future.

Commercial grade condenser microphones with built in preamplifier can be expensive but can eliminate the need of the analog interface circuit. Characteristics and specifications of the probe calibration environment (anechoic chamber) itself can be checked if more precise calibration is required. The reflection and diffraction effects of the probe's supporting structure on the intensity measurements were investigated, and corrections were made in this report. A topic of future research would be to compare this intensity probe against other commercial probes of similar nature. Analytical expressions used in computing the three-dimensional intensity vectors, and potential energy densities in this paper can be compared with other methods.

Source localization applications using an intensity probe and other microphone arrays have been explored over the last two decades [2, 3, 4, 5, 6]. Improvements in the software and hardware will be necessary to use this probe in the real-time applications. Identification and characterization of noise sources in the automotive interior; and recording acoustic signatures of the different automotive modules (engines, muffler, exhaust, braking system, etc) can be done with the intensity probe designed in this report with some changes in the software, and the inclusion of a spectrum analyzer.

References

[1] B. S. Cazzolato and C. H. Hansen, "Errors arising from three-dimensional acoustic energy density in one-dimensional sound fields," *J. Sound Vib.,* vol. 238, pp. 375-400, 2000.

[2] H. Silverman, W. Patterson, J. Flanagan, and D. Rabinkin, "A digital processing system for some location and sound capture by large microphone arrays," *in Proc. IEEE Int. Conf. Acoust., Speech, Signal Processing (ICASSP-97)*, Munich, Germany, pp. 251-254, April, 1997.

[3] M. Brandstein, J. Adcock, and H. Silverman, "Microphone array localization error estimation with application to sensor placement," *J. Acoustic. Soc. Am.,* vol. 99, no. 6, pp. 3807-3816, 1996.

[4] C. H. Knapp and G. C. Carter, "The generalized correlation method for estimation of time delay," *IEEE Trans. Acoust. Speech Signal. Process.,* vol. ASSP-24, pp. 320-327, August, 1976.

[5] M. Brandstein and H. Silverman, "A practical methodology for speech source localization with microphone arrays," *Computer, Speech, and Language*, vol. 11, pp. 91-126, April, 1997.

[6] M. Brandstein and D. Word, "*Microphone arrays: Signal Processing Techniques and application*," Chapter 8, Springer-Verlag, Berlin, 2007.

Appendix A: Measurement Units

In this report, acoustical quantities such as the sound pressure, intensity, and power levels were measured in the decibel (dB) unit. Decibels are the ratio of the measured quantity to a reference level. The intensity level can be described as,

$$L_I = 10 \cdot \log\left(\frac{I}{I_{ref}}\right),$$

where L_I is the intensity level, I is the sound intensity (unit: watt/meter^2), and

$$I_{ref} = \frac{10^{-12}\, watt}{meter^2}.$$

Sound pressure is also described as,

$$L_p = 20 \cdot \log\left(\frac{P}{P_{ref}}\right),$$

where L_p is the sound pressure level in dB, P is the sound pressure (unit: Pascal), and

$$P_{ref} = 20\mu \text{ Pascals}.$$

This level approximates the threshold of the human hearing at 1 kHz tone.

Appendix B: Systematic Error Analysis

The pressures estimates, P_e at the midpoint between the two microphone centers, can be written using the Taylor series approximation as

$$p_e(t) = p(t) + \frac{d^2}{2} p^{//}(t) + \frac{d^4}{24} p^{iv}(t) + \ldots\ldots\ldots\ldots\ldots \quad \text{(B.1)}$$

In the above equation *p(t)* is the approximation of the pressure between the two microphones, *d* is the half distance between the two microphones, and the rest is the *cos(d)* to the higher order. Superscripts on the *p(t)* indicates the spatial derivatives. *p(t)* can be written as,

$$p(t) \approx \frac{1}{2}\left[p_1(t) + p_2(t)\right] \quad \text{(B.2)}$$

Now , the *p(t)* term in the equation B.1 is taken on the left side. So, the equation B.1 can rewritten as,

$$p_e(t) - p(t) = \frac{d^2}{2} p^{//}(t) + \frac{d^4}{24} p^{iv}(t) + \ldots\ldots\ldots\ldots\ldots \quad \text{(B.3)}$$

Now, dividing both sides of the equation B. 3 by *p(t)* gives this following equation:

$$\frac{p_e(t) - p(t)}{p(t)} = \left[\frac{d^2}{2} p^{//}(t) + \frac{d^4}{24} p^{iv}(t) + \ldots\ldots\right] \frac{1}{p(t)} \quad \text{(B.4)}$$

This equation (B.4) is the normalized error in the pressure estimates (as referred in the Chapter 4, equation 4.1) except the time dependence is omitted from the left side of the equation 4.1.

Now, the normalized errors in particle velocity vector estimates are discussed below:

$$v(t) \approx \frac{1}{\rho d} \int_{-\infty}^{t} [p_1(\tau) - p_2(\tau)] d\tau \tag{B.5}$$

$$v_e(t) = -\frac{1}{\rho} \int_{-\infty}^{t} \left[p'(\tau) + \frac{d^2}{6} p'''(\tau) + \frac{d^4}{120} p^{v}(\tau) + ... \right] d\tau \tag{B.6}$$

In the two above equations, *v(t)* is the approximations of the particle velocity, while $v_e(t)$ is the estimates of the particle velocity. Now, using equations B.5 and B.6,

$$\frac{v_e(t) - v(t)}{v(t)} = \frac{-\frac{1}{\rho} \int_{-\infty}^{t} \left[p'(\tau) + \frac{d^2}{6} p'''(\tau) + \frac{d^4}{120} p^{v}(\tau) + ... \right] d\tau - \frac{1}{\rho d} \int_{-\infty}^{t} [p_1(\tau) - p_2(\tau)] d\tau}{\frac{1}{\rho d} \int_{-\infty}^{t} [p_1(\tau) - p_2(\tau)] d\tau} .$$

(B.7)

Now, with some algebra and $p'(\tau) = \frac{p_1(\tau) - p_2(\tau)}{d}$, the Equation B.7 can be rewritten as,

$$\frac{v_e(t)-v(t)}{v(t)} = \frac{\int_{-\infty}^{t}\left[\frac{d^2}{6}p'''(\tau)+\frac{d^4}{120}p^{v}(\tau)+.....\right]d\tau}{\int_{-\infty}^{T}[p'(\tau)]d\tau} \quad . \tag{B.8}$$

This above equation is same as the equation 4.2 in the Chapter 4 of the dissertation. The capital " T" in the upper limit of the integration in the denominator of the equation 4.2 signifies that the upper limit of the two integrations is not necessarily the same. " T " is the time interval up to time T where as " t " could be the entire measurement length.

For the equation 4.3, 4.4, and 4.5 of the Chapter 4, the plane progressive wave model was used. The spatial derivatives of the sound pressure, p can be written as,

$$\begin{aligned} p &= A\exp(-ikx) \\ p' &= -ikp \\ p'' &= -k^2 p \\ p''' &= -k^2 p' = -ik^3 p, \text{ etc.} \end{aligned} \tag{B.9}$$

Now, the Equation B.9 can used in the Equation B.4 and B.8, the result are the Equation 4.3 and 4.4 of the Chapter 4. The equation 4.5 of the Chapter 4 is also derived from the Equations 4.3 and 4.4. The derivation of the Equation 4.5 and other equations (4.1, 4.2, 4.3, and 4.4) were collected from a book "Sound Intensity" by F. J. Fahy.

Appendix C: Near-field and far-field

As discussed in the section 4.1.1 in the context of plane wave justification in the anechoic chamber, the intensity probe was placed 2m from the loudspeaker (sound source). In general, up to one wavelength distance from the source is considered near-field. For the measurements made in the anechoic chamber, the probe was placed 2 meters from the sound source and it was in the far-field position with respect to the source. The distance of one wavelength at 200 Hz, and the sound speed of 346.1 m/s is 1.73 meters. The distance is smaller than the 2 meters distance of the probe location from the source. In the plane wave case, the term *kr* (*k* is the wave number, and *r* is the distance from the source) should be very large. *kr* can be written as:

$$kr = \frac{2\pi}{\lambda} r,$$

where λ is the wavelength, and *r* is the distance of the probe from the sound source. For a probe distance of 2 meters, the *kr* at 200 Hz, 1.0 kHz, and 6.5 kHz are calculated to be 7.26, 36.31, and 236.05, respectively. The center (origin) microphones were calibrated at 1 kHz. At this frequency (*kr* = 36.31), the systematic error in the probe intensity measurement is about -1.5 dB (from Figure 4.1 plot, f).

Appendix D: Relevant Illustrations

Figure D.1: Seven microphone Intensity probe.

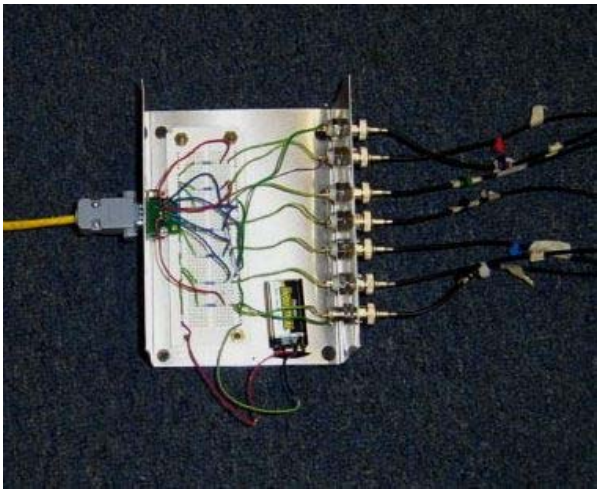

Figure D.2: Interface circuit (battery powered).

Figure D.3: The intensity probe in the anechoic chamber resting on a tripod.

Figure D.4: The reverberation chamber measurement setup.

Figure D.5: Sound source (Large loudspeaker) covered with a sound absorptive material.

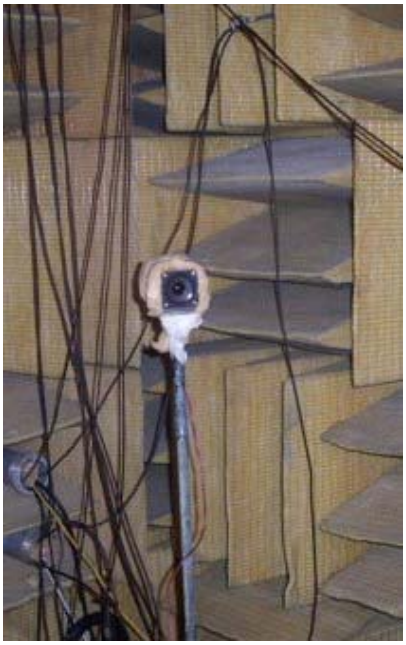

Figure D.6: Sound source (small loudspeaker) covered with a sound absorptive material (used in the source localization measurements).

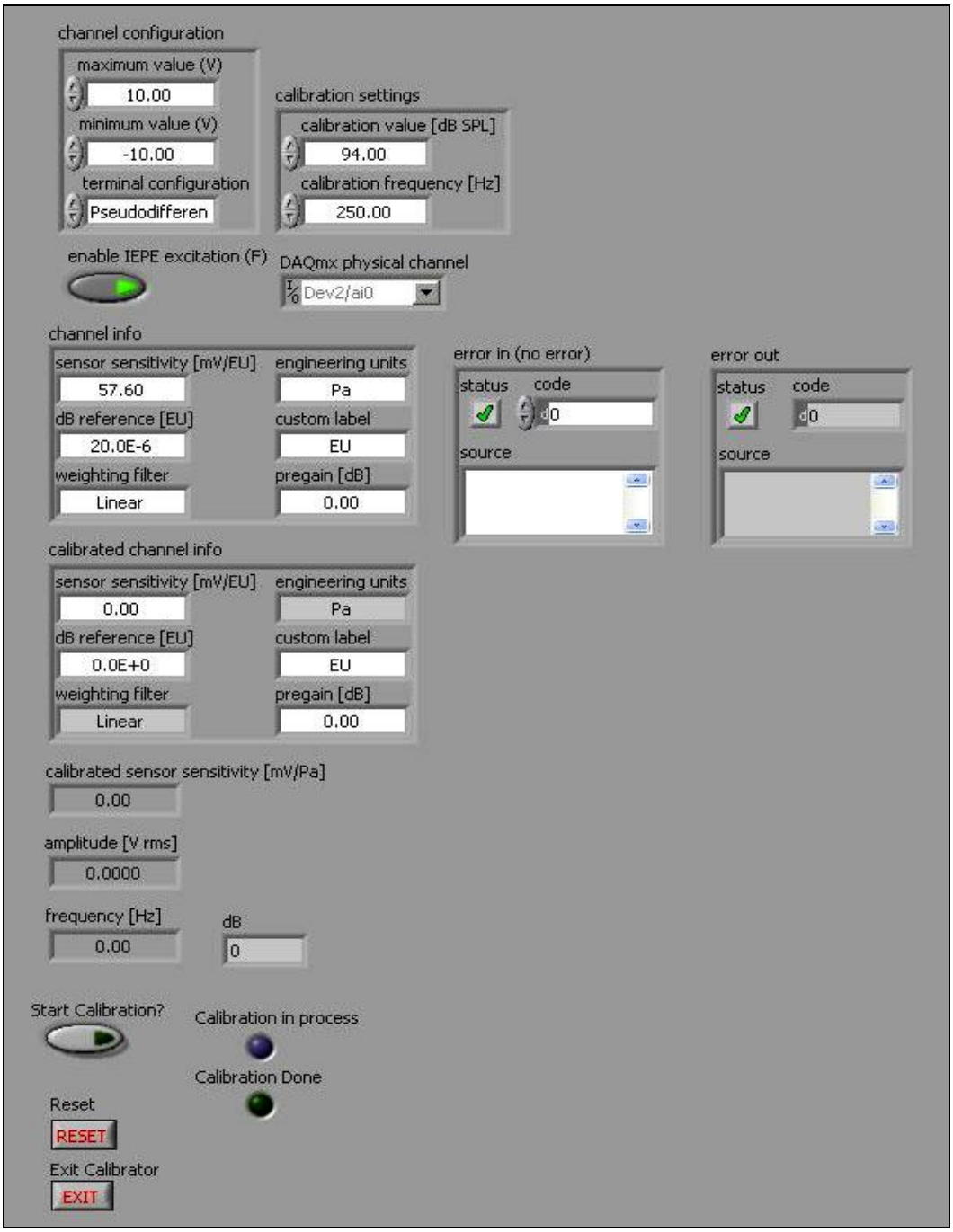

Figure D.7: A custom LabView microphone calibration tool.

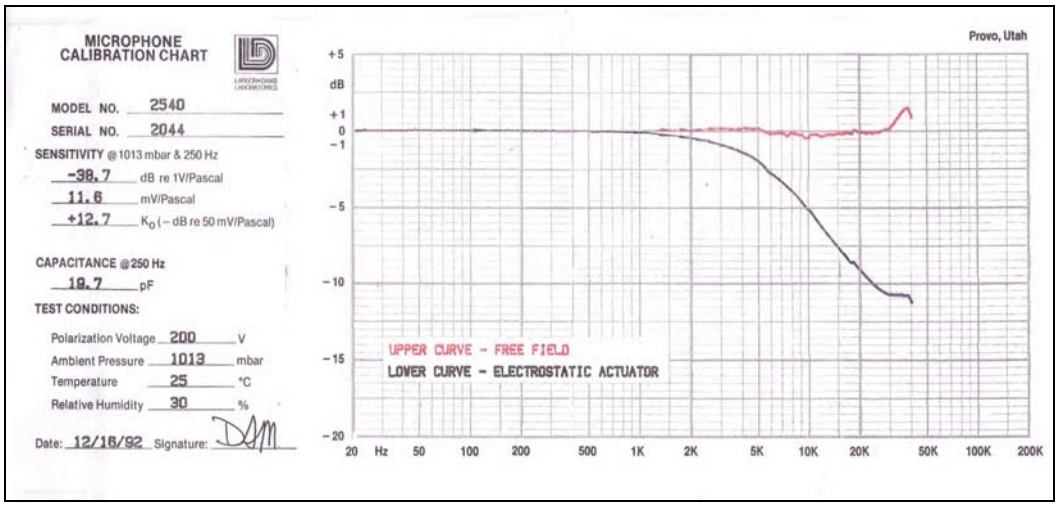

Figure D.8: Manufacturer provided frequency response plot of the standard reference microphone (courtesy: LARSON-DAVIS).

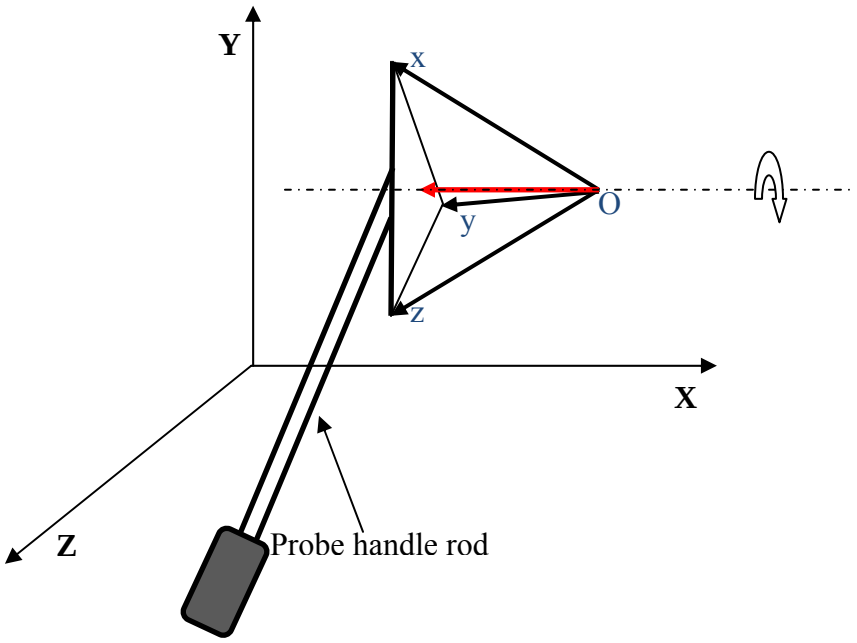

Figure D.9: A schematic of the reference coordinate system (upper case **bold**) and probe coordinate system (lower case), used in the directivity pattern plots in chapter 6.

Bibliography

J. B. Allen and D. A. Berkley, "Image method for efficiently simulating small-room acoustics," *J. Acoust. Soc. Am.,* vol. 65, pp. 943-950, 1979.

J. B. Allen and D. A. Berkley, "Image method for efficiently simulating small-room acoustics," *J. Acoust. Soc. Am.,* vol. 65, pp. 943-950, 1979.

M. Brandstein, J. Adcock, and H. Silverman, "Microphone array localization error estimation with application to sensor placement," *J. Acoustic. Soc. Am.*, vol. 99, no. 6, pp. 3807-3816, 1996.

M. Brandstein and H. Silverman, "A practical methodology for speech source localization with microphone arrays," *Computer, Speech, and Language*, vol. 11, pp. 91-126, April, 1997.

M. Brandstein and D. Word, "*Microphone arrays: Signal Processing Techniques and application*," Chapter 8, Springer-Verlag, Berlin, 2007.

B. S. Cazzolato and J. Ghan, "Frequency domain expressions for the estimation of time-averaged acoustic energy density," *J. Acoust. Soc. Am.*, vol. 117, pp. 3750-3756, 2005.

B. S. Cazzolato and C. H. Hansen, "Errors arising from three-dimensional acoustic energy density in one-dimensional sound fields," *J. Sound Vib.,* vol. 238, pp. 375-400, 2000.

B. Champagne, M. Eizenman, and S. Pasupathy, "Exact maximum likelihood time delay estimation for short observation intervals," *IEEE Trans. Signal Processing*, vol. 39, pp. 1245-1257, June, 1991.

Y. T. Chen and K. C. Ho, "A simple and efficient estimator for hyperbolic location," *IEEE Trans. Signal Processing*, vol. 42, pp. 1905-1915, Aug., 1994.

Y. T. Chen and K. C. Ho, "An efficient closed-form localization solution from time difference of arrival measurements," *in Proc. IEEE Int. Conf. Acoust., Speech, Signal Processing*, vol. II, pp. 393-396, 1994.

J. Y. Chung, "Cross-spectral method of measuring acoustic intensity without error caused by instrument phase mismatch," *J. Acoust. Soc. A.*. vol. 64, pp. 1613-1616, 1978.

R. K. Cook and P. A. Schade, "New method for the measurement of the total energy density of sound waves," *Proceedings of Inter-Noise*, vol. 74, pp. 101-106, 1974.

H. P. Corporation, "*Application Note 1230: Sound Power Measurements*," Hewlett-Packard Co., Singapore, 1992.

G. W. Elko, "*Frequency domain estimation of the complex acoustic intensity and acoustic energy density*," Ph.D. thesis, The Pennsylvania State University, 1984.

F. J. Fahy, "*Sound Intensity*," second edition, E & FN SPON (Chapman & Hall), London, 1995.

F. J. Fahy, "*Sound Intensity*," second edition, E & FN SPON, London, sec 6.2, pp. 108-114, 1995.

F. J. Fahy, "Measurement of acoustic intensity using the cross-spectral density of two microphone signals," *J. Acoust. Soc. Am.*, vol. 62, pp. 1057-1059, 1977.

E. Fredriksen and O. Schultz, "*Pressure microphones for intensity measurement with significantly improved phase properties*," In Brüel Kjaer Technical Review, no. 4-1986, Brüel & Kjaer, Naeurm, Denmark, pp. 11-23, 1986.

G.R.A.S. Sound & Vibration, "*Vector Intensity Probe Type 50VT*", Product Data and Specification sheet, Holte, Denmark, 2002.

Y. Huang, J. Benesty, and J. Chen, "*MIMO Acoustic Signal Processing*," Springer-Verlag, Berlin, 2007.

E. C. Ifeachor and B. W. Jervis, "*Digital Signal Processing – A Practical Approach,*" ADDISON-WESLEY, Wokingham, England, pp. 62, 1995.

P. M. Morse and K. U. Ingard, "*Theoretical Acoustics*," McGraw-Hill, New York, 1968.

C. H. Knapp and G. C. Carter, "The generalized correlation method for estimation of time delay," *IEEE Trans. Acoust. Speech Signal. Process*., vol. ASSP-24, pp. 320-327, August, 1976.

H. Kuttruff and A. Schmitz, "Measurement of sound intensity by means of multi-microphone probes," *Acoustica*, vol. 80, pp. 388-396, 1994.

L. E. Kinsler, A. R. Frey, A. B. Coppens, and J. V. Sanders, "*Fundamentals of Acoustics,*" 3rd edition, John Wiley, New York, 1982.

G. Krishnappa, "Cross-spectral method of measuring acoustic intensity by correcting phase and gain mismatch errors by microphone calibration," *J. Acoust. Soc. Am.,* vol. 69, pp. 307-310, 1981.

J. A. Moryl and E. L. Hixson, "A total acoustic energy density sensor with applications to energy density measurement in a reverberation room," *Proceedings of Inter-Noise, vol. 87*, pp. 1195-1198, 1987.

M. Möser, "*Engineering Acoustics-An Introduction to Noise Control*," second edition, Springer, Berlin, 2004.

S. Nagata, K. Furihata, T. Wada, D. K. Asano, and T. Yanagisawa, "A three-dimensional sound intensity measurement system for source identification and sound power determination by ln models," *J. Acoust. Soc. Am.,* vol. 118, pp. 3691-3705, 2005.

P. J. Nashif and S. D. Sommerfeldt, "An active control strategies for minimizing the energy densities in enclosures," *Proceedings of Inter Noise*, vol. 92, pp. 357-361, 1992.

Y. C. Park and S. D. Sommerfeldt, "Global attenuation of broadband noise fields using energy density controls," *J. Acoust. Soc. Am*., vol. 101, pp. 350-359, 1997.

G. Pavic, "Measurement of sound intensity," *J. Sound Vib.,* vol. 51, pp. 533-546, 1977.

J. W. Perkins, S. D. Sommerfeldt, and J. Tichy, "Error analysis of a particle energy density sensor," *J. Acoust. Soc. Am.,* vol. 108, pp. 211-222, 2000.

T. J. Poterek, "*Energy density analysis of acoustic intensity*," Master's thesis, The University of Texas at Austin, 2001.

M. Schumacher, "*A transducer and processing system for acoustic energy density sensing in one-dimensional sound fields*," Master's thesis, The University of Texas at Austin, 1984.

S. D. Sommerfeldt and P. J. Nashif, "A comparison of control strategies for minimizing the sound field in enclosures," *Proceedings of Noise-Con.*, vol. 91, pp. 299-306, 1991.

S. D. Sommerfeldt and J. W. Perkins, "Active control of energy density in three dimensional enclosures," *J. Acoustic. Soc. Am.,* vol. 95, pp. 2989, 1994.

W. Shen and J. Q. Sun, "A study of shell interior noise control," *SPIE,* vol. 3041, pp. 812-818, 1997.

H. Silverman, W. Patterson, J. Flanagan, and D. Rabinkin, "A digital processing system for some location and sound capture by large microphone arrays," *in Proc. IEEE Int. Conf. Acoust., Speech, Signal Processing (ICASSP-97)*, Munich, Germany, pp. 251-254, April, 1997.

M. Suzuki, H. Anzai, S. Oguro, and T. Ono, "Performance evaluation of a three dimensional intensity probe," *J. Acoust. Soc. Jpn (E).,* vol. 16, pp. 233-238, 1995.

J. K. Thompson and D. R. Tree, "Finite Difference approximation errors in acoustic intensity measurements," *J. Sound Vib.,* vol. 75, pp. 229-238, 1981.

M. P. Waser and M. J. Crocker, "Introduction to the two-microphones cross-spectral method of determining sound intensity," *Noise Control Eng. J.*, vol. 22, pp. 76-85, 1984.

P. S. Watkinson, "The practical assessment of errors in sound intensity measurement," *J. Sound Vib.*, vol. 105, pp. 255-263, 1986.

T. Yanagisawa and N. Koike, "Cancellation of both phase mismatch and position errors with rotating microphones in sound intensity measurements," *J. Sound Vib.,* vol. 113, pp. 117-126, 1987.

A. J. Zuckerwar and G. C. Herring, "Calibration method of the pressure sensitivity of microphones by a far-field method at frequencies up to 80 kHz," *J. Acoust. Soc. Am.*, vol. 119, pp. 320-329, 2006.

Vita

Khalid Hossain Miah was born on January, 01, 1974 in Dhaka, Bangladesh. He is the son of Moazzem Hossain and Khadiza Begum. He has completed his Post Secondary School education from the Notredame College, Dhaka, Bangladesh in 1990. Then he attended the Dhaka Medical College in Dhaka, Bangladesh from 1991 to 1994 before moving to the United States in 1994. In the US, he has attended the first two years of undergraduate education in the Oklahoma State University from 1994 to 1996. He then transferred to the University of Texas at Austin and completed Bachelor of Science in the Aerospace Engineering in 1999. He then worked in the Applied Materials, Austin, TX as a Manufacturing Processing Engineer from 1999 to the end of 2001. He then started his graduate school in the Electrical and Computer Engineering dept at the University of Texas at Austin in 2002. He earned Master of Science (M.S.) degree in the Electrical and Computer Engineering in 2003 from. He then continues his studies at the University of Texas at Austin to pursuit a Ph.D. in the Acoustics and signal processing field. In between M.S. and Ph.D. degrees, he held internships and research positions with Schlumberger, HART Communication Foundation, Nelson Acoustical Engineering, and Institute for Geophysics at UT Austin. His research interests include microphone array signal processing, and seismic imaging using inversion methods.

Permanent address: P.O. Box 7155, Austin, TX 78713

This dissertation was typed by the author.